Synthesis and Characterization of Na-doped $Cu_{0.5}Tl_{0.5}Ba_2Ca_2Cu_{3-x}Na_xO_{10-\delta}$ (x=0, 1, 2,2.5, 3) and $Cu_{0.5}Tl_{0.5}Ba_2CaMgCu_{3-x}Na_xO_{10-\delta}$ (x=0, 1, 2, 3) samples

Ambreen Akhtar

Department of Physics

Quaid-i-Azam University

Islamabad,

2022

Synthesis and Characterization of Na-doped $Cu_{0.5}Tl_{0.5}Ba_2Ca_2Cu_{3-x}Na_xO_{10-\delta}$ (x=0, 1, 2, 2.5, 3) and $Cu_{0.5}Tl_{0.5}Ba_2CaMgCu_{3-x}Na_xO_{10-\delta}$ (x=0, 1, 2, 3) samples

A dissertation submitted to the department of physics, Quaid-I-Azam University, Islamabad, in partial fulfillment of the requirement for the degree of

Master of Philosophy

in

Physics

By

Ambreen Akhtar

Material Science Laboratory

Department of Physics

Quaid-I-Azam University

Islamabad, Pakistan

2022

Certificate

This is to certify that Ms. **Ambreen Akhtar** D/O **Ghulam Mustafa** has carried out the experimental work in this dissertation under my supervision in Materials Science Laboratory, Department of Physics, Quaid-i-Azam University, Islamabad, and satisfying the dissertation requirement for the degree of Master of Philosophy in Physics.

Supervisor

Dr. Nawazish Ali Khan
Department of Physics
Quaid-i-Azam University
Islamabad, Pakistan.

Submitted through

Chairman

Prof. Dr. Nawazish Ali Khan
Department of Physics
Quaid-I-Azam University Islamabad, Pakistan.

DEDICATED

TO

MY FAMILY

ACKNOWLEDGEMENTS

All the praises to Almighty ALLAH, the most merciful and sovereign power, who made me able to accomplish this research work successfully. I offer my humble and sincere words of thanks to his Holy Prophet Muhammad (P.B.U.H) who is forever a source of guidance and knowledge for humanity.

This work would have not been possible without the invaluable contributions of many individuals. First and foremost, I wish to thank my supervisor Dr. Nawazish Ali Khan for all of his support, advice, and guidance during the whole period of my study. I am thankful to him. I would like to thank all my seniors, juniors and fellows . My humble and heartfelt gratitude is reserved for my beloved Parents and brother. Without their prayers, support, and encouragement the completion of this study task would have been a dream.

.

Ambreen Akhtar

List of Figures

Table of Contents

Chapter:1

Introduction

Chapter:2
Literature Review

Chapter:3
Preparation of Sample & Experimental Techniques

Chapter:4
Results & Conclusion

Abstract:

To examine the role played by lighter alkali atoms in oxide superconductors of high critical-temperature(Tc) superconductivity, the samples of the following compounds $Cu_{0.5}Tl_{0.5}Ba_2Ca_2Cu_{3-x}Na_xO_{10-\delta}$(x=0,1,2,2.5,3) and $Cu_{0.5}Tl_{0.5}Ba_2CaMgCu_{3-x}Na_xO_{10-\delta}$ (x=0, 1, 2, 3) have been prepared. These analyses would clarify the significance of interactions of electrons with phonons in the process of the high critical-temperature(Tc) superconductivity as well as the involvement of extra electrons in the CuO_2 planes. These samples show an orthorhombic crystal structure with decreased unit cell volume due to higher Na-doping in the final product. In terms of resistivity measurements, the metallic variations in resistivity down to 77K and critical temperatures at zero resistivity are 94.91K, 94.7K, 91.63K and 95.2K, 93.6,K 92.8K values for the prepared $Cu_{0.5}Tl_{0.5}Ba_2Ca_2Cu_{3-x}Na_xO_{10-\delta}$ (x= 0, 1, 2) and $Cu_{0.5}Tl_{0.5}Ba_2CaMgCu_{3-x}Na_xO_{10-\delta}$ (x= 0, 1, 2) samples respectively. Suppression of the velocity of fermi surface 'V_F', the zero resistance coherence length (along c-axis) '$\xi_c(0)$', the interlayer coupling constant 'J', and the phase relaxation time of the carriers 'τ_ϕ' are demonstrating a loss in the superconducting carriers' density in Na-doped, according to the Fluctuation-induced conductivity(FIC) analysis of $Cu_{0.5}Tl_{0.5}Ba_2Ca_2Cu_{3-x}Na_xO_{10-\delta}$ (x=0, 1, 2) samples. However, compared to undoped samples, the values for $B_{C0}(T)$, $B_{C1}(T)$, and, $J_c(0)$ is increased indicating an increase in the population of inadvertently localized defects that acts as the pining centers and hence also shows an increasing trend in the values for these mentioned superconducting-parameters. While the zero resistance coherence-length (along c-axis) '$\xi_c(0)$', the velocity of fermi surface 'V_F' , the inter layer coupling constant 'J', and the phase relaxation time of carriers 'τ_ϕ' are marginally increased for $Cu_{0.5}Tl_{0.5}Ba_2CaMgCu_{3-x}Na_xO_{10-\delta}$ (x=0, 1, 2) samples, demonstrating a small increase in the carriers' density in the above mentioned samples. The marginal suppression of $B_{C0}(T)$, $B_{C1}(T)$, and $J_C(0)$ values in $Cu_{0.5}Tl_{0.5}Ba_2CaMgCu_{3-x}Na_xO_{10-\delta}$ (x= 0, 1, 2) samples showing an increase in the population of inadvertently localized defects. By increasing the doping concentration of Na to pure 1223 samples, the phonon modes of oxygen(O_2) are going softened which is most likely caused by the suppressed oscillator strength in Na-doped materials. The doping concentration of Na in the final(1223) samples shows the reduction in the density of free carriers at the planar sites of CuO_2/NaO_2 in these samples, which in turn shows suppression in the real (ε')part, imaginary-part(ε'') of the dielectric constant, & the ac-conductivity(σ_{ac}).

Chapter:1

Introduction to Superconductivity

We will let to know about the historical background, and some theories and applications of superconductivity in this chapter.

1.1 Historical background of Superconductivity

When a sample is chilled to a sufficiently low temperature, a phenomenon known as superconductivity occurs in which the electrical resistance of man-made metals and alloys abruptly reduces to zero. Kamerlingh Onnes and his student first noticed it in Leiden in 1911 **[1]**. The first metal that shows superconductivity is Mercury(Hg), during the experiment, its critical temperature of 4.2K is observed below which its resistivity goes down to zero.

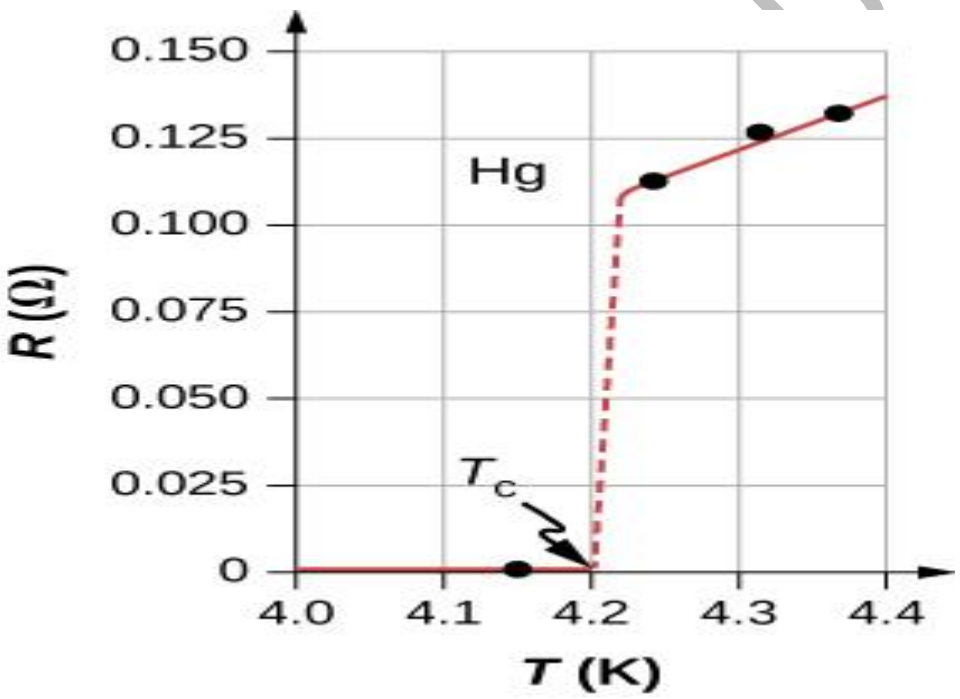

Figure 1.1 Resistivity versus temperature graph of Mercury [1]

Superconductivity occurs in metals, alloys, intermetallic compounds, and doped semiconductors. In 1911 the superconductivity for Hg is observed with Tc=4.2K. In 1973, it was observed for Nb_3Ge with 23K.In 1986, it was observed for $LaBaCuO_4$ with Tc=35K and $YBa_2Cu_3O_7$ with Tc=92K. In 1987, it was observed for $BiCaSrCu_2O_9$ with Tc=110K. In 1988, it was observed for $Tl_xSr_xBa_xCu_xO_x$ with Tc=125K **[2].**

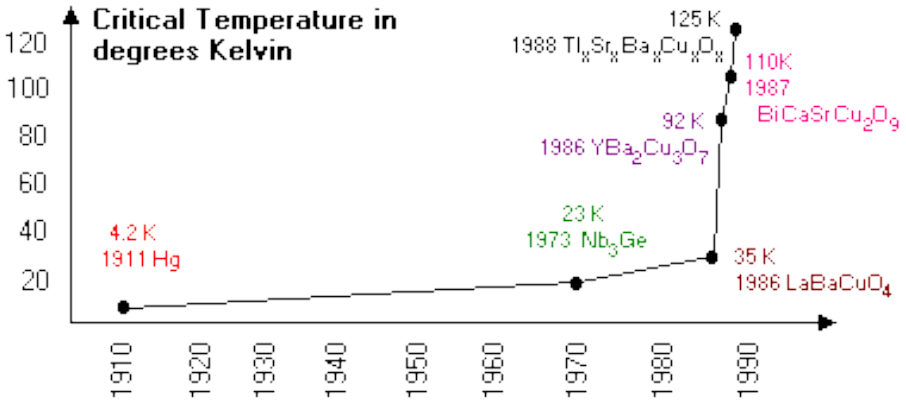

Figure 1.2 History of Superconductor's discovery

1.2 Important Properties of Superconductors:

There are two fundamental properties of superconductors **[3]**:

a) Zero resistance(R=0)
b) Perfect diamagnetism(B=0)

1.2.1 Zero resistance:

The blockage to the flow of electrons is termed resistance. In atoms, there are many free electrons around the lattice cores (fixed atoms). In the normal state, there are unlimited collisions of electrons with fixed atoms. The electrons carry kinetic energy during their motion and finally vibrate and loss, then convert that kinetic energy into heat energy after making collisions with lattice cores of atoms.

The resistivity is the property of a material to measure the resistance in the material. Resistivity is defined as

$$\rho = \frac{RA}{l}$$

Also, resistivity is the reciprocal of conductivity

$$\rho = \frac{1}{\sigma}$$

$$\sigma = ne^2 \frac{\tau}{m} \qquad (1.1)$$

Also

$$\rho = \frac{m}{n\tau e^2} \qquad (1.2)$$

Here the electron's mass is denoted by 'm', the mean free time is denoted by 'τ', the electronic charge by 'e' and the number density of the electron by 'n'.

The lattice vibrations ceased if the sample is cooled slowly to a very low value of temperature below a critical(Tc) temperature. As a result, the electron-lattice motion is stopped.

if the sample is chilled slowly to a very low temperature below a, critical temperature. As result, the electron-lattice motion is stopped.

From equation (1.2): If there is quite large change in mean free time, then at low temperatures, the superconductors' electrical resistivity drops down. In the superconducting state, the pair of electrons are bound together by cooper's pairs (via phonons) **[4].**

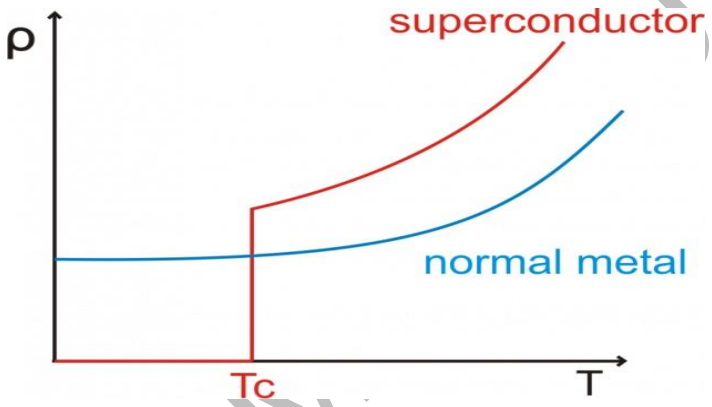

Fig 1.3 Temperature v/s resistivity curve.

1.2.2 Diamagnetism:

The magnetic behavior is extremely weak, and there are no permanent magnetic dipole moments in such diamagnetic substances. But when this substance is exposed by external (magnetic)B-field, the magnetic dipole moments begin to align in opposite to that magnetic field.

1.2.3 Meissner's Effect:

Meissner and Ochsenfeld made their first discovery of this effect in 1933**[5].** the magnetic field being ejected from inside the superconductor material.

Since

$$B = \mu_o(H + M) \qquad (1.3)$$

In superconductors, loss of the magnetic field B=0,

$$M = -H$$

Susceptibility is given as

$$\frac{M}{H} = \chi = -1 \qquad (1.4)$$

As susceptibility for perfect diamagnetic materials is also -1 hence superconductors show perfect diamagnetism.

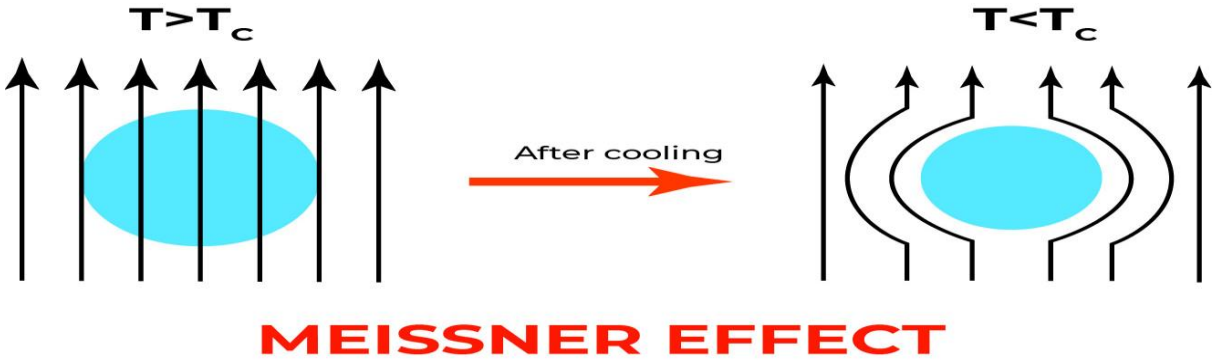

Fig 1.4 Meissner Effect in normal and superconducting materials

1.3 Parameters of Superconducting states:

There are many parameters that affect the superconducting characteristics of superconductors. Following are the three essential parameters by which superconductors are classified and restrict the existence of superconductivity:

- Critical temperature (T_c)
- Critical magnetic field (H_c)
- Critical current density (J_c)

1.3.1 Critical temperature:

This is the transition temperature at which a material's electrical resistivity reduces to zero. At this temperature, there will be a transition of the phase of the material, and the material will act as a superconductor.

Two States are present;
When $T>T_C$; The state of the material is normal
When $T<T_C$; The state of the material is superconducting

The discovered range of critical temperature for a material to remain in a superconducting state is from a fraction of 1K to slightly above 100K. the superconductors having critical temperatures near this range are classified as ***"high-temperature superconductors".*** For practical purposes, the superconducting materials are required to be kept below their critical temperatures and this purpose can be attained by immersing the material in liquid helium; which has a 4.2K critical temperature. But liquid helium evaporates instantly and thus, it is required to be replenished continuously. So in comparison to this, liquid nitrogen; having $T_c >> 77$ K, bath proves to be inexpensive and cost-effective that can maintain the superconductivity of the material.

1.3.2 Critical current density:

This is the maximum current limit that could pass through a wire's cross-section while causing the material to transition into its normal state. These small wires can only carry a very limited amount of current. It was first identified by Kunzler in 1961 **[6]**. The material's current flow will produce a magnetic field on its own. The magnetic-field that forms on the surface of the material may go beyond the critical field limit at very high current densities, which would ultimately cause the material to lose its superconductivity and return to its original state.

The critical transition current for a straight superconducting wire is:

$$I_c = 2\pi a B_c / \mu_o \qquad (1.5)$$

The critical transition current is proportional to the radii 'a' of the wire. Since the critical transition magnetic-field is the function of temperature; as the temperature(T) is increased to critical temperature(Tc), the field strength drops to zero. Inconsistent with this relation, a wire carrying a superconducting current will, also, drop with the approaching of temperature to the critical temperature. Due to this reason, in real applications, superconductors are operated at half of the critical temperature; since the B_c, and I_c are more than 75% of the critical values. Practically the J_c value must be larger than 1000 (A/mm^2)

1.3.3 Critical magnetic field:

Another significant factor that defines the material's state for superconductivity is the critical transition (magnetic)B-field. Its critical magnetic-field 'Hc' is the greatest field which may be provided to material at a given temperature T to maintain the material in the superconducting condition. If the given field is greater than the material's critical magnetic-field(Hc), the superconductivity of the material is lost. The critical field will be zero at critical temperature 'Tc' and will grow as the temperature drop.

The effect of the (Hc) by temperature is shown in the following mathematical formula:

$$Hc(T)=Hc(0)[1-T/Tc] \qquad (1.6)$$

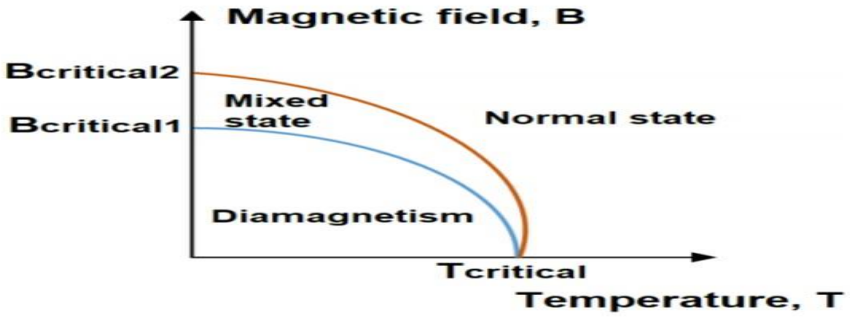

Fig 1.5 Temperature-dependent critical Magnetic field

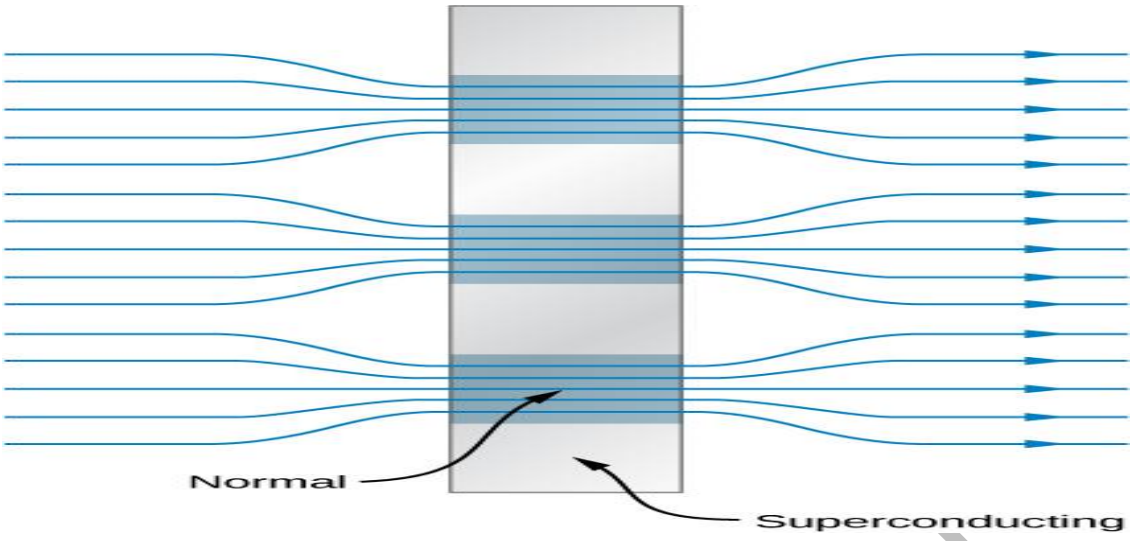

Fig 1.6 The behavior of applying Magnetic field in normal and superconducting material

The table showing the critical temperature and magnetic field of various materials is as follows:

Materials	Critical temperature (Kelvin)	Critical Magnetic Field (Tesla)
Al	1.2	0.011
Pb	7.2	0.080
NbTi	9.3	15
Th	1.4	0.00016
$YBa_2Cu_3O_7$	92	100
Nb_3Al	18	32

Table 1.1: Tc and Hc in significant materials

1.3.4 Relation between critical parameters:

Although superconductivity is characterized by all these three critical parameters; T_c, J_c, and H_c. A superconducting material may lose its superconducting properties if any one or more of these parameters get beyond their critical limits. But the material will, surely, not lose all its superconductivity at a time; only those areas will destroy its superconductivity that are exceeding the critical limits while other areas will hold their state. At zero temperature, we can estimate the maximum values of J_c, and H_c, but the most appropriate value of T_c can be estimated when $J_c=H_c=0$.

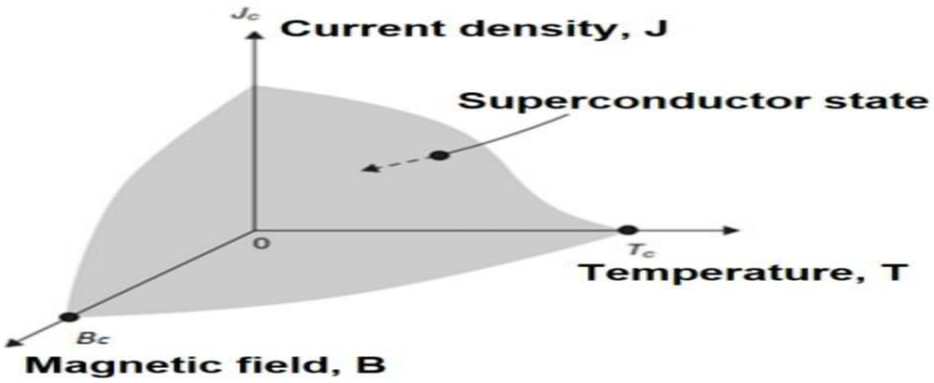

Fig 1.7 Relationship between Tc, Hc, and Jc.

1.4. Superconductors' Types:

1. Type-1
2. Type-2

1.4.1. Type-1 superconductor:

These superconductors purely obey the Meissner effect (i.e. B=0 inside the superconductors). These have a very low critical temperature(0K to 10K) and a very low critical magnetic field(4.9μT to 1T). These have only one critical transition magnetic field. Such superconductors are also known as soft superconductors because they lose their superconducting state by applying low magnetic field intensity. They are diamagnetic. They are pure metals e.g. Pb, Zn, Hg, etc. BCS theory can be used to explain its behavior. No mixed state exists in type-1 superconductors. The shifting of superconducting to normal state is sharp and abrupt for Type-1 superconductors.

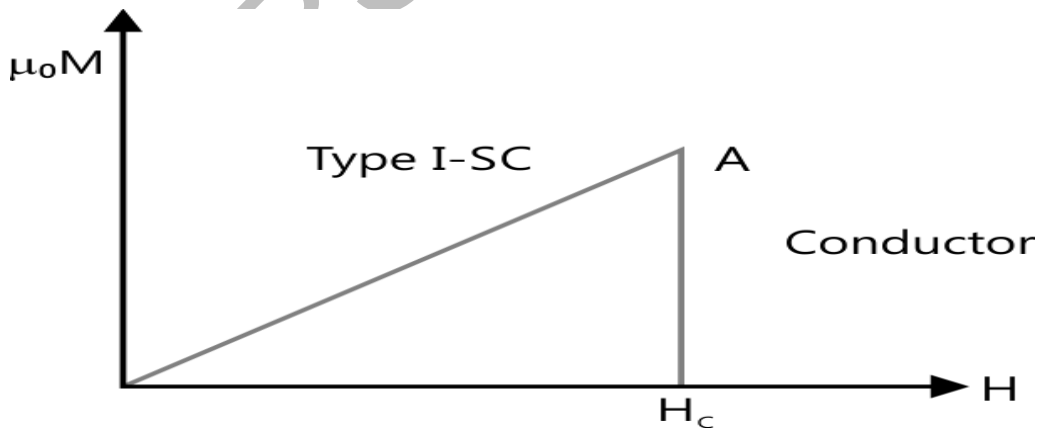

Fig 1.8: type-1 superconductor

1.4.2. Type-2 superconductor:

These superconductors partly obey the Meissner effect (i.e. B can penetrate inside the superconductors). These have a high Tc (greater than 10K) and a high Hc (greater than 1T) and a high value of resistivity by applying a magnetic field **[7]**. These have two critical fields. Type-2

superconductors **[8]** are also called hard superconductors because they cannot lose their superconducting state by applying low magnetic field intensity. They are diamagnetic. They are alloys and ceramic oxides e.g. NbTi, Nb_3Sn, etc. BCS theory can be used to explain its behavior. A mixed state exists in type-1 superconductors. For type-2 superconductor, the transition from the superconducting to the normal state is not sharp and abrupt.

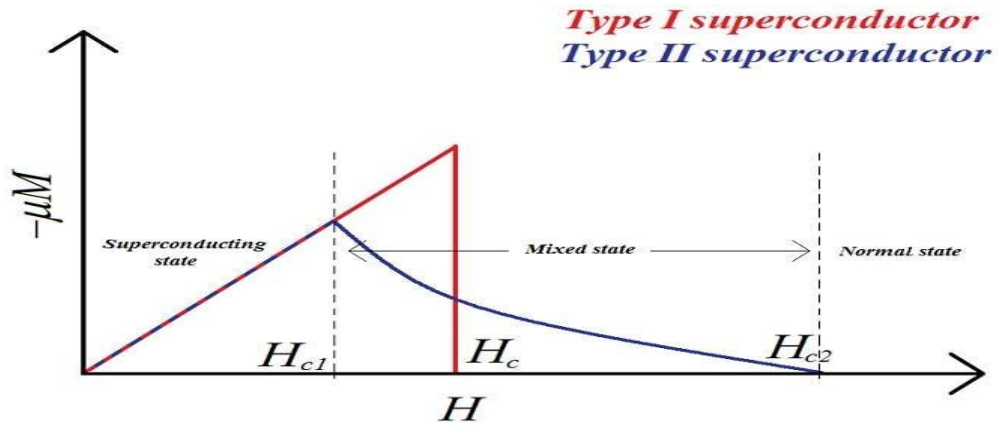

Fig 1.9: type-1 & type-2 superconductor's response to an applied external B- field

1.5 Thermal-Properties of Superconductors:

1.5.1 Entropy:

The entropy of superconducting state S_s is lesser than normal-state S_N which means that there is more regular arrangement of superconducting state over the normal state. The reason for less entropy is that the electrons are more ordered in superconductors. At T_c, the entropy of both states is the same **[8]**.

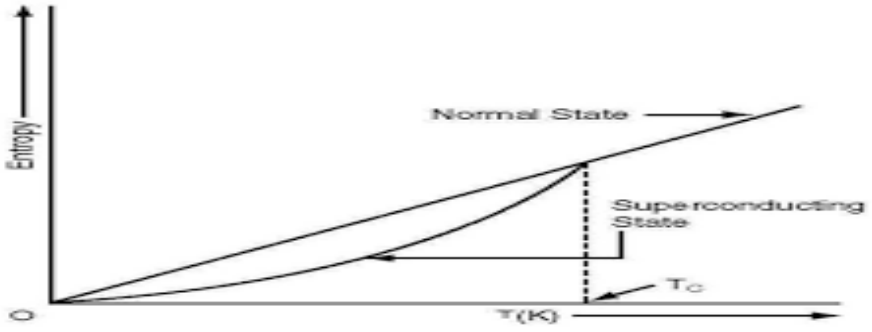

Fig 1.11: The Temperature dependent entropy difference

$$S_N - S_S = -\frac{H_c dH_c}{dt} \qquad (1.7)$$

At $T=T_c$ $H_c=0$ so $S_N-S_S=0$

At T=0K again S_N-S_S=0

1.5.2 Specific Heat:

The specific heat of normal metal has the following relation with temperature:

$$C_n(T) = \gamma T + \beta T^3 \quad (1.8)$$

Here the first term shows the electronic specific heat while the second term is for lattice vibrations' contribution to the specific heat. Superconductors have a clear jump at T_c. But it is noticeable that the lattice properties like Debye temperature and crystal structure remain unaffected even after the transition from normal to superconducting state so specific heat in both cases remains the same due to lattice vibrations. The important role is played by electronic specific heat **[9].** Experimentally it has been shown that the electronic specific heat varies exponentially with temperature:

$$(Cel)_s = Aexp(\frac{-\Delta}{k_B T}) \quad (1.9)$$

Here Δ represents the gap of energy and A is it's constant.

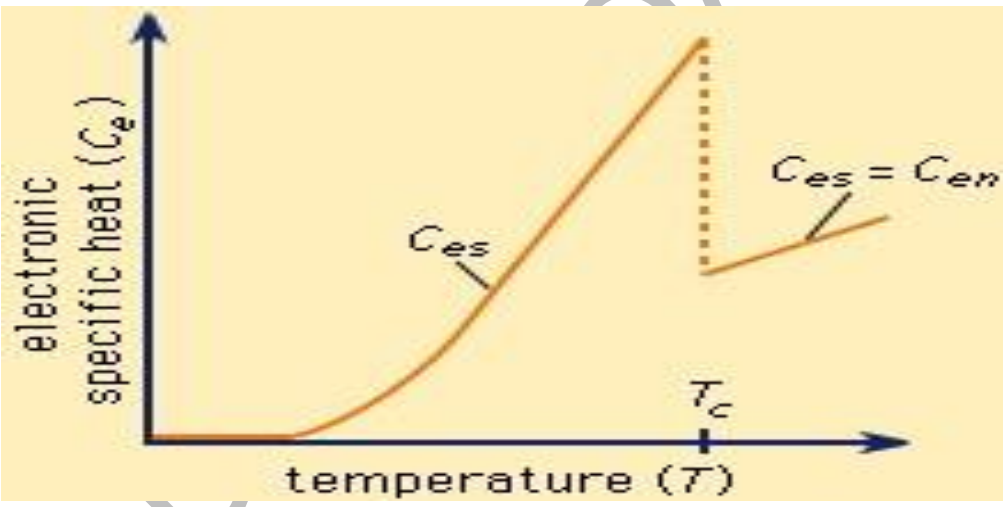

Fig 1.12: The Temperature-dependent electronic specific heat

1.6 Dielectric Properties:

1.6.1 Superconducting Capacitor:

A device is used to store charge in an electric field. It consists of layers of conductor around and dielectric is in between.

$$C = \varepsilon_r \frac{A}{d} \quad (1.10)$$

1.6.1.1 Dielectric Constant:

It is a complex constant which has real ε' as well as imaginary part ε''.

1.6.1.2 Dielectric Loss:

It is the ratio between the imaginary constant to the real constant. It is also known as the dissipation factor.

$$\tan\delta = \frac{\varepsilon''}{\varepsilon'} \quad (1.11)$$

1.6.1.3 AC-Conductivity:

$$\sigma_{ac} = 2\pi f\varepsilon_o\, \varepsilon' \tan\delta \quad (1.12)$$

1.7 Theoretical Evaluation of Superconductivity:

The following theories are given by some physicists after the discovery of superconductivity.

i)London Theory

ii)BCS Theory

1.7.1 London Theory:

In 1935, Heinz and Fritz London gave the first theory based on two-fluid models. The London equations relate the electromagnetic fields to current in and around a superconductor. It is the macroscopic study of the thermodynamic behavior of superconductors. In the two-fluid model, the electrons of superconducting-material have two types, (i) Normal electrons $\mathbf{n_n}$ and (ii) Superconducting electrons $\mathbf{n_s}$ as given by:

$$n = n_n + n_s \quad (1.12)$$

$$T \to Tc, n_n \to 0 \;\; so \;\; n_s \to \max for\; (T<Tc)$$

And $$T \to Tc, n_s \to 0 \; so \; n_n \to \max as \;\; for\; (T>Tc)$$

The equation of motion in E-field for Superconductors: -

$$F=ma$$

$$eE=m(dv/dt) \quad (1.13)$$

$$n_s eE=mn_s(dv_s/dt) \quad (1.14)$$

where '$\mathbf{v_s}$' **is** the superfluid velocity, the mass of electrons is denoted by 'm', and the electron's charge denoted by 'e'.

So supercurrent density

$$J_s=ev_sn_s \quad (1.15)$$

$$dJ_s/dt = en_s(dv_s/dt) \quad (1.16)$$

$$dJ_s/dt = e^2n_sE/m \quad (1.17)$$

This is the first London equation.

In static state E=0 inside the superconductors: -

$$dJ_s/dt=0 \quad (1.18)$$

According to Maxwell's equation: -

$$\nabla xE = -dB/dt \quad (1.19)$$

As E=0 so B is constant according to the above equation which is inconsistent with the Meissner effect. So London made some modifications to it and finally, we get the 2nd London equation **[10]**:

$$\nabla xJs = -(n_s e^2/m)B \quad (1.20)$$

Which is inconsistent with the Meissner effect.

1.7.1.1 London's penetration depth:

It is the characteristic length that defines the limit of distance to which lines of magnetic field B penetrate into the material of superconductors. The magnetic field is not completely zero but is decaying exponentially from the material of the superconductor.

As Maxwell's equation: -

$$\nabla xB= \mu_o Js \quad (1.21)$$

$$\nabla x(\nabla xB)=-(\mu_o n_s e^2/m) \quad (1.22)$$

$$\nabla x(\nabla xB) =-(1/\lambda^2) B \quad (1.23)$$

So

$$\lambda=(m/ \mu_o n_s e^2)^{1/2} \quad (1.24)$$

$$\nabla x(\nabla xB) = \nabla (\nabla. B)- \nabla^2 B \quad (1.25)$$

According to Maxwell's equation: -

$$\nabla. B=0$$

Put in equations (4) and (5): -

$$\nabla^2 B =(1/\lambda^2) B \quad (1.26)$$

$$B=B_0 e^{-(x/L)} \quad (1.27)$$

It shows magnetic field decays exponentially by London theory.

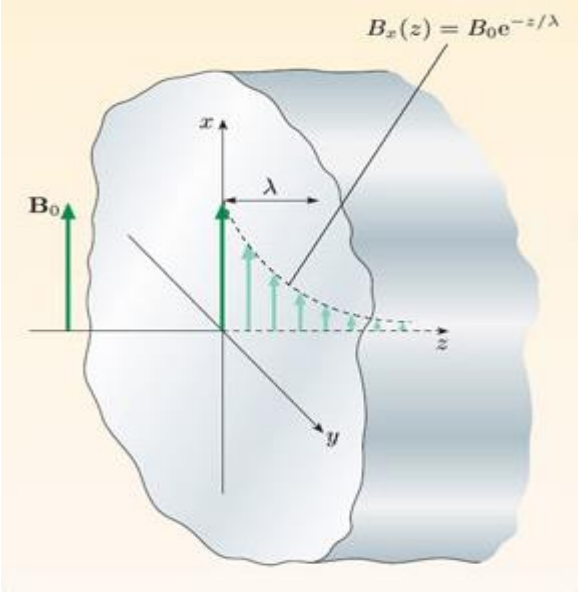

Fig 1.13: Exponential decay of magnetic field

$\lambda^2 = (m_e/\mu_0 n_s e^2)$ implies that

$$\lambda_L = (m_e/\mu_0 n_s e^2)^{1/2} \quad \text{(London Penetration depth) [11]}$$

$$\lambda(T) = \frac{\boldsymbol{\lambda(0)}}{[\mathbf{1} + (\frac{\mathbf{T}}{\mathbf{T_c}})^{\mathbf{4}}]^{\mathbf{1/2}}} \qquad (1.28)$$

1.7.2 G-L Theory: -

Through a phenomenological theory known as the GL theory, L.D. Landau and V.L. Ginzburg gave the quantum mechanical explanation of superconductors in 1950**[12]**. The importance of this theory over the London theory is due to the following reasons:

1) This theory gave an explanation for why the superconducting state' entropy is higher than the normal state' entropy.
2) This theory explains the second-order transition of phase diagram (i.e., transition from normal(state) to superconducting(state)), this give rise to order parameter **[13]** 'ψ' which is defined as the 'complex wave function**'** **[14]** of superconducting-electrons: -

$$\Psi = 0 \quad \text{at} \quad T > T_c$$

$$\Psi \text{ is non-0} \quad \text{at} \quad T < T_c$$

The second-order transition of phase diagram explained by the G-L theory which has the expansion of the free energy in terms of the power of the parameter's order, that is negligible at the transition temperature(Tc). This theory, therefore, holds good near Tc, the critical temperature.

$T-T_c << T_c$

Normalization of order parameter ψ gives the density of superconducting electrons n_s:

$$|\psi|^2 = n_s/2 \qquad (1.29)$$

Ψ is independent of position: -

$$F = F_n + \alpha|\psi|^2 + (\beta/2)|\psi|^4 \qquad (1.30)$$

Fn is the density of free-energy in normal state, and F is the density of free-energy. The phenomenological expansion coefficients for superconducting material are α and β.

When magnetic field is applied: -

$$F = F_n + \alpha|\Psi|^2 + \frac{\beta}{2}|\Psi|^4 + \frac{1}{2m^*}|(-i\hbar\nabla - 2e^*A)\Psi|^2 + \frac{|B|^2}{2\mu_0} \qquad (1.31)$$

The generalized equations are:

$$\alpha\Psi + \beta|\Psi|^2\Psi + \frac{1}{2m^*}\left(-i\hbar\nabla - \frac{e^*}{c}A\right)^2\Psi = 0 \qquad (1.32)$$

$$j_s = -\frac{i\hbar e}{2m^*}(\Psi^*\nabla\Psi - \Psi\nabla\Psi^*) - \frac{2e^2}{mc}|\Psi|^2 A \qquad (1.33)$$

The two characteristic lengths ξ and λ are also defined by GL theory:

$$\xi = \sqrt{\frac{\hbar^2}{2m|\alpha|}} \qquad (1.34)$$

$$\lambda = \sqrt{\frac{m}{4e^2\Psi\mu_0}} \qquad (1.35)$$

Coherence length provides information for the order parameter length or thermal fluctuation, whereas penetration depth provides information on the depth to which a B-field enters into the surface of superconductors **[15]**.

The κ (Ginzberg-Landau parameter) specifies the coherence length to penetration depth ratio.

$$\kappa = \frac{\xi}{\lambda} \qquad (1.36)$$

It discriminates type-1 and type-2 superconductors as,

$\kappa < \frac{1}{\sqrt{2}}$ (for type-1 superconductors)

$$\kappa > \frac{1}{\sqrt{2}}$$ (for type-2 superconductors)

The main difference between the both these superconductors 'types raised due to their response to the B-field.

Type-1 Superconductor totally expel the magnetic field from its interior surface but Type-2 Superconductor expel it partially up to higher field but completely at lower field. The reason is: the interface energy of normal to superconducting phase which is positive for type 1 and negative for type 2. It also gave the concept of critical magnetic field which destroy superconductivity.

Type-1 has only one critical field but Type-2 has two fields, one is H_{c1} and other is H_{c2} due to presence of vortices. Below Hc1 the material completely expelled the magnetic field but above the Hc1 magnetic field starts to penetrate through vortices. Each vortex behaves like non-superconducting hole where B is so strong and order parameter $\psi=0$.

1.7.3 BCS Theory: -

The first microscopic theory to provide a quantum mechanical explanation for superconductivity, was first proposed by Bardeen, Cooper, and Schrieffer in 1957 [16]. This theory enlightened the phenomenon of pairing of two electrons via the interaction between the electrons & phonons, which is the basis of superconductivity. It also explained that how weak-coupled superconductors like aluminium have superconducting characteristics. Its basic idea lies in the involvement of interaction of electrons with phonons. Two important phenomena are described by this theory:

1) Cooper pair formation
2) Isotopic effect

1.7.3.1 Cooper pairs formation: -

An important microscopic mechanism that is responsible for superconductivity is the electron-phonon interaction. When an electron passes through ionic cores of lattice then it creates the distortion and positive ions start vibrating so phonons are created due to its vibrations then two electrons that carry negative charges interact with each other indirectly with the help of phonons **[17]**. And cooper pairs are formed due to electron-electron interaction via phonons. One electron carries the spin up momentum and the other has spin down so their net momentum is zero. The requirement that the electron pairs have an energy lower than fermi energy, indicating that the pair is in the bound state, is essential for the creation of cooper pairs.

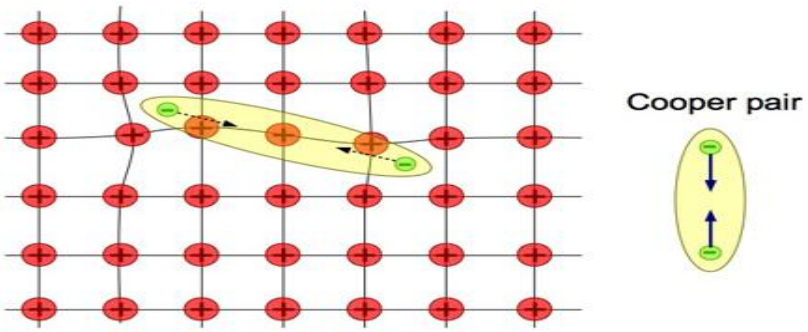

Fig 1.14 Cooper pairs' Formation

Both electrons have opposite and equal momentum (+k and –k) and total spin of both

electrons are zero because both electrons carry opposite spins to each other i.e., (+1/2 and -1/2) respectively. Electron with +k momentum is in +1/2 spin up state (↑) and second electron of –k is in -1/2 spin down state (↓). Excitation occurs together in cooper pair, this is very important property of a cooper pair i.e. if the state occupied with '–k' momentum while spin-down stays occupying then it's obvious that state with '+k' momentum while spin-up is to be occupied. There are many electron pairs that overlap strongly in a superconducting state and collectively form highly "condensate". And it follows the Bose-Einstein statistics. As electrons gets energy from phonons and start vibrating with Debye temperature (The temperature at which mechanical oscillator oscillate at specific frequency with large amplitude at Tc). As the electron behave as quantum mechanical oscillator.

1.7.3.2 Isotopic effect: -

This is the essential key to the development of BCS theory **[18]**. The dependence on the phonon parameters was experimentally determined by this fact that for different isotopes of same metal,

Tc depends upon mass of ion. It states that: - "The critical-temperature for a superconducting material behaves inversely to its isotopic-mass"

$$T_C \propto M^{-\alpha} \qquad (1.37)$$

where α=0.5 and near to zero for high-temperature superconductors.

It shows that by adding neutrons to the atoms of elements, there arises the isotopic effect that the atoms become heavier and heavier and this effect causes the occurrence of superconductivity at a very low critical temperature. By figuring out the energy gap "2Δ " at the Fermi level, the BCS Theory prediction can also be made in this manner. Many physical aspects of the state of superconductors are provided by the BCS quantum Theory. ."2Δ"is the minimum required amount of energy to break a cooper pair, resulting into the formation of two quasi-particle excitations. At T<Tc, the equation for the energy gap given by BCS theory is:

$$2\Delta(T<\mathrm{Tc}) = 3.52 k_B T_c \qquad (1.38)$$

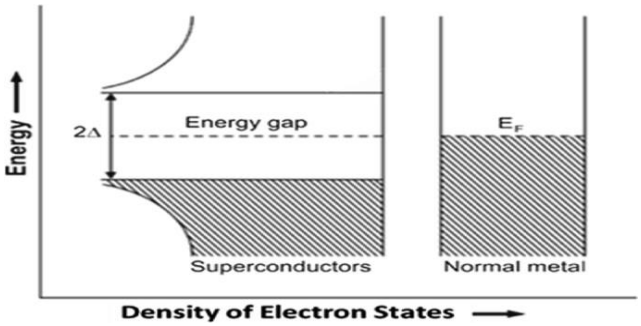

Fig 1.15 graph between energy and density of free electron states

1.7.3.3 Coherence Length: -

Two electrons (cooper pairs) interact via phonons separated by small distance called coherence length(ξ).

BCS theory defines coherence length as:

$$\xi = \frac{\hbar V_F}{2\Delta} \qquad (1.39)$$

Here the Fermi velocity is represented by 'V_F' and the energy gap is denoted by '2Δ'

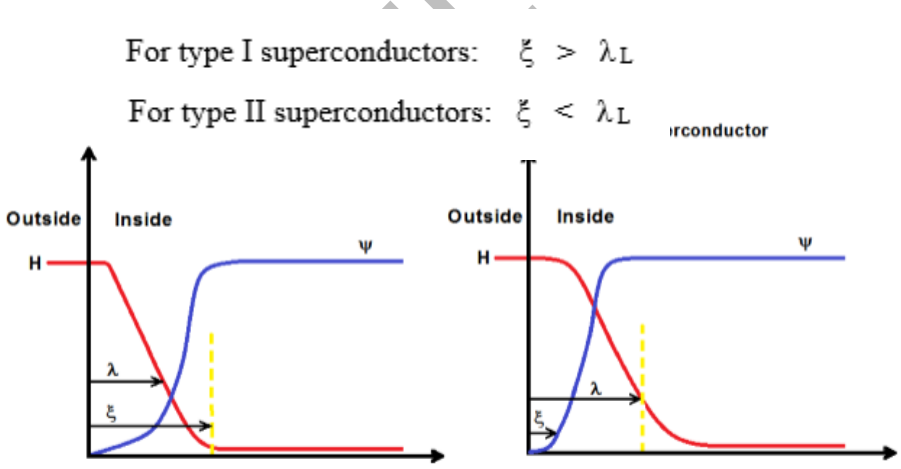

Fig 1.15 "penetration depth" and "coherence length" in superconductors

1.8 Josephson' Effect: -

In 1962, scientist named as Brian David Josephson gave a new quantum mechanical tunnelling effect that occurs in superconducting samples called Josephson Effect **[19].** This effect is a new quantum mechanical tunnelling effect lies in superconductors. It shows that when we separate down the two superconducting materials by an insulating medium inserted between them, the electron would tunnel between them. The connection between the two superconducting layers is due to that thin layer of dielectric medium which is called Josephson junction **[20].**

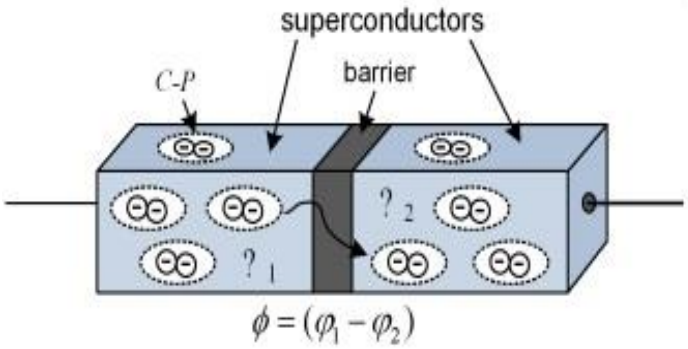

Fig 1.16 Josephson Effect

Josephson effect has two types:

- Effect of AC Josephson
- Effect of DC Josephson

1.8.1 DC Josephson effect: -

It refers to the current produced by the cooper pairs' tunnelling process' when the voltage is zero**.** At zero bias or V=0, a Direct Current flow through the junction, in the absence of an E-field and B-field. The critical current is obtained which is dependent on the following factors: magnetic field, temperature, and shape.

1.8.2 AC Josephson effect: -

In this effect when DC voltage applied across the junctions of superconducting material, then AC supercurrent and normal DC current flows through the junction **[21]**. This AC super current (oscillating current) raised due to the cooper pairs.

1microVolts produces by a DC voltage with ($\omega = \frac{2eV}{\hbar}$)483.6MHZ (high frequency).

1.9 High temperature superconductors:

Those superconducting materials with critical temperature more than 23.2K is identified as High temperature superconductors (HTSC). These two scientists provide great superconductive evidence in a new class of superconducting elements in LaBaCuO ceramic at the Tc of 30K. This marvellous discovery has increase the interest towards superconductivity phenomenon. Then in 1987, "P. W. Chu and M. K. Wu", both of them declared together a disclosure of a 93K superconductor Y-Ba-Cu-O (replacing La by Y). Just after one year in 1988, superconducting cuprates of Bi and Tl based having critical temperatures 110K and 125K respectively were discovered. Then in 1933, Hg-based cuprates having T_C=135K were discovered and their critical temperature increased to 164K. Fig shows the cuprates with different critical temperatures as a function of their time evolution and T_C of other metallic superconducting materials. They depend upon the doping of holes. In 1989, one family of doping of free electrons in cuprates are discovered. Its name was (Nd, Pr and Sm)-Ce-Cu-O. Their maximum critical temperature is $T_{C,\,max}$=24K.

We have used the unconventional high-temperature superconductors which have tetra/orthorhombic perovskite crystal structure having p4m space group. They are highly anisotropic.

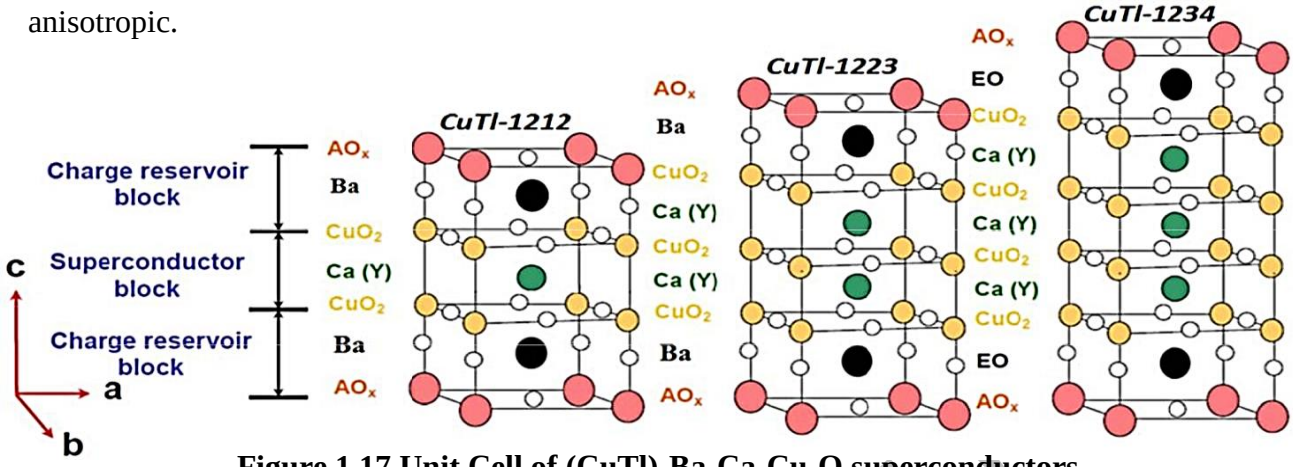

Figure 1.17 Unit Cell of (CuTl)-Ba-Ca-Cu-O superconductors

1.10 Important Applications of Superconductivity: -

In this era, superconducting materials are used mostly in industries and in many research works **[22]**. Some applications of superconductors, due to their properties, are listed below;

- Magnetic shielding
- Magneto cardiogram
- NMR ("nuclear magnetic resonance spectroscopy")
- Magnetic levitation trains
- SQUIDS (stands for superconducting quantum interference devices).
- Logic elements of superconductors
- Very fast computers
- MRI ("magnetic resonance imaging")
- Non-destructive computer chips
- Non-destructive aircrafts
- Magnetic flux detectors
- Single electron transistor
- Mineral prospecting

References:

[1] R. Simon and A. Smith, *Superconductors: Conquering Technology's New Frontier*. New York, NY: Springer, 2013.

[2] Andrei Mourachkine, *High-temperature superconductivity in cuprates: the nonlinear mechanism and tunneling measurements*. Dordrecht; Boston: Kluwer Academic Publishers, 2002.

[3] D. van Delft, "History and significance of the discovery of superconductivity by Kamerlingh Onnes in 1911," *Physica C: Superconductivity*, vol. 479, pp. 30–35, Sep. 2012, doi: 10.1016/j.physc.2012.02.046.

[4] S. O. Pillai, *Solid state physics*. London, Uk: New Academic Science, An Imprint of New Age International (Uk) Ltd, 2018.

[5] W. Meissner and R. Ochsenfeld, "Ein neuer Effekt bei Eintritt der Supraleitf higkeit," *Die Naturwissenschaften*, vol. 21, no. 44, pp. 787–788, Nov. 1933, doi: 10.1007/bf01504252.

[6] J. E. Kunzler, E. Buehler, F. S. L. Hsu, and J. H. Wernick, "Superconductivity inNb3Sn at High Current Density in a Magnetic Field of 88 kgauss," *Physical Review Letters*, vol. 6, no. 3, pp. 89–91, Feb. 1961, doi: 10.1103/physrevlett.6.89.

[7] ŠmidtV. V. and Muller P., *The Physics of superconductors: introduction to fundamentals and applications*. Berlin Springer, 2010.

[8] R. K. Puri and V. K. Babbar, *Solid state physics and electronics*. New Delhi: S. Chand, 2009.

[9] S. O. Pillai, *Solid state physics*. London, Uk: New Academic Science, An Imprint of New Age International (Uk) Ltd, 2018.

[10] "The electromagnetic equations of the superconductor," *Proceedings of the Royal Society of London. Series A - Mathematical and Physical Sciences*, vol. 149, no. 866, pp. 71–88, Mar. 1935, doi: 10.1098/rspa.1935.0048.

[11] J. Bardeen, L. N. Cooper, and J. R. Schrieffer, *Theory of superconductivity*. [Lancaster, Pa.]: [Lancaster Press], 1957.

[12] V. L. Ginzburg and L. D. Landau, "On the Theory of Superconductivity," *On Superconductivity and Superfluidity*, pp. 113–137, doi: 10.1007/978-3-540-68008-6_4.

[13] S. Rajput and S. Chaudhary, "On the Fluctuation Induced Excess Conductivity in Stainless Steel Sheathed MgB_2 Tapes," *Journal of Materials*, vol. 2013, pp. 1–6, Mar. 2013, doi: 10.1155/2013/898607.

[14] S. Rajput and S. Chaudhary, "On the Fluctuation Induced Excess Conductivity in Stainless Steel Sheathed MgB_2 Tapes," *Journal of Materials*, vol. 2013, pp. 1–6, Mar. 2013, doi: 10.1155/2013/898607.

[15] H. Ibach and H. Lüth, *Solid-State Physics: An Introduction to Principles of Materials Science*. Springer Science & Business Media, 2009.

[16] S. Rajput and S. Chaudhary, "On the Fluctuation Induced Excess Conductivity in Stainless Steel Sheathed MgB_2 Tapes," *Journal of Materials*, vol. 2013, pp. 1–6, Mar. 2013, doi: 10.1155/2013/898607.

[17] J. Bardeen, L. N. Cooper, and J. R. Schrieffer, “Microscopic Theory of Superconductivity,” *Physical Review*, vol. 106, no. 1, pp. 162–164, Apr. 1957, doi: 10.1103/physrev.106.162.

[18] H. Ibach and H Lüth, *Solid-state physics: an introduction to principles of materials science*. Berlin; New York: Springer, 2009.

[19] “Quantum Theory of Solids,” *silo.pub*, Dec. 25, 421AD. https://silo.pub/quantum-theory-of-solids-m-2556692.html (accessed Aug. 29, 2022).

[20] B. D. Josephson, *Possible new effects in superconductive tunneling*. [Amsterdam.]: [North-Holland Publishing Company], 1960.

[21] W. Anacker, “Josephson tunneling devices,” *Proceedings of the December 5-7, 1972, fall joint computer conference, part II on - AFIPS ’72 (Fall, part II)*, 1972, doi: 10.1145/1480083.1480171.

[22] B. D. Josephson, “The discovery of tunneling supercurrents,” *Reviews of Modern Physics*, vol. 46, no. 2, pp. 251–254, Apr. 1974, doi: 10.1103/revmodphys.46.251.

[23] D. P. Tunstall and W. Bradford High-temperature *superconductivity*. Boca Raton: CRC Press, 2021.

Chapter:2

Literature Review

2.1 Thallium Based Superconductors

Z. Z. Sheng et al. **[1]** discovered thallium-based superconductors for the very first time in 1988. They investigated a new Tc of above 100K for Tl-Ba-Ca-Cu-O (TBCCO) compounds. They reported that thallium-based superconductor $Tl_2Ca_2Ba_2Cu_3O_{10+y}$ has been shown to exhibit very stable behavior with high critical temperatures.

K. Gopala Krishnan et al. **[2]** prepared the Tl-Ba-Ca-Cu-O superconductor and found its zero resistance for Tc(R=0) of 125K. They found it stable and reproducible. XRD analysis shows that the c-axis decreases with decreasing the temperature from 300K to Tc(R=0). They also described the anisotropic thermopower of $Tl_2Ba_2CaCu_2O_8$ single crystals.

Parkin et al. **[3]** In $Tl_2Ba_2Ca_2Cu_3O_x$ superconductors, got zero resistance critical temperature ranges between 118 and 127 K [6]. They discovered that Tc(R=0) varies with respect to the environment. The $Tl_2Ba_2Ca_2Cu_3O_x$ superconductor has a body-centered tetragonal configuration.

2.2. CuTl-based HTSC Superconductors

Nawazish A. Khan et al. **[4]** prepared the (CuTl1223) $Cu_{0.5}Tl_{0.5}Ba_2Ca_2Cu_3O_{10-\delta}$ superconductor with Mg-doping at the calcium-site,,, to improve interplane coupling . They stated that the Tc(R=0) and [Jc(H=0)] increased by 10K & 2 orders of magnitude, respectively, while the a-axes and c-axes are reduced. Through X-ray diffraction, the main crystal phase of $Cu_{1-x}Tl_xBa_2Ca_{2-y}Mg_yCu_3O_{10-\delta}$ (y=0, 0.5, 1.0, and 1.5) was identified.

Nawazish A. Khan et al **[5]** synthesized the $Cu_{0.5}Tl_{0.5}Ba_2Ca_{n-1-y}Be_yCu_nO_{2n+4-\delta}$ superconductor by adding the Be-doping concentration, at the Calcium site to enhance the interplane coupling. For the synthesization of $Cu_{0.5}Tl_{0.5}Ba_2Ca_{2-y}Be_yCu_3O_{2n+4-\delta}$ (y : 0.7,1.7)and

$Cu_{0.5}Tl_{0.5}Ba_2Ca_{3-y}Be_yCu_4O_{12-\delta}$ (y: 1.5, 2.0), solid-state reaction approach was used. 95K was described as the zero resistance phase transition temperature Tc(R=0). Its crystal structure may be verified using XRD. Based on XRD measurements, Be-doping was used to reduce the cell parameter c-axis and J. Their FTIR results demonstrate a softening of the apical oxygen absorption mode around wavenumber of 500 cm^{-1} and wavenumber 575 cm^{-1} is the mode plane of CuO_2 . They also demonstrate an increase of the inter-plane coupling in superconductors, which is caused by Be's higher electronegativity than Ca's. The magnitude of diamagnetism and the critical-temperature Tc(R=0) were raised.

Nawazish A. Khan et al **[6]** synthesized $Cu_{0.5}Tl_{0.5}Ba_2Ca_2Cu_{3-y}Zny O_{10-\delta}$ (y:0.75,1.5,2.25, 2.65) by solid-state reaction method. XRD analysis shows that this compound has a tetragonal shape. They found that Tc(R=0), magnitude of diamagnetism, and [J_c (H = 0)] are increased with increasing the doping of Zinc in this compound (1223) at Cu-site. They found Tc(R=0) was 121K and Tc(^{onset})

was 127K with increasing the doping concentration of Zinc at the Copper site. Both the Tc(R=0) and magnitude of diamagnetism are increased. By showing that samples of Zn-doped materials that had undergone the post-annealing in air showed the biggest gain in superconducting properties, It was found that the final substance had the best carrier doping in ZnO2 planes. Because the superconducting characteristics of Zn-doped samples are slightly reduced by post-annealing in the presence of oxygen and nitrogen' atmospheres, we have determined that the process of breakage of pairs suggested in earlier studies, entirely lacks in our $Cu_{0.5}Tl_{0.5}Ba_2Ca_2Cu_{0.35}Zn_{2.65}O_{10-d}$ superconductor. This method makes $Cu_{0.5}Tl_{0.5}Ba_2Ca_2Zn_3O_{10-d}$ superconductor highly reproducible.

Nawazish. A. Khan et al. **[7]** synthesized the $Cu_{0.5}Tl_{0.5}Ba_2Ca_{2-y}M_yCu_3O_{10-\delta}$ (M = Mg, Pr) superconductor to enhance the coupling of CuO_2 planes 'J' and this is evidenced by experimental results of XRD, Fourier transform Infrared spectroscopy, Four Probe resistivity method and FIC analysis. They found that the c-axis was decreased, and apical oxygen mode was softened. The Tc(R=0) and Jc(H=0) were enhanced by the Mg-doping in the pure sample. But when Pr was doped to a pure 1223 sample then there was decreased behavior of coupling constant 'J' according to the FTIR results. FTIR results show the hardening of mode Cu (1)–O_A–Cu (2) from 534cm^{-1} to 564 cm^{-1} while the other apical mode of oxygen Tl–O_A–Cu (2) is softened from 485 cm^{-1} to 436 cm^{-1} with increased doping of Pr-concentration.

2.3. Literature about FIC analysis

S. Firdous. et al **[8]** studied the intrinsic parameters of superconductivity on the basis of analysis of excess conductivity for the samples of $YBa_2Cu_3O_{7-\delta}$, $YBa_2Cu_4O_8$,& $Y_2Ba_4Cu_7O_{15-\delta}$) The superior measurements of V_F of the carriers, the c-axis oriented coherence length) and J in the $YBa_2Cu_3O_{7-\delta}$ sample prepared by using $Cu_2(CN)_2$ in comparison with the Synthesization of $YBa_2Cu_3O_{7-\delta}$ sample using CuO.The synthesized $YBa_2Cu_3O_{7-\delta}$ sample using CuO is, however, show the superiority in their B-field characteristics compared with $Cu_2(CN)_2$ synthesized sample, i.e., have large values of Bc0(T) and Bc1(T). The $YBa_2Cu_3O_{7-\delta}$sample has superior B- characteristics of prepared using CuO due to the large density of defects of oxygen that is acting as the microscopic pinning centers. The superiority of $YBa_2Cu_4O_8$ sample over $YBa_2Cu_3O_{7-\delta}$ samples due to their the c-axis coherence length and the V_F of carriers but the reason of the inferiority of, magnetic characteristics is the low number defects(impurities) in double - Cu_2O chains.

For device fabrication, the superiority trend has:

$YBa_2Cu_3O_{7-\delta}$, > $YBa_2Cu_4O_8$, > $Y_2Ba_4Cu_7O_{15-\delta}$, respectively.

Nawazish. A. Khan et al. **[9]** used the solid state reaction technique to create the samples of the single phase $(Tl_{1-y}C_y)$ Ba_2 Ca_3 Cu_4 $O_{12-\delta;}$ (y=0, 0.25, 0.5, 0.75) superconductor. The charge reservoir layer $(Tl_{1-y}C_y)$ Ba_2O_{4-d}'s doping of carbon at the thallium site has been validated by FTIR

absorption studies. The analysis of grain boundaries of the $Tl_{0.75}C_{0.25}$-1234 sample has been improved, as evidenced by the SEM (scanning electron microscope) analysis. In order to attain a large Tc [R=0] and enhanced grain's shape, it was discovered that y :0.25 was the ideal C-doping concentration. The Tc [R=0] of the $(Tl_{1-y}C_y)$ -1234 (y = 0.5 and 0.75) samples decreased, the superconducting transition temperature Tc [R=0] of the $Tl_{0.75}C_{0.25}$-1234 sample has been raised to 100K. However, in all of the carbon-replaced samples, the degree of diamagnetism has been reduced.

G.Hussain.et.al**.[10]c**reated (Ag)x/CuTl1223 (x = 0, 0.5, 1.0, 2.0and 4) wt. %, NanoSuperconductor composites, silver(Ag) nanoparticles were added to $Cu_{0.5}Tl_{0.5}Ba_2Ca_2Cu_3O_{10-\delta}$ (CuTl1223) HTSC superconductor. With increasing concentrations of Ag nanoparticles in the (CuTl1223) phase up to x = 2.0 weight percent, the U (eV)(the activation energy)and Tc (0) rose.The carriers'interaction with the metallic Ag nanoparticles found at the host CuTl1223 superconducting matrix's grain boundaries is most likely what is reasoning behind for that change in U (eV) . It is possible that better intergrain coupling resulted from the addition of metallic Silver-based nanoparticles) at the grain boundaries, which filled the gaps and pores and gradually decreased the resistivity of normal state at 300 K (Ω cm^{-1}). There are two possible mechanisms for the addition of Silver based nanoparticles: the first is the creation of non-superconducting parts, which raises U (eV); the second (dominant) is the enhanced inter-grain connection, which promotes Tc[R=0]. The microscopic characteristics that were derived from the analysis of excess charge carrier's conductivity, such as Jc (0), ξc (0), α etc., explained fully the experimental results.

A. Raza et al. **[11]** used two steps solid-state reaction method at 860 ◦C to prepared the -$Cu_{0.5}Tl_{0.5}Ba_2Ca_2Cu_3O_{10-d}$ and $Cu_{0.5}Tl_{0.5}Ba_2Ca_2Cu_{1.5}M_{1.5}O_{10-d}$ (M: Cd, Zn, and Ni) samples . The XRD analysis shows that the above samples show orthorhombic crystal structure which has the enhancement of unit-cell volume by increasing the concentration of M (dopant atoms). The Tc(R=0) and onset temperature T_c^{onsett} are decreased in case of adding the Cd in the pure samples while Tc(R=0) and onset temperature T_c^{onsett} are enhanced with adding the Ni and Zn doping. In FTIR measurements, there was hardening of Tl–O–Cu (2) mode by the addition of (M = Cd, Zn, and Ni) atoms. In FIC (fluctuation-induced conductivity), the V_F of carriers , ξc (0) , and the J with the Cd-doping , are decreased, whereas with doping of zinc and nickel these parameters are increased. There has been induction of enhancement of some flux pinning characters which are Bc_0 (T), Bc_1 (T), and J_c (0) with Cadmium-concentration doping but these values are decreased in Ni and Zn-doped samples. GL's parameter 'κ' and the penetration depth (λp.d) of B-field are suppressed that is observed in Cadmium-doped samples. Cadmium-doping samples show that superconductivity is weakened by reducing the energy needed to split down the Cooper pairs. These studies demonstrate that the solid-state medium's anharmonic oscillations are caused by doped Cd atoms and that these oscillations decrease the phonons' density and, in turn, the Cooper pairs' density, highlighting the significance of interaction of electron-phonon in the process of HTSC superconductivity.

Nawazish. A. Khan et al**. [12]** investigated the excess conductivity (FIC) in $Cu_{0.5}Tl_{0.5}Ba_2Ca_{n1}Cu_nO_{2n+4}$ thin film samples (n = 2, 3, 4) has been studied. The c-axis-oriented thin films have exhibited a tetragonal structure where the samples' Tc (R = 0) rises the CuO2 planes, with an increasing number (n). An FIC analysis is performed using the Ginzburg-Landau and the Aslamazov-Larkin theory critical regimes number. The Ginzburg-Landau theory is used and has determined critical superconducting variables. Although the values of ξc (0), V_F, and $\tau\phi$ rise but their coupling constant J of CuO2 conducting planes is reduced with more CuO2 planes present in these samples. The $\lambda_{p.d}$, nevertheless, is reduced, while Bc(T), Bc1(T), values and Jc(0) grow as n conducting planes in $Cu_{0.5}Tl_{0.5}Ba_2Ca_{n1}Cu_nO_{2n+4}$ (n = 2, 3,4) rise. This shows how flux pinning has increased which is most probably caused by deficiencies of thallium in the characteristics of the layer that stores charge.

2.4. Literature about Dielectric Properties

Nawazish. A. Khan et al. **[13]** examined, the diectric-properties of $Cu_{0.5}Tl_{0.5}Ba_2Ca_2Cu_{3-y}Zn_yO_{10-\delta;}$(for y:0-2.5) samples. The T_c is enhanced and the diamagnetism was observed. The negative capacitance was observed at low frequency because of the reduction in the sample capacitance to the negative values from its geometrical capacitance (without sample). It's due to positive charges that started gathering near electrodes and so displaced the mobile charge from their mean position resulting in the generation of dipolar capacitance. The real and imaginary dielectric constant most probably resulted from the polarization due to mobile charges displacement in ZnO_2/CuO_2 conducting plane from the mean position. The enhanced values of these constants by increasing Zn content due to enhanced carrier concentration of conducting planes that increased polarization density. These results strongly suggested the importance of mobile carrier's in conducting planes to determine certain capacitance values. The atoms' polarizability and subsequently their dielectric constants may be improved by the less thermal agitation at 79 K (ε', ε''). Our $Cu_{0.5}Tl_{0.5}Ba_2Ca_2Cu_{3-y}Zn_yO_{10-\delta}$ material shows greater ac-conductivity and smaller losses at 290 and 79 K when compared to the dielectric characteristics of $Tl_2Ba_2Ca_2Cu_2O_x$. Since the $Cu_{0.5}Tl_{0.5}Ba_2O_{4-\delta}$ CRL has localized-charges at the Ba^{+2}, Tl^{+3}, and Cu^{+2} sites while the conducting CuO_2/ZnO_2 planes carry mobile charge "carriers" that are displaced from their fixed mean-point(distorted), by an externally applied frequency, as indicated by the decreased values of dielectric loss with rise of Zinc doping. The polarization is most likely caused by the separate the charges into these two planes. There is also a probability that this material will be used in practical applications.

M. Mumtaz et al. **[14]** worked on $Cu_{0.5}Tl_{0.5}Ba_2Ca_3(Cu_{4-y}Cd_y)O_{12-\delta}$ (y:0,0.25,0.5 and 0.75) and their real dielectric constant was described. The ε' is used to store the amount of energy that is in the superconducting material when the sample is subjected to a field is known as ε'. From the negative capacitance, it is possible to determine the negative values of ε' (real dielectric constant) (a term that shows a decrease in capacitance of a superconducting sample from geometric capacitance without superconducting sample). And the development of positive charges close to the electrodes is the cause of this. These charges are most likely to be concentrated at the device's outer layer due to the flow of negative charges toward the electrodes. Ceramics have high fermi energy levels, making it possible for electrons to move from these ceramics to metal surfaces. Within the samples,

the low-frequency region exhibits negative capacitance. Each material has a different cause for negative capacitance, which is a microscopic physical phenomenon linked to the capture of charge carriers, contact injection, and impact of space charges. They clarified how the imaginary part causes energy to be suppressed and absorbed along surfaces (grain boundaries, localized charge densities, and localized defects). There is a loss of real, imaginary constants & ac-conductivity of dielectric medium properties but the dielectric loss 'tanδ' is increased. While these are enhanced after post-annealing due to consumption of oxygen. The dielectric constants decrease and tanδ increases at normal-state (300 K) due to higher thermal tension and decreased polarization, which is the opposite at lower temperatures. The working frequency and temperature of the externally applied ac-field have a significant impact on these samples. The post-annealing in the presence of O_2 may vary, the oxygen content of the compound's structures and alter the carrier density, it can also control a material's dielectric behavior. On the second side, this process may alter the materials' inter-grain connection, which may impact the material's dielectric characteristics. They came to the conclusion that post-annealing in oxygen caused dielectric loss to increase in all samples.

Nawazish. Ali. Khan et al. **[15]** considered the effect of Zn doping on $Cu_{0.5}Tl_{0.5}Ba_2Ca_2Cu_{3-x}Zn_xO_{10-\delta}$ (y: 0, 1.0, 1.5, 2.0, 2.5) samples. They used solid-state reaction method having two steps to create their sample in the shape of pellets. They used the mutual inductance method, the LCR meter and the four-probe method to characterize their sample, measuring its resistivity, ac susceptibility, and dielectric properties. The tanδ losses, ac conductivity, and real and imaginary dielectric components are all included in the dielectric measurement. With increasing the concentration of Zinc doping, a rise in the zero resistivity critical temperature systematically as seen through measurements of resistivity and ac susceptibility, which in turn improved the diamagnetic character of their samples. The dielectric response was studied over the range of the frequency of (10K - 10M) Hz, and it was discovered that at lower frequencies (10 kHz), the real component of the dielectric was enhanced by an increase in Zn concentration, which resulted in a decrease in tanδ loss at both 79 K and room temperature. They argue that rise in charge carrier concentration, which results in enhancement of polarization density, is the cause of the real component of the dielectric parameter's improvement. The (ε'') of dielectric-constant was observed to be suppressed by increasing frequency and the temperature at 79 K and at room temperature. In contrast, the decreasing behavior seen with increasing doping concentration of zinc, most likely, caused by Zn's lower conductance because its filled $3d^{10}$ shell leads to large band-energy gap of semiconductors rather than metallic Cu. The dielectric response was measured for the range (10K–10 M) Hz of frequencies and found that the lower frequency (10 kHz) real part of the dielectric enhanced with increasing concentration of Zn which leads to a decrease in tanδ loss at 79 K as well as at room temperature. They argue that enhancement in the real part of the dielectric parameter is due to increasing concentration of charge-carriers that leads to an enhanced density of polarization. They reported the suppression of the ε'' with increasing frequency at 79 K and at 300K. On the other hand, the decreasing behavior was also reported with increasing Zn doping probably due to lower value of G(conductance) of Zinc, due to filled shell of $3d^{10}$ leading to large band energy gap of

semiconductor, as compared to metallic Cu having partially filled $3d^9$ shell. The ac conductivity shows an increasing trend at frequency up to 2 MHz with Zn doping reflected enhanced charge carrier. But at greater than 2 MHz they observed that conductivity leads to normal state value.

2.5. Metals-doped 1223 superconductors

T. Aytug et al. **[16]** experienced both Na-doped and un-doped Hg-1223 phases of low-temperature oxygen annealing. By altering the oxygen content of the Hg-O layer, it is hypothesized that Na could disturb the material's electronic band structure, which might then have an impact on the superconductivity of the material after annealing. It has been discovered that by annealing at a temperature of 300 °C for 10 hours, Tc can be raised by more than 20 K, however annealing at temperatures higher than 350 °C results in superconductivity loss because of Hg loss. Up to 400°C, the normal state- starts to diminish as annealing temperatures rise. Additionally, the normal state-curves of the doped samples flattened, indicating a more insulating characteristic.

Nawazish.Ali. Khan et al. **[17]** Two-step solid-state reactions were used to prepare $Cu_{0.5}Tl_{0.5}Ba_2(Ca_{2-x}Be_x)$ (Cu_2Ti) O_{10-d} (x=0, 0.5, and 1.0) samples. After adding the concentration of Be at Calcium site of above given compound, superconducting characteristics were reduced. According to the atomic masses of Titanium (47.90 a.m. u) and Copper (63.54 a.m.u) in conducting CuO_2 plane, oxygen phonon modes varied following Be doping. The decrease value of Cooper pairs' density (arise due to an-harmonic oscillations), below a required level of optimum superconductivity, responsible for the loss in microscopic superconducting parameters that was deduced from the analysis of excess charge carrier conductivity.

Nawazish.Ali. Khan et al. **[18]** investigated Cobalt-doped $Cu_{0.5}Tl_{0.5}Ba_2Ca_2Cu_{3x}Co_xO_{10-d}$ (x=0, 0.05, 0.1, 0.5) superconductor for the most likely reasons of decrease of the values of superconducting properties, such as Tc(R=0), B=0, etc. The research has shown that increase of doping of cobalt at Copper-site in the superconducting conducting CuO_2 planes somehow localizes the charge carriers at cobalt site and reduces the mobile carriers' density. We doped Li at Tl sites in $Cu_{0.5}Tl_{0.5}Ba_2O_4$ CRL to generate an effective carrier doping $(Cu_{0.5}Tl_{0.25}Li_{0.25})Ba_2O_{4-d}$ CRL of $(Cu_{0.5}Tl_{0.25}Li_{0.25})Ba_2Ca_2$ $Cu_{3x}Co_xO_{10-d}$ compound since it is known that alkali metals lose their outermost "s-orbital" electron quickly, which may be provided to the planes of CuO_2. The resulting compound has better superconducting qualities because of the superconducting conducting planes of CuO_2' free charge carrier density.

Nawazish. Ali. Khan et al. **[19]** examined the method of doping the CuO_2 planes in the $Cu_{0.5}Tl_{0.5}Ba_2Ca_2Cu_3O_{10-d}$ superconductor with Na deposition at the $Cu_{0.5}Tl_{0.5}Ba_2O_{4-d}$ CRL for the first time. With doping of Sodium, the diamagnetism' magnitude and the critical-temperature Tc[R=0] for zero resistance are both raised. However, these superconducting properties are suppressed in the sodium-based compounds doping with Magnesium and Beryllium. According to X-ray diffraction analysis, it becomes clear that there is shortage of c-axes with Magnesium and Beryllium doping concentration increase ' J' to the point that carriers begin to repel one another, potentially suppressing the superconducting characteristics. Na-doped samples that have undergone

self-doping have displayed improved superconducting parameters; this was most likely made possible by optimized the charge carriers in the CuO_2 planes.

S.H. Safeer et al. **[20]** compared the $Cu_{0.5}Tl_{0.5}Ba_2(CaMg)Cu_3O_{10-d}$ and $Cu_{0.5}Tl_{0.5}Ba_2(CaMg)Cu_{1.5}M_{1.5}O_{10-d}$ (M: Zn, Ni)-doped samples in terms of their superconducting characteristics. Finding out how electron-phonon interactions contribute to the high-temperature superconductivity mechanism in these oxide superconductors was our main goal. By adding Zn and Ni dopants to the Cu sites in this molecule, we were able to indirectly achieve our goal. Due to the difference in their masses, Zn/Ni atoms replaced Cu and caused an-harmonic oscillations. The closer proximity of the conducting CuO_2/MO_2 (M: Zn, Ni) planes increased the impact of an-harmonic vibrations. When Zn and Ni atoms were doped into a material, the magnitude of diamagnetism was suppressed, on comparing the zero-field-cooled (ZFC)' magnetic moments with the field-cooled (FC)' magnetic moments. They postulated that the doped atoms' lower atomic mass than Cu atoms is what causes the magnetic moments to be suppressed. Magnetic hysteresis loops' critical current density and width are suppressed using Zn and Ni doping. The enormous anharmonic oscillations caused by these reduced values in the doped samples reduces the population of phonons which is main requirement for the process of interactions of electrons with phonons.

R. Awad et al. **[21]** prepared $TlBa2Ca2\text{-}xNaxCu_3O_{9-\delta}$; with $0 \leq x \leq 0.4$. As the Na-content rises, the lattice parameters expand. As x grows from 0 to 0.05, the Tc has been seen to slightly increase before steadily declining for x greater than 0.05. This finding was explained by the evidence that Na changed the (Tl-1223) phase from an overdoped regime to an underdoped regime, which is consistent with the thermos-power data, which showed a transition from (overdoped regime) to a (underdoped regime). Ac magnetic susceptibility experiments have also reported the inter-grain Jc (critical current density) as a function of Na.

J. Z. Wu et al. **[22]** found Hg-based superconductors (HgBa2Can-1 CunO2n+2+8, n=l-4) has recently to exhibit superconductivity above 130 K. The greatest superconducting transition temperature (Tc) has been determined to be 135K for ambient pressure and > 160K for hydrostatic pressure for Hg-1223. Finding alternate methods, such chemical doping, to raise the Tc of the Hg-1223 phase is interesting since greater Tc means higher operation temperature for a superconducting device. On the other hand, manufacturing of high-quality thin films of Hg-1223 is required in order to utilize this material effectively in a variety of microelectronic devices. However, the severe film/substrate interface reaction brought on by the high processing temperature Ts > 860 °C required for pure Hg-1223 can occur during the formation of the Hg-1223 thin film. Thus, lowering the processing temperature is required to produce high-quality Hg-1223 thin on a variety of substrates that work with current technology. Alkali doping has been shown to raise Tc in Bi-based cuprates by up to 10K and decrease Ts by more than 100 °C. It should be noted that other high Tc superconductors have not shown these effects, and it is not known whether or not the dopants enter the lattice. Studying the impact of alkali doping in the Hg-based Cuprate system is thus important.

References:

[1] Z. Z. Sheng and A. M. Hermann, "Bulk superconductivity at 120 K in the Tl–Ca/Ba–Cu–O system," *Nature*, vol. 332, no. 6160, pp. 138–139, Mar. 1988, doi: 10.1038/332138a0.

[2] K. Gopala Krishnan, P. V. P. S. S. Sastry, K. Gangadharan, G. M. Phatak, J. V. Yakhmi, and R. M. Iyer, "Synthesis and properties of a 125 K superconductor in the Tl-Ca-Ba-Cu-O system," *Applied Physics Letters*, vol. 53, no. 5, pp. 414–416, Aug. 1988, doi: 10.1063/1.100606.

[3] S. S. P. Parkin *et al.*, "Bulk Superconductivity at 125 K in $Tl_2Ca_2Ba_2Cu_3O_x$" *Ten Years of Superconductivity: 1980–1990*, pp. 309–312, 1988, doi: 10.1007/978-94-011-1622-0_44.

[4] N. A. Khan and A. A. Khurram, "Enhanced superconducting properties of $Cu_{1-x}Tl_xBa_2Ca_{2-y}Mg_yCu_3O_{10-\delta}$ (y=0, 0.5, 1.0, and 1.5)," *Applied Physics Letters*, vol. 86, no. 15, p. 152502, Apr. 2005, doi: 10.1063/1.1899254.

[5] N. A Khan, G. Husnain, and K. Sabeeh, "Superconductivity in Be substituted by Ca in $Cu_{0.5}Tl_{0.5}Ba_2Ca_{n-1-y}Be_yCunO_{2n+4-\delta}$ (n= 3, 4 and y= 0.7, 1.5, 1.7, 2.0)," *scholar.google.com.pk*, Apr. 01, 2006.

[6] N. A. Khan and M. Mumtaz, "A new $Cu_{0.5}Tl_{0.5}Ba_2Ca_2Cu_{3-y}Zn_yO_{10-\delta}$high-temperature superconductor with three ZnO_2planes," *Superconductor Science and Technology*, vol. 19, no. 8, pp. 762–766, Jun. 2006, doi: 10.1088/0953-2048/19/8/012.

[7] N. A Khan, A. Javaid, A. Khurram, and N. Haider, "The study of inter-plane coupling in $Cu_{0.5}Tl_{0.5}Ba_2Ca_2Cu_3O_{10-\delta}$ superconductor by Mg and Pr substitution at Ca site," *scholar.google.com.pk*, Sep. 15, 2006.

[8] S. F. Akhtar, N. A. Khan, and S. H. Safeer, "Excess Conductivity Analysis of Y-Ba-Cu–O Superconductor Phases," *Journal of Low-Temperature Physics*, vol. 206, no. 1, pp. 106–119, Jan. 2022, doi: 10.1007/s10909-021-02629-0.

[9] N. A. Khan and S. Ahmad, "Para-conductivity and critical regime of $(Tl_{1-x}C_x)Ba_2Ca_3Cu_4O_{12-\delta}$ superconductors," *Journal of Applied Physics*, vol. 112, no. 3, p. 033912, Aug. 2012, doi: 10.1063/1.4740238.

[10] G. Hussain *et al.*, "Activation energy and excess conductivity analysis of (Ag)x/CuTl-1223 nano-superconductor composites," *Journal of Applied Physics*, vol. 116, no. 10, p. 103911, Sep. 2014, doi: 10.1063/1.4895051.

[11] A. Raza, S. H. Safeer, and N. A. Khan, "The Role of Mass of Doped Atoms in the Superconductivity of $Cu_{0.5}Tl_{0.5}Ba_2Ca_2Cu_3O10-d$ and $Cu_{0.5}Tl_{0.5}Ba_2Ca_2Cu_{1.5}M_{1.5}O_{10-d}$ (M = Cd, Zn, and Ni)," *Journal of Superconductivity and Novel Magnetism*, vol. 30, no. 5, pp. 1153–1160, Dec. 2016, doi: 10.1007/s10948-016-3922-3.

[12] N. A. Khan, S. H. Safeer, M. Rahim, M. N. Khan, and N. Hassan, "Excess Conductivity Analysis of $Cu_{0.5}Tl_{0.5}Ba_2Ca_{n-1}Cu_nO_{2n+4-\delta}$ (n = 2, 3, 4) Thin Films," *Journal of Superconductivity and Novel Magnetism*, vol. 30, no. 6, pp. 1493–1498, Dec. 2016, doi: 10.1007/s10948-016-3942-z.

[13] N. A. Khan, M. Mumtaz, and A. A. Khurram, "Frequency-dependent dielectric properties of $Cu_{0.5}Tl_{0.5}Ba_2Ca_2Cu_{3-y}Zn_yO_{10-\delta}$ (y=0, 1.0, 1.5,2.0, 2.5) superconductors," *Journal of Applied Physics*, vol. 104, no. 3, p. 033916, Aug. 2008, doi: 10.1063/1.2967823.
[14] M. Mumtaz, M. Rahim, N. A. Khan, K. Nadeem, and K. Shehzad, "Dielectric properties of oxygen post-annealed $Cu_{0.5}Tl_{0.5}Ba_2Ca_3(Cu_{4-y}Cd_y)O_{12-\delta}$ bulk superconductor," *Ceramics International*, vol. 39, no. 8, pp. 9591–9598, Dec. 2013, doi: 10.1016/j.ceramint.2013.05.078.
[15] N. A. Khan, M. Mumtaz, and A. A. Khurram, "Frequency-dependent dielectric properties of $Cu_{0.5}Tl_{0.5}Ba_2Ca_2Cu_{3-y}Zn_yO_{10-\delta}$ (y=0, 1.0, 1.5,2.0, 2.5) superconductors," *Journal of Applied Physics*, vol. 104, no. 3, p. 033916, Aug. 2008, doi: 10.1063/1.2967823.
[16] T. Aytug, A. A. Gapud, S. H. Yoo, B. W. Kang, S. D. Gapud, and J. Z. Wu, "Effect of sodium doping on the oxygen distribution of Hg-1223 superconductors," *Physica C: Superconductivity*, vol. 313, no. 1–2, pp. 121–126, Feb. 1999, doi: 10.1016/s0921-4534(98)00699-6.

[17] N. A. Khan, M. A. Rafique, M. Mumtaz, and G. Hussain, "Investigation on Critical Regime of $Cu_{0.5}Tl_{0.5}Ba_2(Ca_{2-x}\ Be_x)(Cu_2Ti)O_{10-\delta}$ Superconductor via Excess Conductivity Analysis," *Journal of Superconductivity and Novel Magnetism*, vol. 28, no. 11, pp. 3243–3248, Aug. 2015, doi: 10.1007/s10948-015-3185-4.

[18] N. A. Khan, M. Mumtaz, A. Ullah, N. Hassan, and A. A. Khurram, "Suppression of Tc in Co-doped $(Cu_{0.5}Tl_{0.5})\ Ba_2Ca_2Cu_{3-x}Co_xO_{10-\delta}$ superconductor," *Journal of Alloys and Compounds*, vol. 507, no. 1, pp. 142–145, Sep. 2010, doi: 10.1016/j.jallcom.2010.07.141.

[19] N. A. Khan and S. Hussain, "Enhanced superconductivity by Na doping in $(Cu_{0.5}Tl_{0.25}Na_{0.25})Ba_2Ca_2Cu_3O10-\delta$," *Journal of Alloys and Compounds*, vol. 475, no. 1–2, pp. 652–657, May 2009, doi: 10.1016/j.jallcom.2008.07.091.

[20] S. H. Safeer, A. Raza, N. A. Khan, and M. N. Khan, "Suppression of Superconductivity by Anharmonic Oscillations in Zn- or Ni-doped $Cu_{0.5}Tl_{0.5}Ba_2(CaMg)Cu_{1.5}M_{1.5}O_{10-\delta}$ (M=Zn, Ni) Superconductors; Evident by Magnetic Measurements," *Journal of Electronic Materials*, vol. 50, no. 11, pp. 6518–6524, Sep. 2021, doi: 10.1007/s11664-021-09195-x.

[21] R. Awad, A. I. Abou-Aly, S. Isber, and W. Malaeb, "Effect of the partial replacement of Ca by alkaline element Na on Tl-1223 superconductor," *Journal of Physics: Conference Series*, vol. 43, pp. 474–479, Jun. 2006, doi: 10.1088/1742-6596/43/1/118.
[22] J. Z. Wu, "Superconductivity in lithium- and sodium-doped mercury-based cuprates," *risweb.st-andrews.ac.uk*, 1998.

Chapter:3

Preparation of Sample & Experimental Techniques

A brief explanation of the techniques required to make thallium-based high-temperature superconductors explained in this chapter. A variety of methods were used to analyze the characteristics of superconducting samples.

3.1 Preparation of Samples:

The solid-state reaction approach **[1]** helps to prepare the superconducting sample $Cu_{0.5}Tl_{0.5}Ba_2Ca_2Cu_3O_{10-y}$ series $Cu_{0.5}Tl_{0.5}Ba_2Ca_2(Cu_{3-x}Na_x)O_{10-y}$ for (x=0,1,2,2.5,3) and $Cu_{0.5}Tl_{0.5}Ba_2CaMg(Cu_{3-x}Na_x)O_{10-y}$ for (x=0,1,2, 3).

The following chemicals are used to make the above samples: -

For $Cu_{0.5}Tl_{0.5}Ba_2Ca_2(Cu_{3-x}Na_x)O_{10-y}$ for (x=0,1,2,2.5,3): -

- CuCN
- $CaCO_3$
- $BaCO_3$
- Na_2CO_3
- Tl_2O_3

For $Cu_{0.5}Tl_{0.5}Ba_2CaMg(Cu_{3-x}Na_x)O_{10-y}$ for (x=0,1,2, 3): -

- $Cu_2CN_2+H_2O$
- $CaCO_3$
- $Ba(NO_3)_2$
- MgO
- Na_2CO_3
- Tl_2O_3

Using a mortar and pestle, these substances were thoroughly mixed and ground for an hour in accordance with their chemical formulae and in the correct ratios. The mixture was subsequently exposed to a 24-hour quartz boat firing at 860°C. Then, it is left there to gradually cool to T_{room}(300K) . The obtained product is then re-ground for 1 hour and heated for a further 24 hours in the same conditions using an alumina boat. Our precursor material $Cu_{0.5}Tl_{0.5}Ba_2Ca_2(Cu_{3-x}Na_x)O_{10-y}$ / $Cu_{0.5}Tl_{0.5}Ba_2CaMg(Cu_{3-x}Na_x)O_{10-y}$ was now available. We then ground the precursor material for 45 minutes in an agate mortar and pestle after mixing it with Tl_2O_3 in the proper proportions. The pressure of 5 tons/cm^2 was applied to a hydraulic press

to create a pellet of this mixed precursor. The pellet was covered in gold foil for sintering and heated for about 10 minutes to 860^0C before being cooled to T_{room}(300K)., to produce the stable form of 1223.

3.2 Characterizations: -

In order to characterize the synthesized samples, the following methods were used:

- X-rays diffraction
- Four Probe DC-resistivity measurements
- Two Probe Dielectric measurements and AC conductivity
- Fourier Transform Infrared Spectroscopy (FTIR)
- Fluctuation-induced conductivity(FIC)

3.2.1 X-ray diffraction(XRD):

The information about the crystalline nature and structure of the substance is discovered using the X-ray diffraction (XRD) technique **[2]**. This study is performed to determine whether the material is crystalline or not and to determine the crystal lattice cell parameter, and phase of crystals. The electromagnetic radiations with a short wavelength are known as X-rays (0.01 to 10 nm). The size of the material's atoms must be similar to the wavelength of X-Rays. In general, it is impossible to create a well-diffraction grating that can satisfy X-ray diffraction requirements. As a result, the distance between crystal lattice atoms is nearly equivalent to the wavelength of X-rays. Because the crystal naturally has a grating, it can be used for diffraction. Understanding a material's crystal structure is the most important aspect of material science. The most common materials used to create X-rays of wavelengths about 1.54 and 0.8, respectively, are Cu or Mo **[3-4]**. Bragg was the first researcher to suggest that crystalline materials could cause X-rays to be diffracted.

The energy of an X-ray photon is,

$$E = h\vartheta \quad (3.1)$$

Or

$$E = hc/\lambda \quad (3.2)$$

If λ =0.0998nm, as hc= 1240 eV.nm

$$E = 12.42 \text{ Kev} \quad (3.3)$$

The majority of traditional techniques for analyzing indeterminate 3D objects are based on the fact that X-rays with a range of energy of 10 and 100 keV may easily penetrate below the crystal.

3.2.1.1 Working Principle:

Bragg's law: - The law that is used to explain the diffraction of X-rays through crystalline material is known as Bragg's law.

"William Henry(WH) Bragg" and his son "William Lawrence(WL) Bragg were the first to suggest X-ray diffraction **[5]**. They observed that crystalline materials produced strong reflections

at certain wavelengths and λ at starting angles. Though their wavelength should be equivalent to the inner distance of atoms, Bragg's law can be used for both electron and neutron diffraction. The crystal has a regular arrangement of atoms in a pattern with interatomic spacing that is comparable to the wavelength of X-rays, acting as a perfect three-dimensional diffraction grating as a result.

The most common materials utilized are Cu or Mo to create X-rays with 1.54 and 0.8 values of λ, because these two X-ray sources create intense beams with 0.8 and 1.5 micron wavelengths, respectively.

The distance spanned by two parallel X-ray beams must be an integral multiple of λ being used for the diffraction of X-rays from the crystal, which is made up of parallel planes. This phenomenon is referred to as Bragg's law.

An incident ray makes an angle θ with a crystal plane. For the path difference 'd' of these two X-rays,

path difference = AB + BC, AB = dsinθ, BC = dsinθ

So path differences = 2dsinθ

These reflected rays constructively interfere and bright spots are visible on the photographic plate used as a screen. These rays are in phase because the optical path difference is an integer multiple of the wavelength, and 2dsinθ is the condition for constructive interference **[6]**.

Therefore,

$$2d\sin\theta = n\lambda \text{(Bragg's law)} \qquad (3.4)$$

where 'λ' shows the wave-length of the incident light and 'n' is a positive integer (n=1, 2, 3…). If the λ of the incident X-ray is known, the internal distance can be obtained. Bragg's law thus formed the basis of the study of crystal structure called X-ray crystallography.

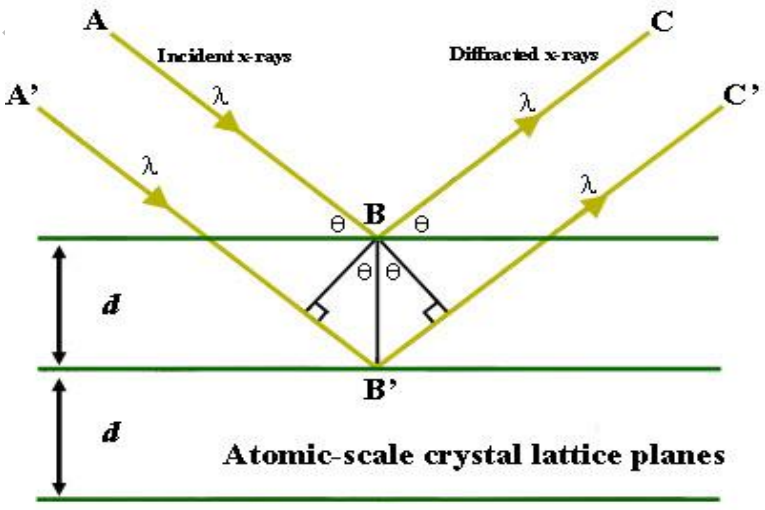

Fig 3.1 The Bragg's Law

The foundation of X-ray crystallography was created by crystal structure analysis using Bragg's Law.

3.2.1.2 Methods of X-rays: -

- Laue method
- Rotating Crystal method
- Powder method

3.2.1.3 Working: -

XRD analysis is now being used to characterize the earlier generated samples. We used a Bruker D8 Focus XRD machine. It utilizes the powder diffraction technique. Cu is employed as an X-ray source with 1.5406Å wavelength k_α lines. The utilized range for "2θ" is 4-60°. 0.3seconds each step was the fixed scan speed. A computer system collects diffraction data. The sample in an X-ray diffractometer is supported by a smooth plate in such a way that it can rotate about an axis that is perpendicular to the paper's surface. By passing the beams from a slit within an X-ray tube, monochromatic X-rays are created. When a specimen is in the path of the beam, diffraction occurs. With a counter, beam intensities that are diffracted can be seen. Specimen and counter are the sources of X-rays in the same plane. The counter has a rotational axis. The counter's angular position is expressed in terms of 2θ. The counter and the sample are set up so that if the sample rotates through an angle, the counter rotates through 2θ as a result. As a result, both the incidence angle and the reflection angle are kept constant. Intensity is measured as a function of 2θ as long as the counter's angular velocity is constant. In order to determine the specimen's crystal arrangement, the diffractometer's data is reviewed. Check cell, a piece of computer software is used to identify the crystal arrangement and determine the matrix parameters.

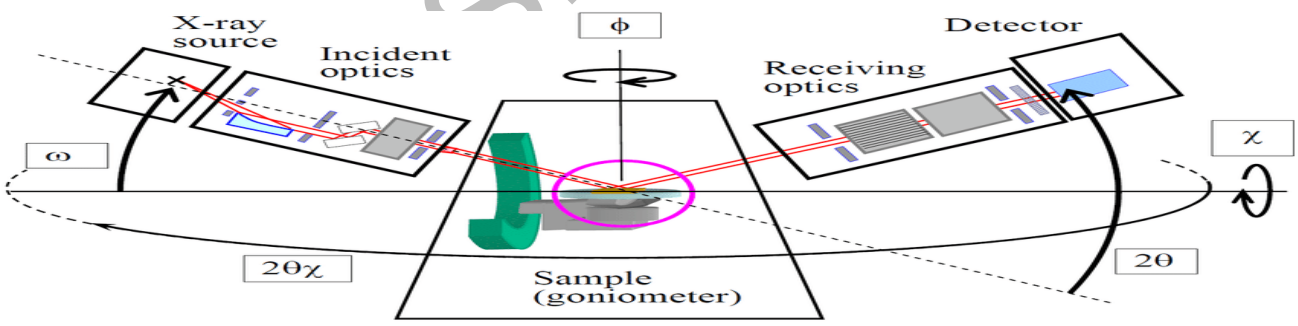

Fig 3.2 XRD's Working

3.2.2 Electrical resistivity:

Resistance refers to obstructions to the movement of charges. The measure of a material's resistance to electrical conduction at a certain size is referred as resistivity. Resistivity can alternatively be referred to as volume resistivity or specific electrical resistance, even though these terms are less prominent. All materials work against the flow of electricity, even if some are more effective at carrying electrical current than others. The resistivity is a measure that makes it possible to compare the degree to which various materials permit or hinder the flow of electricity.

There are two main causes of having electrical resistivity, which is following as:

- Average Collision Time
- Temperature

3.2.2.1 Average Collision Time: -The sample's applied external electric field accelerates the atoms' electrons, which causes them to begin colliding with the atoms. Therefore, this is the resistance that atoms give to the flow of electrons.

The formula for resistivity is:

$$\rho = \frac{m}{n\tau e^2} \qquad (3.5)$$

Electrons may potentially encounter lattice collisions in addition to atomic resistance. The total resistivity is therefore

$$\rho = \rho_i + \rho_{ph} \qquad (3.6)$$

Where 'ρ_i' is the residual resistivity, which does not depend upon the temperature, and 'ρ_{ph}' is the ideal resistivity, which is temperature dependent.

In equation (3.5), "n" is the number density, "τ" is the average-time between collisions, and "$1/\tau$" is chance of an electron collision (scattering) per unit time. Every crystal contains flaws, as we all know. Therefore, as electrons are flowing, they may collide with lattice phonons. In this way , the total probability of an electron colliding (scattering) is equal to the sum of the electron scattering caused by phonons $\frac{1}{\tau_{ph}}$and lattice defects $\frac{1}{\tau_i}$.

$$\frac{1}{\tau} = \frac{1}{\tau_{ph}} + \frac{1}{\tau_i} \qquad (3.7)$$

We already know that different substances can scatter electrons in a variety of ways, including phonon scattering, electron scattering via defects, and electron scattering via impurities. These scattering mechanisms lead to the development of resistivity. The total resistivity of the compound is equal to the sum of these separate reasons, according to Mathieson's rule.

The formula is

$$\rho_{phonon} = \rho_{defect} + \rho_{impurity} + \rho_{boundary} \qquad (3.8)$$

In which ρ_{phonon} shows the resistivity of electron-scattering via phonons, ρ_{defect} shows the resistivity of electron-defect scattering, $\rho_{impurity}$ shows the resistivity of electron scattering through impurities, and $\rho_{boundary}$ is the resistivity that results from electron scattering at the material's boundary. Residual resistivity is the collective name for the final three temperature-independent variables in equation (3.8). Despite the fact that the first part in equation (3.8) depends on temperature **[7]**.

3.2.2.2 Temperature: -

The resistance provided by atoms to the electrons increases as the temperature of a superconducting sample rises because more electrons are colliding with them. Conversely, as the

temperature drops, the number of collisions decreases and the resistance diminishes. For alkali metals, the temperature-dependent resistivity, also known as the ideal resistivity due to phonons, is confirmed to be of the order of T^5. The mean square amplitude of phonons depends upon temperature for resistivity in simple metals at high temperatures.

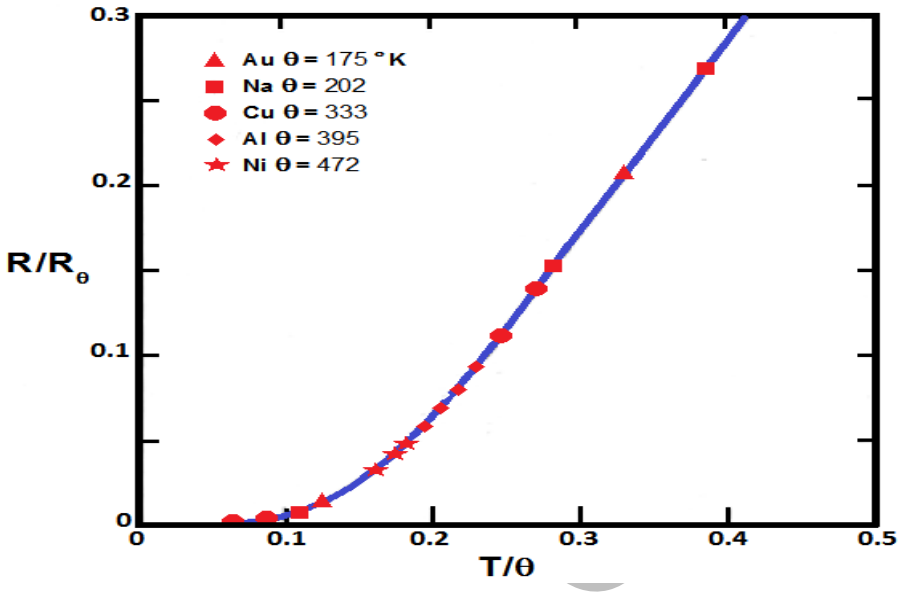

Fig. 3.3: The phonon contribution to the resistivity in normal metals.

3.2.2.3 The DC Measurements of Electrical Resistivity:

The critical temperature Tc of superconductors can be determined using DC electrical resistivity, which also aids in the analysis of other superconducting and normal state properties. The "four-probe method," which is based on "Ohm's law," is used to determine the DC electrical resistivity.

$$V = IR \qquad (3.8a)$$

'I' stands for applied current and 'V' for the applied voltage.

'R' is the resistance, and its experimental dependence on the conductor's length and surface area is as follows:

$$R \propto L$$

$$R \propto 1/A$$

Temperature affects resistivity, which can be expressed as

$$R \propto L/A$$

$$R(T) = \rho\,(T)\frac{L}{A} \qquad (3.9)$$

$$\rho(T) = R(T)\frac{A}{L} \qquad (3.10)$$

according to Ohm's Law.

$$R(T) = \frac{V}{I}$$

So equation (3.10) becomes $$\rho(T) = \frac{VA}{IL} \quad (3.11)$$

The SI symbol for resistivity is "Ω-m".

3.2.2.4 Working:

We used pallet-form samples to measure resistivity. Two methods:

- Two Probe method
- Four Probe method

3.2.2.5 Four Probe method: -

This method is preferable for HTSC (high-temperature superconductors) as we used it for the calculations of the resistivity of conductors, superconductors, and semiconductors. But two probe method is used for conductors as it measures the resistance in a few ohms. Four connections were made at the flat surface of the superconducting material in this occurrence. By applying silver paste to the sample, these contacts are created, creating a very strong, tight bond that will not break when the sample is placed in liquid nitrogen to cool at extremely low temperatures. In this procedure, two of the four wires are used to aid with the current that passes through the sample while the other two are used to help with the voltage drop through the sample. While a current travel through the sample, a voltage drop occurs as a result of resistance. We recommend the four-probe resistivity method for measuring the sample's resistivity since contact resistance is a very important element. Our measurements are significantly influenced by sample resistance as well as wire resistance. This is why we like this approach **[8]**. For our four-probe resistivity measurement procedures, we employed three Hewlett-Packard digital multimeters, model 3466A. While the second multimeter is used as a voltmeter to detect the voltage drop across the sample, the first multimeter is utilized as an ammeter to measure current. In order to compare the temperature of the sample to a reference temperature, such as liquid nitrogen, a thermocouple wire is needed. The voltage of the thermocouple wire that is temperature dependent is measured using the third multimeter. We converted the voltage (mV) to temperature using the same old reference table for thermocouple voltage and temperature courting (K). We analyzed the experimental data using the Origin software. We obtained the current (I), voltage (V), and temperature (T) readings from the four-probe test. Ohm's law is used to determine the value. We employ a source of constant current in the four-probe technique to provide current to the sample. The potential difference is produced between the outermost and innermost wires. We often provide current in the range of 1 to 2 mA. Below room temperature, the superconductivity phenomena take place. We dipped the sample into liquid nitrogen to chill it down and obtain this low temperature. Thermocouples are required for temperature measurement. It is the intersection of two wires that are joined at the ends of various alloys and metals. The "Seeback effect" serves as the foundation for the thermocouple's operation. When there should be a temperature drop in this effect, there is instead a voltage drop at both ends of the wires. The measuring junction and reference junction are the two junctions that are employed in this. A measuring junction is set up in the environment to calculate its temperature, while a reference junction is known to be set up in liquid nitrogen at a predefined temperature. The

temperature of the heated junction can be determined using the electromotive force that exists between the two junctions. We then obtain the data utilizing original computer software before plotting the resistivity vs temperature graph of the superconducting sample.

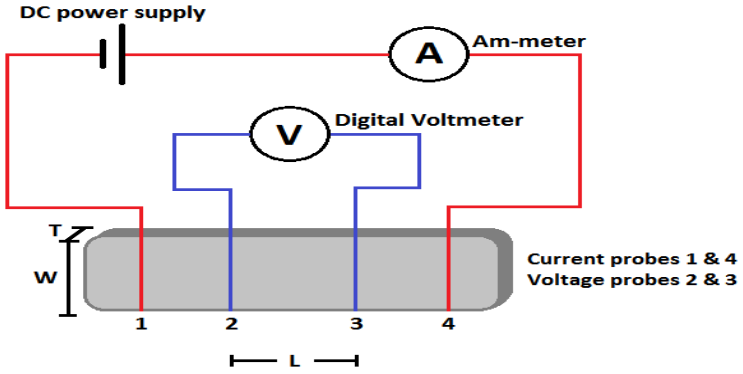

Fig. 3.3: Four probe resistivity measurements

3.2.3 Fourier-Transform Infrared Spectroscopy (FTIR):

Atomic vibrations in solids take place about their equilibrium location. The mass of the atoms, the lengths of their bonds with other atoms, and the bond angle all directly affect these vibrations or phonons. These interdependencies changed the vibrations of various solid materials. These vibrations are still there at absolute zero. The calculation of energy associated with these lattice vibrations by applying the approximation of simple harmonic oscillations quantum mechanically, is:

$$E_n=(n+1/2)\hbar\omega_o \qquad (3.12)$$

for n=0,1,2,3, ….

The' ħ' Boltzmann constant in this instance has a value: $\hbar=h/2\pi=(6.634x10^{-34})/2\pi=1.054\times10^{-34}$ Js. The harmonic oscillator's frequency is " ω_o ". These vibrations, therefore, have energy $E_o=1/2$ for the ground state energy n = 0. These vibrations of the lattice are crucial for explaining the sample's physical characteristics. Therefore, it is crucial to identify the type of vibrational modes present in a sample in order to explain the characterization of solid materials. We employ a spectrometer known as a (FTIR) to investigate these patterns. The name of this method is FTIR spectroscopy **[9]**.

Michelson interferometer has been instrumental in the FTIR spectrometer's success. This interferometer divides infrared radiation into its various components as part of its operation. Due to the fact that the infrared radiations' frequency is similar to that of phonons (lattice vibrations), infrared rays used for FTIR spectroscopy **[10].**

Resonance is created and an absorption peak occurs in FTIR spectra when the frequency of infrared radiation reaches the natural frequency of atom oscillation. However, if the resonance event does not take place, infrared radiation will pass right through the material.

We can use the FTIR spectroscopy technique to:

- Find unknown elements present in the sample;
- Count the variety of substances present in the mixture;
- Verify the sample's purity.

Figure 3.5: The set-up of FTIR

3.2.3.1 Basic Parts of FTIR: -

- Infrared source of radiation
- Michelson's Interferometer
- Detector

In FTIR, infrared sources are air-cooled, which means that the temperature is decreased by releasing heat into the atmosphere. These sources are made of nichrome wire coils and are air-cooled. Due to its high electrical resistivity, nichrome, an alloy of chromium and nickel, emits radiation in the mid-infrared spectrum as an electric current flows through it **[11].** In the Michelson interferometer, there are three active parts. moving mirror, fixed mirror, and beam splitter, in that order.

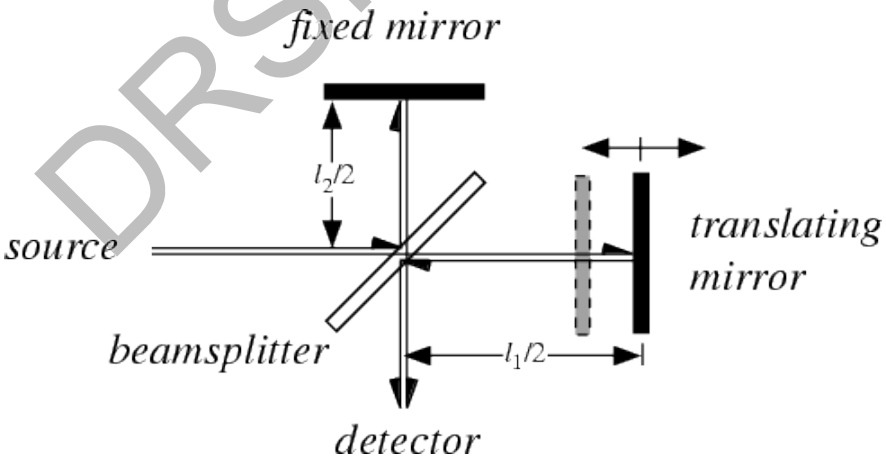

Figure 3.5: Michelson interferometer.

Here two mirrors are positioned via perpendicular to one another as shown in Figure 3.5. The beam-splitter is typically created by depositing a germanium's thin layer on a KBr substrate. It is a semi-reflecting device. Radiation from the source is created toward the interferometer and hits the beam splitter, where it is reflected toward the fixed mirror in half and transmitted toward the moving

mirror in the other half. The radiations are reflected by these two mirrors and then recombined at the beam splitter. The resultant beam, known as an interferogram, is created when the two reflected radiation beams collide. The frequency of the sample that absorbs or transmits is then sent through the interferogram **[12]**.

To transform light energy into electrical impulses is what it does. In FTIR spectroscopy, two types of detectors are often used.

- Mercury cadmium telluride (MCT),
- Deuterated triglycine sulphate (DTGS)

3.2.3.1.1 Deuterated triglycine sulphate

Temperature affects its electrical polarization. Current flows through it as a result of temperature change. It is regarded as a weak detector since it reacts slowly to changes in the intensity of infrared radiation.

3.2.3.1.2 Tellurium mercury cadmium

It is an alloy of tellurium (Te), mercury (Hg), and cadmium (Cd). Light can flow through it. Compared to a DTGS detector, it is faster and less noisy **[13]**. However, liquid nitrogen cooling is essential for noise reduction. Furthermore, the spectrum range of these detectors is poor. In our experimental setup, a Nicolet 5700 model spectrometer was used. We used tiny pellets of KBr as the background spectrum. A little amount of material is mixed with KBr powder and pelletized at a pressure of 3.8 tons/cm^2 after obtaining a background spectrum. The pellet is then put in a spectrometer's sample holder. 200 scans were taken for each sample within the 400–700 cm^{-1} wavenumber range. With the aid of the computer program Omnic, the raw data is examined. Different vibrational modes are observed for each sample and lastly, we compare the vibrational modes of all samples.

3.2.3.2 Working: -

- A background of pure KBr pellet was first placed in the beam's path, and 200 scans were obtained with a range of 400–700 cm^{-1}.
- We then added roughly 5 mg of a superconductor to 50 mg of KBr compound, mixed them thoroughly, and created the pellet. Once more, we performed 200 scans of the mixed sample spectrum, with the range previously set at 400-700 cm^{-1}.
- After removing the background spectrum and using KBr as a background, the computer only showed the spectrum of our sample.
- To analyze and examine the spectrum of our samples, we employed the OMNIC software.

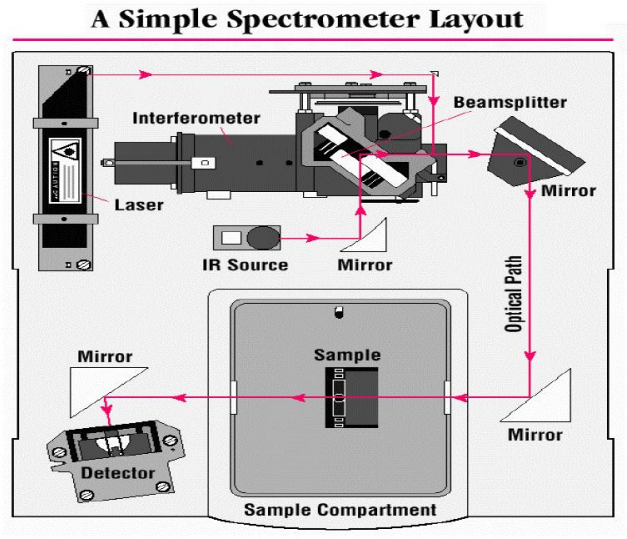

Figure 3.6: FTIR's Working

3.2.4 Dielectric measurements: -

The way a material reacts to an external electric field is determined by its dielectric characteristics. There is movement of charges about their mean position by applying the external electric-field, which causes polarization to happen. Four different polarization's types which depends on the 'f' of the external E-field **[14].**

Electronic Polarization: It appears as a result of the shifting of the atom and ion electronic charge clouds. High frequency of observations like this (10^{15} Hz)

Atomic polarization: This polarization occurs due to displacement of the ionic core and the electronic-charge distribution working together. These polarizations operate in the 10^{10}–10^{13} Hz frequency band.

Dipolar polarization: It results from permanently activated dipoles that operate between 10^{3} and 10^{6} Hz.

Interfacial polarization requires a minimum amount of charge dipole movement in an applied field and has a low-frequency response range of 100 to a few thousand Hertz.

Due to their limited frequency range, the dipolar and interfacial polarization is significant in our situation. The superconducting samples can become normal materials at high frequencies **[15].**

3.2.4.1 Parts of Dielectric Setup:

- Sample holder
- LCR meter
- Thermocouple
- Liquid Nitrogen

- Digital meter

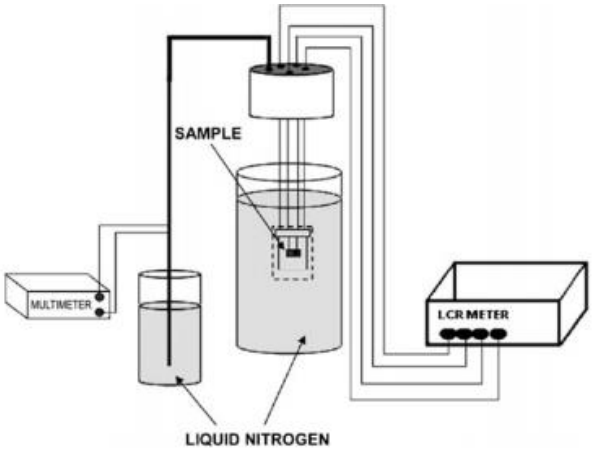

Figure 3.7: Dielectric measurements experimental set-up.

We apply silver to both sides of our sample to create a capacitor so that we can measure its dielectric properties of it. The silver paste behaves like a plate with a sample of dielectric material in between. We use a Wayne Kerr 4275 LCR meter to test the capacitance and conductance of our samples over the range of frequency of 20 Hz to 1 MHz. We determined the constants for dielectric (ε', ε''), and AC-conductivity('σ_{ac}') and dielectric loss ($\tan\delta$) values from these values of capacitance (C) and conductance (G)**[16].**

$$\varepsilon' = \frac{Cd}{A\varepsilon_0} \quad (3.13)$$

$$\varepsilon'' = \frac{Gd}{A\omega\varepsilon_0} \quad (3.14)$$

$$\text{Tan}\delta = \frac{\varepsilon''}{\varepsilon'} \quad (3.15)$$

$$\sigma_{ac} = 2\pi f\varepsilon_o\, \varepsilon' \tan\delta \quad (3.16)$$

'A' stands for the electrode's surface area, 'd' for its thickness, 'C' for capacitance, 'G' for conductance. The '2πf' shows the angular frequency and ε_o shows the permittivity of free space.

3.2.5 Fluctuation Induced Conductivity Analysis (FIC): -

Superconductors show outstanding property both in their regular state and in their superconducting state. The production of cooper pairs, which enhances the conductivity of a substance known as superconducting fluctuations, can begin above the Tc. Cooper pairs only vary from each other in the superconducting state because they do not exist above Tc in a long-range order, which is what gives the material its superconducting features. The cooper couples are swiftly formed and destroyed as a result of thermodynamic fluctuations above Tc. These variations are necessary for the temperature regime known as the Ginzburg criterion temperature, which is located close to Tc (TG). For low-temperature superconductors, Ginzburg's value for TG is less than 1 K, however, it is more like (1-2) K for high-temperature superconductors.

The superconducting thermodynamic fluctuations have a significant impact on resistivity outside of the critical regime and just above the critical temperature of a superconductor. There is a variation from resistivity's linear (undeviating) dependency at somewhat higher temperatures. The fluctuation-induced conductivity is caused by the superconducting transition's divergence from linearity, and is represented by;

$$\Delta\sigma(T) = \frac{\rho_n(T) - \rho(T)}{\rho_n(T)\rho(T)} \tag{3.17}$$

While ρn(T)= a + bT shows the resistivity of the normal conducting state, ρ(T)is recognized as the actual (definite) resistivity. When considering Δσ (T), there are two primary fluctuation factors. Contributions from Aslamazov-Larkin (AL) and Maki-Thompson (MK) come first and second, respectively. The first one is caused by extra current carried by cooper pairs, which raises variations over the threshold temperature **[17]**. The second contribution explains about how superconducting fluctuations affect the conductivity of the electrons in their normal state. In high-temperature superconductors, the Lawrence-Doniach (LD) model explains the AL term, and the AL term predicts that as temperature rises, the system will transition from a 3D to a 2D electronic state. In the phenomenon of moderate breaking of cooper pairs, the 'AL' term becomes more dominant as one gets nearer to the critical-temperature, although, in the 2D fluctuation area, the MT term becomes 'tφ-dependent' and has quite important **[18]**. From FIC analysis, we can obtain accurate data on the coherence length ξc(T), phase-relaxation time 'tφ', and dimensionality of the superconductor. Given that high-temperature superconducting oxides have shorter Ginsburg-Landau coherence lengths ξGL (0), " Δσ (T)" should occur at temperatures above the critical temperature. Numerous research teams informed the crossover temperatures in LD model expressions while the MT role was expected to be unclear, therefore the prospect of evaluating tφ was neglected. Ginzburg was the first to calculate the variations' contributions to the heat capacity in a superconductor. He has demonstrated that these oscillations raise the heat capacity above Tc. He used the LT of second-order phase-transition to apply the heat capacity jump that happens at Tc. Ginzburg predicted the temperatures for bulk superconductors at which the fluctuation adjustment to the heat capacity is significant Thus, it is possible that such thermal fluctuations will be measured. Different investigations, including susceptibility tests, D.C. resistivity measurements, specific heat capacity tests, etc. near Tc, can verify these thermal oscillations. At temperatures just above Tc, these oscillations prevent the resistivity from decreasing towards zero. The heat capacity begins to diverge at Tc.

$$\frac{\Delta \boldsymbol{T}}{\boldsymbol{T_c}} \sim \left[\frac{(\boldsymbol{Tc})^{\boldsymbol{4}}}{\varepsilon \boldsymbol{f}}\right] \sim \left[\frac{(\boldsymbol{\alpha})^{\boldsymbol{4}}}{\boldsymbol{\xi}}\right] \sim \mathbf{10^{-4}}\boldsymbol{to}\mathbf{10^{-4}} \tag{3.18}$$

where " $\boldsymbol{\alpha}$ " denotes the interatomic distance among the lattice-sites and "ξ" shows the coherence length. Since the value of $\Delta T/T$ is so small, these fluctuations have long been unnoticeable to experimenters.

3.2.5.1 Aslamazov-Larkin Theory:

The fluctuations in Ψ(r) of HTSC are primarily caused by low coherence lengths and high Tc. These fluctuations can be detected in laboratories using fluctuating conductivity, fluctuating magneto-conductivity, and fluctuating specific heat. The first theoretical approximations for fluctuation-induced conductivity (FIC), which were used to analyze the resistivity readings of a sample, were developed by Aslamazov and Larkin. In 1968 **[19]**, Aslamazov and Larkin developed the FIC of crystallites based on the Ginzburg-Landau theory. They claim that the FIC is characterized by "2D" and "3D" in the two- and three-dimension regimes, respectively.

$$\Delta\boldsymbol{\sigma 2D} = \frac{\mathbf{e^2}}{\mathbf{16\hbar d}}\left(\frac{\mathbf{T}}{\mathbf{T-Tc}}\right) \tag{3.19}$$

$$\Delta\boldsymbol{\sigma 3D} = \frac{\mathbf{e^2}}{\mathbf{32\hbar \xi_0}}\left(\frac{\mathbf{T}}{\mathbf{T-Tc}}\right)^{\mathbf{1/2}} \tag{3.20}$$

Using A.K. Ghosh et al. **[20]**, it is recommended that the polycrystalline samples undergo FIC analysis. Actually, the AL equations were adjusted as

$$\Delta\sigma_{2D} = \frac{e^2}{64\hbar d}\varepsilon^{-1}\left[1+\left(1+\frac{8\xi_c^4(0)\varepsilon^{-1}}{d^2\xi_{ab}^2(0)}\right)^{\frac{1}{2}}\right] \tag{3.21}$$

$$\Delta\sigma_{3D} = \frac{e^2}{32\hbar\xi_p(0)}\varepsilon^{\frac{-1}{2})} \tag{3.22}$$

where "ξp (0)" denotes the polycrystalline materials' response or effective coherence length, and "ε" denotes the lower temperature. ξp (0) is presented as

$$\frac{1}{\xi_p(0)} = \frac{\frac{1}{\xi_c(0)}+\left(\frac{1}{\xi_c^2(0)}+\frac{1}{\xi_{ab}^2(0)}\right)^{\frac{1}{2}}}{4} \tag{3.23}$$

where "ξab (0)" denotes the zero resistance coherence-length within the CuO_2 conducting planes & "ξc (0)" denotes the zero resistance coherence length along the c-axis.

References

[1] S. Kumar Shrivastava, "Synthesis of High-Tc Superconducting Cuprate Materials through Solid State Reaction Route," *International Journal of Engineering, Science and Mathematics*, vol. 7, no. 3, Mar. 2018.

[2] J. S. Blakemore, "Solid State Physics," *Cambridge University Press*, Dec. 1985, doi: 10.1017/cbo9781139167871.

[3] Ashcroft, N.W., and N.D. Mermin, Solid state physics (saunders college, Philadelphia, 1976). Appendix N, 2010. 166.

[4] Ali, M.O., Elementary Solid State Physics, Principles, and Applications, Addison-Wesley publishing company. (1993).

[5] W. H. Bragg and W. L. Bragg, "The Reflection of X-rays by Crystals," *Proceedings of the Royal Society A: Mathematical, Physical and Engineering Sciences*, vol. 88, no. 605, pp. 428–438, Jul. 1913, doi: 10.1098/rspa.1913.0040.

[6] B. E. Warren, *X-ray diffraction*. New York: Dover Publications, 1990.

[7] N. W. Ashcroft and N David Mermin, *Solid state physics*. Fort Worth: Saunders College, 1988, p. 166.

[8] S. H. Han and Ö. Rapp, "Superconducting fluctuations in the resistivity of Bi-based 2:2:2:3," *Solid State Communications*, vol. 94, no. 8, pp. 661–666, May 1995, doi: 10.1016/0038-1098(95)00072-0.

[9] Nicolet, T, "Introduction to Fourier Transform Infrared Spectrometry," Thermo Nicolet Corporation. 2001.

[10] P. Griffiths and J.A. De Haseth," Fourier Transform Infrared Spectroscopy", 2nd edition, Willey, New York (2007).

[11] J. R. Ferraro, "Vibrational studies of solid inorganic and coordination complexes at high pressures," *Coordination Chemistry Reviews*, vol. 29, no. 1, pp. 1–66, Aug. 1979, doi: 10.1016/s0010-8545(00)80362-8.

[12] F. A. Settle, *Handbook of instrumental techniques for analytical chemistry*. Upper Saddle River, Nj: Prentice Hall Ptr, 1997.

[13] J. Kauppinen and J. Partanen, *Fourier Transforms in Spectroscopy*. Weinheim: John Wiley & Sons, 2011.

[14] A. YOUNIS and N. A. KHAN, "$Cu_{0.5}K_{0.25}Tl_{0.25}Ba_2Ca_3Cu_4O_{12-\delta}$ SUPERCONDUCTOR AND ITS DIELECTRIC PROPERTIES," *Modern Physics Letters B*, vol. 24, no. 32, pp. 3097–3107, Dec. 2010, doi: 10.1142/s0217984910025401.

[15-16] Ş. Cavdar, H. Koralay, N. Tugluoglu, and A. Gunen, "Frequency-dependent dielectric characteristics of Tl–Ba–Ca–Cu–O bulk superconductor," *Superconductor Science and Technology*, vol. 18, no. 9, pp. 1204–1209, Jul. 2005, doi: 10.1088/0953-2048/18/9/010.

[17] A. I. Larkin and A. A. Varlamov, "Fluctuation Phenomena in Superconductors," *arXiv:cond-mat/0109177*, Sep. 2001, Accessed: Aug. 31, 2022. [Online]. Available: https://arxiv.org/abs/cond-mat/0109177

[18] L. G. Aslamasov and A. I. Larkin, "The influence of fluctuation pairing of electrons on the conductivity of normal metal," *Physics Letters A*, vol. 26, no. 6, pp. 238–239, Feb. 1968, doi: 10.1016/0375-9601(68)90623-3.

[19] A. K. Ghosh, S. K. Bandyopadhyay, P. Barat, P. Sen, and A. N. Basu, "Fluctuation-induced conductivity of polycrystalline Y1−xCaxBa2Cu3O7−δ superconductors," *Physica C: Superconductivity*, vol. 264, no. 3–4, pp. 255–260, Jun. 1996, doi: 10.1016/0921-4534(96)00257-

Chapter:4

Results and Conclusion

4.1 Introduction:

Low-dimensional, high-Tc superconductors have a charge reservoir layer (CRL) that is made up of a carrier-supplying $Cu_{0.5}Tl_{0.5}Ba_2O_{4-\delta}$ layer having one or more $nCuO_2$ conducting planes (for n=2, 3, 4,5,... etc.). $Cu_{0.5}Tl_{0.5}Ba_2Ca_2Cu_3O_{10-\delta}$ (CuTl-1223) superconductor (with n=3) of $nCuO_2$ [**1–5]** has highest critical temperature. Superconductivity is established by the conducting CuO_2 planes which has charge carriers, supplied by the $Cu_{0.5}Tl_{0.5}Ba_2O_{4-\delta}$ CRL. The (CuO_2) planes has charge carriers, the density of that carriers are affected by the post-annealing of the produced compounds. The movement of the charge carriers from the $Cu_{0.5}Tl_{0.5}Ba_2O_{4-\delta}$ CRL to the (CuO_2) planes is controlled by O_2(Oxygen) because of its higher electronegativity. Due to the wide temperature range of these oxides' oxygen intercalation temperatures, which ranges from 250-650^{o}C, the generated samples' superconducting properties may vary depending on the temperature at which such samples are post-annealed. In order to replenish the indirect flow of the carriers from the $Cu_{0.5}Tl_{0.5}Ba_2O_{4-\delta}$ CRL, it is advised to dope the elements at the CuO_2 planar-sites that are capable of donating their extra electron at the these planar-sites of CuO_2 planes. Our prior investigations revealed the importance of the interactions of electrons with phonons in such compounds and shown that the final compound's critical temperature is suppressed by soft phonons. The contribution of hard phonons, which arises due to the vibrations of lighter atoms, in the mechanism of HTSC, has not yet been determined. We have synthesized the samples of $Cu_{0.5}Tl_{0.5}Ba_2Ca_2Cu_{3-x}Na_xO_{10-\delta}$ (x=0, 1, 2, 3) that are doped with Na in order to complete the aforementioned task. Alkali metal while the mass of Na is approximately half that of Cu atoms, may readily donate its $3S^1$ electron and would replenish the free carriers in the CuO_2 planes, producing hardened phonons in that solid-state medium. Therefore, we can fix these unresolved problems in such oxide high-temperature superconductors by doping Na at the CuO_2 planar sites. The $Cu_{0.5}Tl_{0.5}Ba_2O_{4-\delta}$ CRLis fixed in the first part of this research, but the doping of conducting CuO_2 planes with Na atoms has to be done with the synthesization of $Cu_{0.5}Tl_{0.5}Ba_2Ca_2Cu_{3-x}Na_xO_{10-\delta}$ (x=0, 1, 2, 2.5 , 3) samples. In 2nd part of these investigations, the samples of $Cu_{0.5}Tl_{0.5}Ba_2CaMgCu_{3-x}Na_xO_{10-\delta}$ (x=0, 1, 2, 3) were prepared in order to dope Mg at the Calcium sites and reduce the distance between the superconducting CuO_2/Na_2O planes.

4.2 Experimental Approach:

Using a solid-state reaction method of two stages, the sample series of $Cu_{0.5}Tl_{0.5}Ba_2Ca_2Cu_{3-x}Na_xO_{10-\delta}$ (x=0, 1, 2, 2.5, 3) & $Cu_{0.5}Tl_{0.5}Ba_2CaMgCu_{3-x}Na_xO_{10-\delta}$ (x=0, 1, 2, 3) were synthesized. In the first phase, measured amounts of the substances $CaCO_3$, $BaCO_3$, Na_2CO_3, and CuCN for $Cu_{0.5}Tl_{0.5}Ba_2Ca_2Cu_{3-x}Na_xO_{10-\delta}$ (x=0, 1, 2, 2.5, 3) samples & $CaCO_3$, $Ba(NO_3)_2$, Na_2CO_3, $Cu_2(CN)_2+H_20$ for $Cu_{0.5}Tl_{0.5}Ba_2CaMgCu_{3-x}Na_xO_{10-\delta}$ (x=0, 1, 2, 3) samples, were ground for about 1h pestle & mortar to determine the composition of the reactants. For a 24-hour period, the ground

material was heated by being fired twice at 860 °C in quartz boats inside a preheated chamber furnace. The furnace was then cooled to Troom(300K). In 2nd step, the fired precursor was mixing with a measured quantity of Tl_2O_3(thallium oxide) and mixed for 45 minutes to produce the final reactant compositions of $Cu_{0.5}Tl_{0.5}Ba_2Ca_2Cu_{3-x}Na_xO_{10-\delta}$ (x=0, 1, 2,2.5, 3) and $Cu_{0.5}Tl_{0.5}Ba_2CaMgCu_{3-x}Na_xO_{10-\delta}$ (x=0, 1, 2, 3). After being palletized under 5 tons/cm^2 of pressure, the thallium mixed precursor was then heated for (10-12) minutes in a pre-heated chamber furnace at 860^{o}C. Pellets were then enclosed inside gold capsules. X-ray diffraction(XRD), temperature-dependent four probe resistivity measurements, dielectric properties, and FTIR measurements were used to characterize the produced samples. CuKα radiations with a wavelength of 1.54056Å were used in an X-ray diffraction scan to evaluate the structural phases of the materials, and the Checkcell computer program was used to determine cell parameters. The four-probe approach was used to calculate the sample's temperature-dependent resistance. NICOLET 5700 was used to measure the 400-700cm^{-1} wavenumber's range of FTIR absorption spectra. The KBr pallets were used to obtain the background spectra of the samples.

4.3 Experimental Results:

4.3.1 $Cu_{0.5}Tl_{0.5}Ba_2Ca_2Cu_{3-x}Na_xO_{10-\delta}$-(x=0, 1, 2, 2.5,3) Samples: -

4.3.1.1: Analysis of X-ray diffraction(XRD)

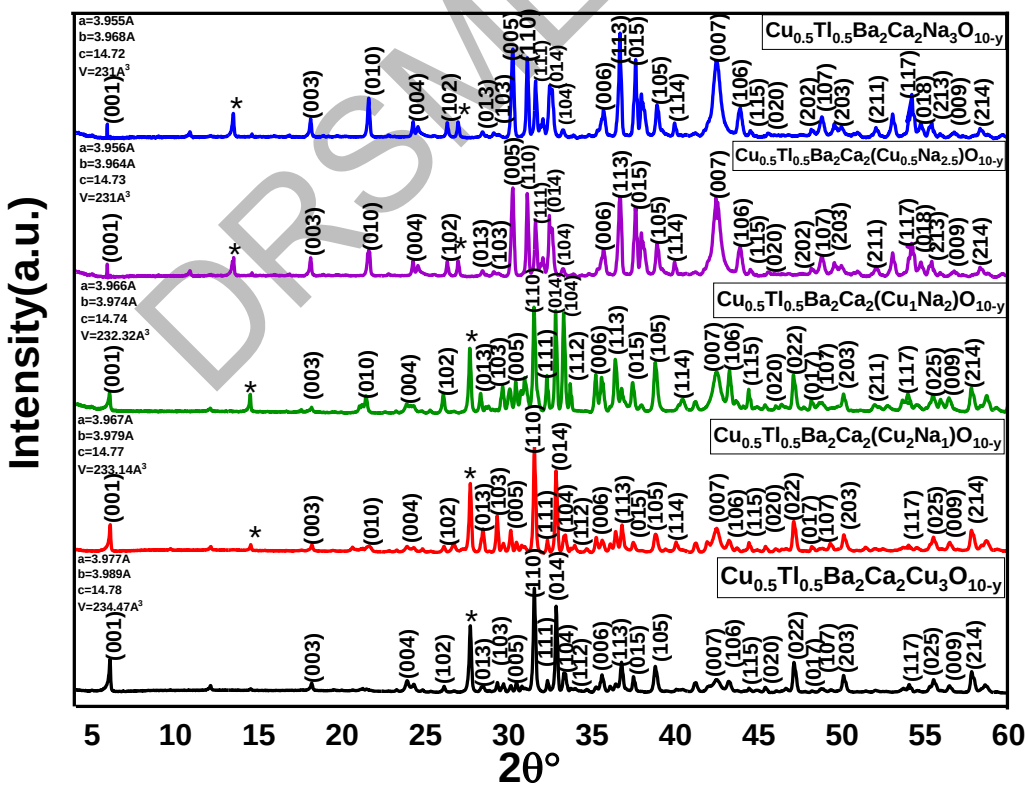

Fig. 4.1: The scanned diffraction of X-rays for $Cu_{0.5}Tl_{0.5}Ba_2Ca_2Cu_{3-x}Na_xO_{10-\delta}$ (x=0, 1, 2,2.5, 3) samples

In Fig. 4.1, the-scanned diffraction of X-ray for the samples of $Cu_{0.5}Tl_{0.5}Ba_2Ca_2Cu_{3-x}Na_xO_{10-\delta}$ (x=0, 1, 2,2.5, 3) are showing. In these diffraction patterns, a predominant CuTl-1223 superconducting phase can be seen. There is a maximum number of indexed X-ray diffraction lines in the orthorhombic crystal structure that followed the P4/mmm space group. Some of the un-indexed diffraction lines of low intensity are marked as impurity lines that belong to $BaCuO_2$ and Ba_2CuO_3 phases.

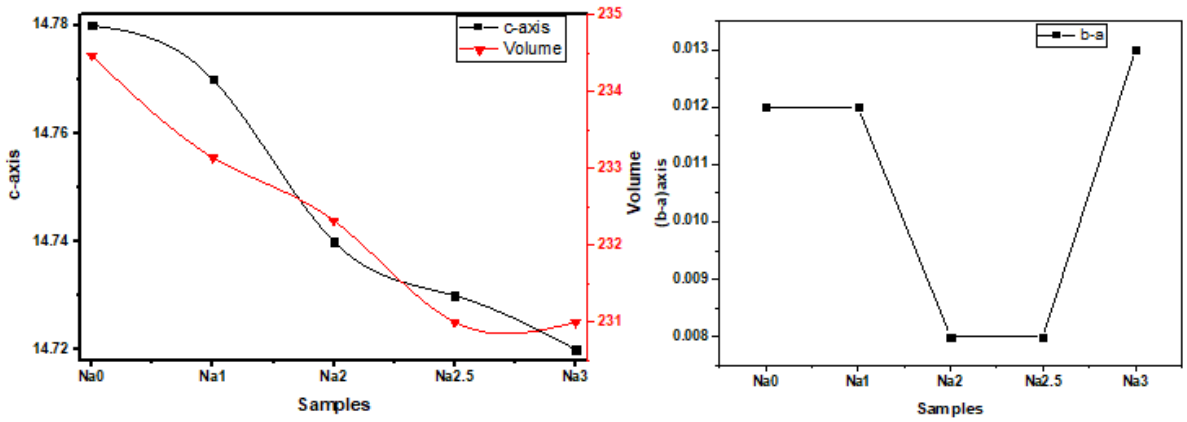

Figure 4.2a: Comparison of b-a axis of $Cu_{0.5}Tl_{0.5}Ba_2Ca_2Cu_{3-x}Na_xO_{10-\delta}$ (x=0, 1, 2,2.5, 3)

Figure 4.2b: Comparison of c-axis parameter and volume of $Cu_{0.5}Tl_{0.5}Ba_2Ca_2Cu_{3-x}Na_xO_{10-\delta}$(x=0, 1, 2,2.5, 3)

Figure 4.2a shows that all Na-doped samples exhibit a rise in orthorhombic distortion by b-a, whereas Figure 4.2b shows that doping Na at the planar CuO_2 sites decreases the *c*-axes length and volume of the unit cell. This is a clear fingerprint that Na was added to the final compound.

4.3.1.2 Temperature-dependent resistivity measurements

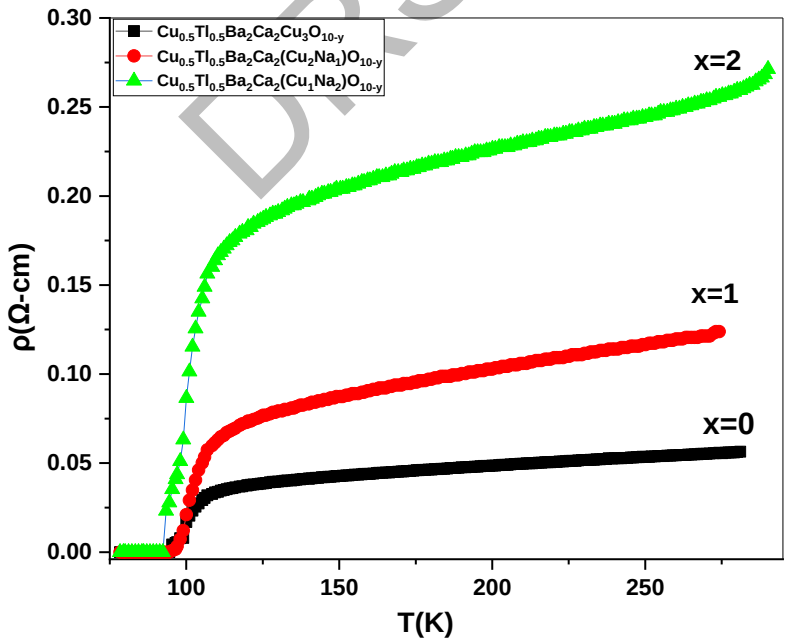

Fig 4.3a: temperature-dependent resistivity measurements for $Cu_{0.5}Tl_{0.5}Ba_2Ca_2Cu_{3-x}Na_xO_{10-\delta}$ (x=0, 1, 2) samples respectively

Fig4.3(a,b,c) represents the temperature-dependent resistivity measurements for $Cu_{0.5}Tl_{0.5}Ba_2Ca_2Cu_{3-x}Na_xO_{10-\delta}$ (x=0, 1, 2) samples . With superconducting'onsets at [Tc(onset)] 109.85K, 108.65K, and 108.01K and the zero resistivity critical temperatures at 94.91K, 94.39K, and 91.63K, respectively, these superconductors have variations of the metallic behavior for the resistivity from Troom down to the Tonsett of superconductivity.

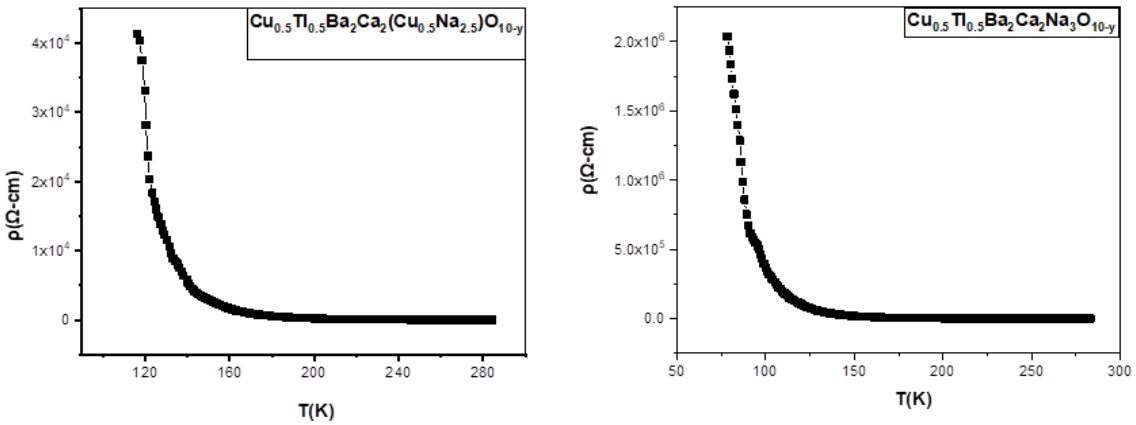

Fig 4.3(b,c): temperature-dependent resistivity measurements for $Cu_{0.5}Tl_{0.5}Ba_2Ca_2Cu_{3-x}Na_xO_{10-\delta}$ (x=2.5,3) samples respectively

The loss of zero resistivity critical temperature indicates that Na-doped samples are being pushed towards the over-doped regimes of the phase diagram; oxide superconductors have displayed a bell-shaped phase diagram of critical temperature versus carriers doping with optimum doping around x=0.3 holes per plane. The critical temperature in such samples suppresses both in over-doping and under-doping of CuO_2 planes. The doped Na atoms donate their $3s^1$ electron in CuO_2 planes, increasing the free electron density since the alkali metal is a good donor of free carriers. Since holes are the predominant carriers in the superconducting-state in such compounds, the higher density of free electrons in the Copper oxide planes promotes electro-hole recombination processes, suppressing the population holes in the superconducting state.

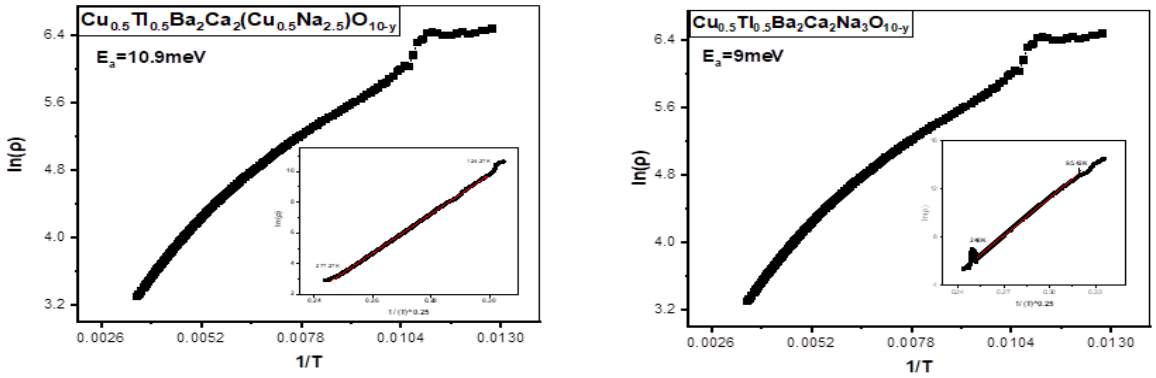

Fig 4.4(a,b): Activation energy curves of $Cu_{0.5}Tl_{0.5}Ba_2Ca_2Cu_{3-x}Na_xO_{10-\delta}$ (x=2.5,3) samples respectively

4.3.1.3 Fluctuation-induced conductivity analyses

By applying fluctuation conductivity analyses (FIC) on conductivity data, the parameters determining intrinsic superconductivity in such samples are identified. These analyses were conducted using the "Aslamazov-Larkin(AL)" and "Lawrence-Doniach(LD)" models as represented by the results in Fig. 4.5(a,b,c).

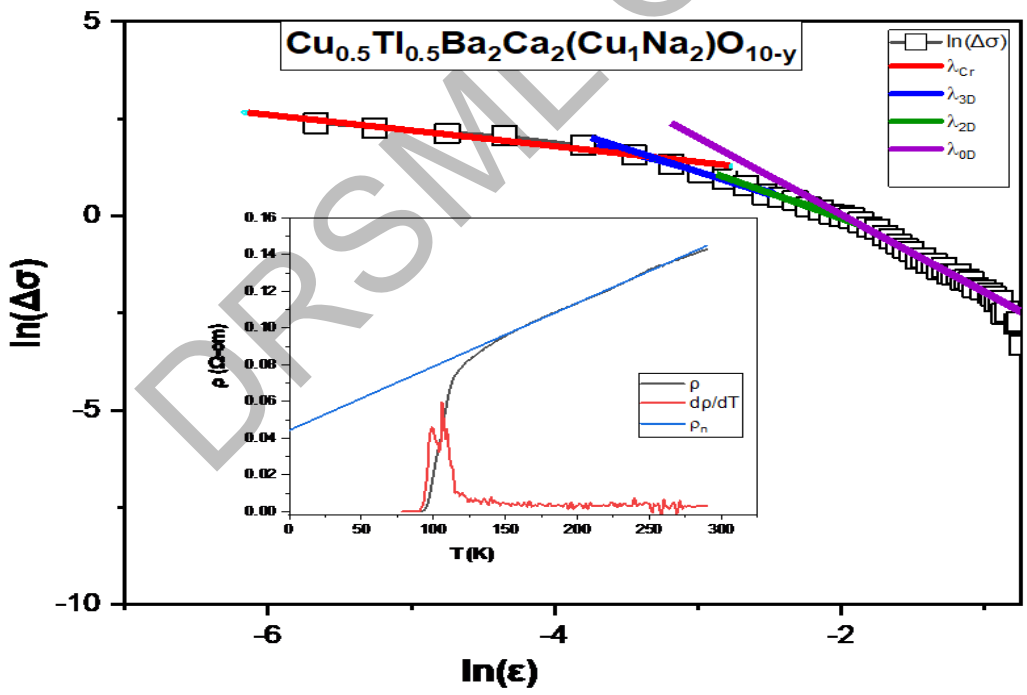

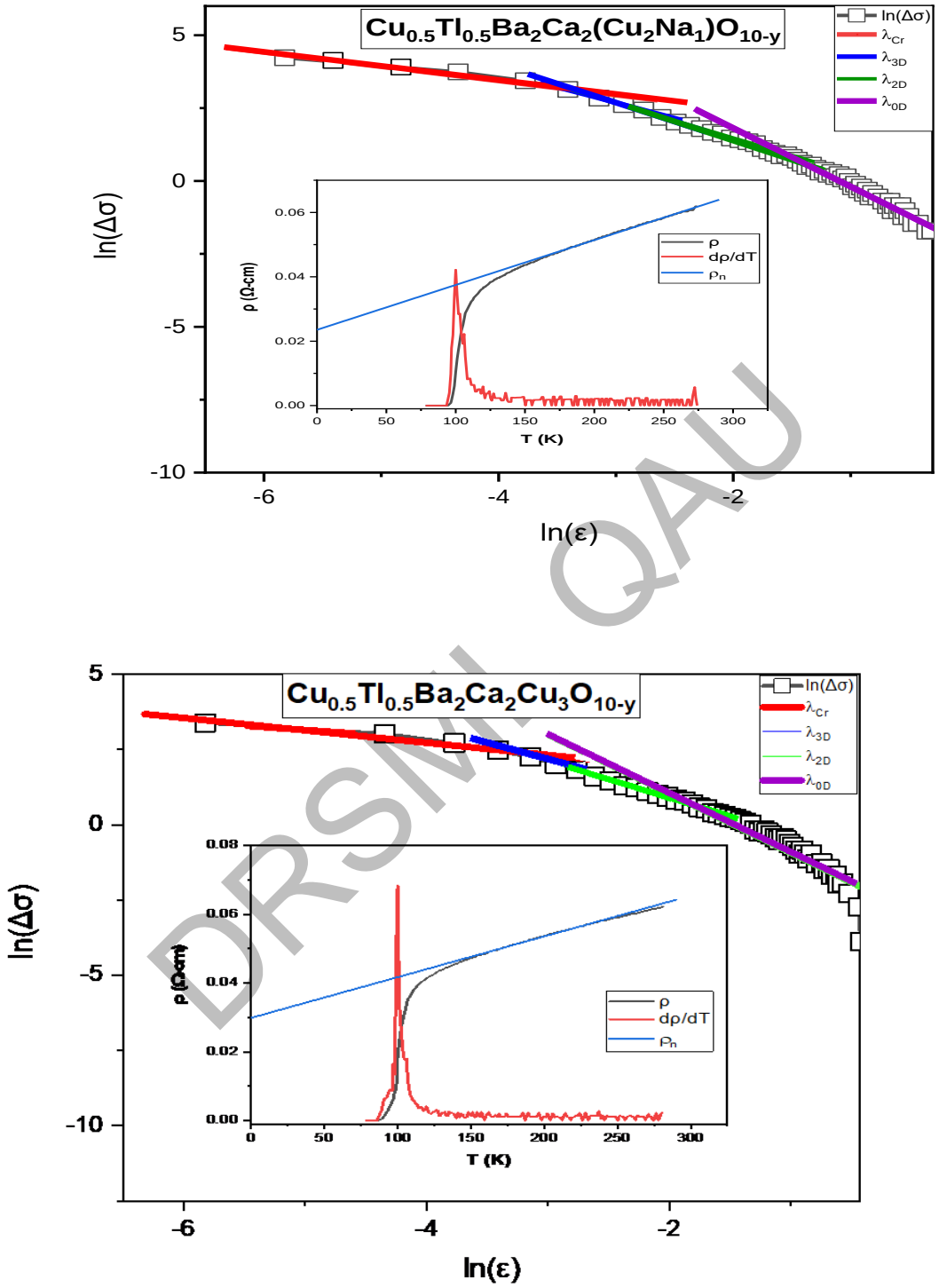

Fig 4.5(a,b,c): Plot between $\ln\Delta\sigma_{(T)}$ and $\ln\varepsilon$ for the samples of $Cu_{0.5}Tl_{0.5}Ba_2Ca_2Cu_{3-x}Na_xO_{10-\delta}$ (x=0,1,2) respectively

Following the equation of the form $\Delta\sigma_{(T)} = \Delta\sigma_{RT}\varepsilon^{-\lambda_D}$ in the temperature range around and beyond T_c gives these results. It is possible to rewrite this equation as follows:

$$ln\Delta\sigma_{(T)} = ln\Delta\sigma_{RT} - \lambda_D ln(\varepsilon) \qquad (4.1)$$

Where dimensional exponent is denoted by 'D' and the reduced temperature is shown by $\varepsilon = \left(T - T_c^{mf}\right)/T_c^{mf}$. Dimensional exponent values for various thermal activated processes during heat and cooling cycles range from 0.3 to 2.0. In these analyses, the critical exponent has a dimensional exponent of around 0.3, the three-dimensional conductivity has a dimensional exponent of about 0.5, the two-dimensional conductivity has a dimensional exponent of about 1.0, and the zero-dimensional conductivity has a dimensional exponent of about 2.0 [6]. Lawrence and Doniach's (LD) model modifies the following formula the polycrystalline samples:

$$\Delta\sigma_{LD} = [e^2/16\hbar d](1 + J\varepsilon^{-1})^{-1/2}\varepsilon^{-1} \qquad (4.2)$$

In this equation, the thickness of the superconducting layers is d, which is equal to (~18 Å in the current case), and $J = \left[2\xi_{c(0)}/d\right]^2$ is inter-layer coupling. Table.2 shows the cross-over temperatures, that are T_G, $T_{3D\text{-}2D}$, and $T_{2D\text{-}0D}$, resulting from analyses of the log-plots of excess conductivity vs reduced temperature. The T_{cmf} is calculated from dρ/dT. All doped samples have suppressed values of Tc, Tcmf, and T_G. The zero resistance coherence length along the c-axis($\xi_{c(0)}$) is given as $\frac{d}{2}\left[\frac{T_{3D-2D}}{T_c^{mf}} - 1\right]^{1/2}$ where the "$T_{3D\text{-}2D}$" is the cross-over temperature**[6]**. The intersection of several dimensional exponents are used to determine the cross-over temperatures of various thermally triggered processes.

The slope below T_G is denoted by λ_{cr}, above T_G it is λ_{3D}, above $T_{3D\text{-}2D}$ it is $\lambda_{2D,}$ and for $T_{2D\text{-}0D}$ it is λ_{0D} having exponent value 2. The value of $\xi_{c(0)}$ is used to calculate the value of the phase relaxation time 'τ_φ' and the Fermi velocity 'V_F' as in the following equation(4.3) and (4.4).

$$V_F = \frac{5\pi k_B T_c \xi_{c(0)}}{2K\hbar} \qquad (4.3)$$

$$\tau_\phi = \frac{\pi\hbar}{8k_B T\varepsilon_0} \qquad (4.4)$$

Here equation (4.3) has a proportionality coefficient which is K ≅ 0.12 according to the reference **[8].** The equations (4.5) and (4.6) are used to calculate the values of inter-plane CuO_2 coupling 'J' & energy that is used to split the Cooper-pairs 'E_{Break}' by determining the value of phase relaxation time $\tau_{\varphi.}$

$$J = \frac{\hbar\tau_\phi^{-1}}{2\pi k_B T} \qquad (4.5)$$

$$E_{Break} = \frac{h}{(1.6 \times 10^{-19})}(eV) \qquad (4.6)$$

Samples	λ_{CR}	λ_{3D}	λ_{2D}	λ_{0D}	$T_{CR-3D} = T_G$ (K)	T_{3D-2D} (K)	T_{2D-0D} (K)	T_c^{mf} (K)	T^* (K)	$\alpha = \rho_n(0K)$ (Ω-cm)
Na0	0.33	.57	1.13	2.06	104.36	114.39	108.37	100.05	157	0.021
Na1	0.33	.56	1.1	2	104.36	105.36	116.4	100.05	161	0.022
Na2	0.32	.55	1.09	2	110.38	111.38	113.39	106	153	0.038

Samples	$\xi_c(0)$ (Å)	J	N_G	$\lambda_{p.d}$ x 10^2 (Å)	$B_{c(0)}$ (T)	B_{c1} (T)	B_{c2} (T)	κ	$J_{c\,(0)}$ x 10^3 (A/cm^2)	V_F x 10^7 (m/s)	E_{Break} (eV)	τ_φ x 10^{-13} (s)
Na0	1.26	.063	.043	390	3.7	.34	128.7	24	5.2	1	.032	1.28
Na1	1.15	.053	.043	343	4.2	.43	128.7	22	6.7	0.93	.037	1.12
Na2	1.13	.05	.041	333	4.4	.45	128.7	21	7.1	0.9	.037	1.12

Table 4.1: Superconducting parameters from the plot of $\ln\Delta\sigma_{(T)}$ and $\ln\varepsilon$ of $Cu_{0.5}Tl_{0.5}Ba_2Ca_2Cu_{3-x}Na_xO_{10-\delta}$ (x=0,1,2) samples respectively

Table 4.2: Superconducting parameters calculated from the FIC of $Cu_{0.5}Tl_{0.5}Ba_2Ca_2Cu_{3-x}Na_xO_{10-\delta}$ (x=0,1,2) samples respectively

The following samples have displaying the temperature-dependent metallic variations for resistivity ,therefore, their resistivity drops with temperature, an extrapolated resistivity to zero temperature determines the α-parameter that demonstrates the intrinsic defects' population in the final material. The rise of 'α' in all Na-doped samples showing enhancement in the population of defects in the final compound. The values of '$\xi_c(0)$', 'V_F' , 'J' , and 'τ_ϕ' of the carriers are suppressed in Na-doped samples. Take a look on table 4.2. The coherence length along the c-axis is related to the Fermi-vector via relation $K_F = [3\pi^2 N/V]^{½}$ and a decrease in values of it with Na doping show that the density of superconducting carriers is decreased in Na-doped samples. It is also

demonstrated by the rise of energy needed to split the cooper pair Na-doped samples which proved that these carriers are strongly coupled. The intersection of the CR regime with the 3D regime gives the Ginzburg number N_G. The CR regime and the 3D-conductivity regimes crossover temperature is T_G. T_G, N_G, and GL equations are used to determine key parameters of superconductivity [**30–31**].

$$N_G = \left[\left(T_G - T_c^{mf}\right)/T_c^{mf}\right] = [1/2]\left[k_B T_c/B_{c(0)}^2 \gamma^2 {\xi_{c(0)}}^3\right]^2 \quad (4.7)$$

$$B_{c(0)} = \Phi_0/2\left(\sqrt{2}\right)\pi\lambda_{pd}\xi_{ab(0)} \quad (4.8)$$

$$B_{c1} = B_{c(0)} \ln\kappa/\left(\sqrt{2}\right)\kappa \quad (4.9)$$

$$B_{c2} = \left(\sqrt{2}\right)\kappa B_{c(0)} \quad (4.10)$$

$$J_c = 4\kappa B_{c1}/3\left(\sqrt{3}\right)\lambda_{pd} ln(\kappa) \quad (4.11)$$

The superconductor anisotropy has a value of 1.67 for CuTl-1234 samples with n = 4, that is $\gamma = \xi_{ab(0)}/\xi_{c(0)} = 5/(n-1)$, where n is the No.of Copper oxide planes. The Bc0(T), Bc1(T), and Jc(0) values in Na-doped samples are increased in comparison to un-doped samples. This demonstrates that Na-doping in the final compounds increased the density of the pinning center turning the material to withstand higher external fields. The London penetration depth and (GL) parameter $\kappa=\lambda/\xi$ in Na-doped samples both decreased as a confirmation of this.

According to Figure 6's variable range hopping (VRH) conductivity, samples of $Cu_{0.5}Tl_{0.5}Ba_2Ca_2Na_3O_{10-\delta}$ and $Cu_{0.5}Tl_{0.5}Ba_2Ca_2Cu_{0.5}Na_{2.5}O_{10-\delta}$ followed the following relation:

$$\rho(T) = \rho_o \exp\left[\left(\frac{T_o}{T}\right)^{1/4}\right] \quad (4.12)$$

The Mott 3D VRH type conducting mechanism (by b :1/4) used to analyze the resistivity vs temperature data of the various samples **[10]**. The experimental data from our samples remain to fit well with the Mott 3D VRH model. According to Fig 4.4(a,b), display the plot of lnρ vs. $1/T^{1/4}$, and a straight line with an activation energy of 2.06 MeV indicates the theoretical prediction for the (VRH) in 3D mechanism. Cu0.5Tl0.5Ba2Ca2Na3O10-d exhibits resistivity of semiconductor-like data changes with temperature fitted in the regime of 77K to 300K.

4.3.1.4 Fourier Transform Infrared spectroscopy(FTIR) measurements

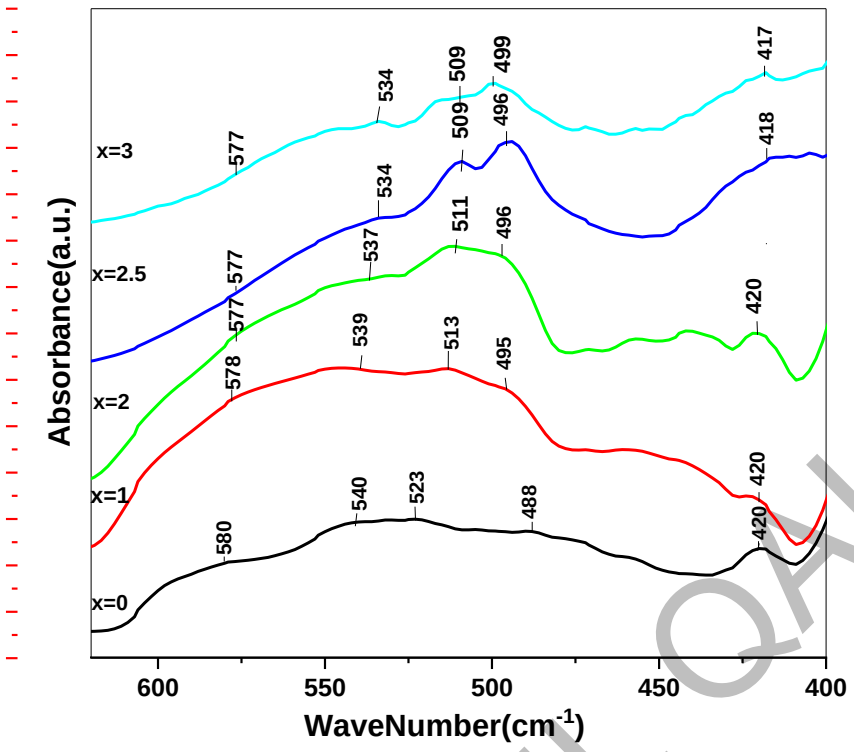

Figure 4.6: the measurements of FTIR results for $Cu_{0.5}Tl_{0.5}Ba_2Ca_2Cu_{3-x}Na_xO_{10-\delta}$ (x=0, 1, 2, 2.5, 3) samples

Figure 4.6 shows the measurements of FTIR results for $Cu_{0.5}Tl_{0.5}Ba_2Ca_2Cu_{3-x}Na_xO_{10-\delta}$ (x=0, 1, 2, 2.5, 3) samples. Two apical oxygen atoms of type Tl-OA-Cu(2) and Cu (1)-OA-Cu(2) are observed at (420–450)cm^{-1} and (480–540)cm^{-1} in the phonon's modes related to the vibrations of different O_2 atoms in the wavenumber range of 400-600 cm^{-1}, as well as a CuO_2 planar oxygen mode at 580 cm^{-1}; the Cu(2) atom is in the CuO_2 plane and the Cu(1) atom is in the (CRL). In Na-doped $Cu_{0.5}Tl_{0.5}Ba_2Ca_2Cu_{3-x}Na_xO_{10-\delta}$ (x=0, 1, 2, 3) samples, all of these modes are softened, demonstrating intrinsic doping of it in the final Compound. These findings also demonstrated how Na-containing compounds' oscillator strength had decreased.

4.3.1.5 Dielectric measurements

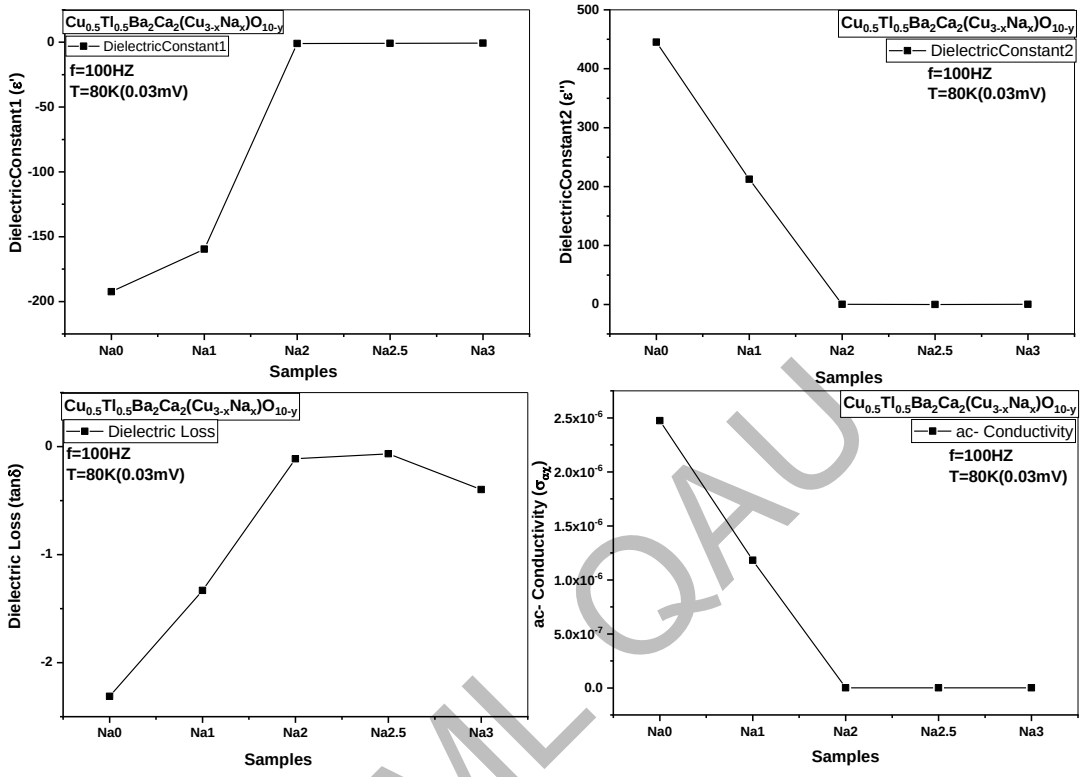

Figure 4.7(a, b, c, d) :the dielectric measurements for the samples of $Cu_{0.5}Tl_{0.5}Ba_2Ca_2Cu_{3-x}Na_xO_{10-\delta}$ (x=0, 1, 2, 2.5, 3)

Figure 4.7(a,b,c,d) shows the dielectric measurements for the samples of $Cu_{0.5}Tl_{0.5}Ba_2Ca_2Cu_{3-x}Na_xO_{10-\delta}$ (x=0, 1, 2, 3). In order to prevent the material from transitioning to the normal state, such measurement sets are carried out at low measuring temperatures of 78K and lower frequencies of 100Hz. Superconducting materials transition to the normal state at higher frequencies. The interfacial polarization dominates the contribution to the dielectric-constant at such low frequencies. With addition of Na to the final compound, the real component and imaginary component of the dielectric-constant are suppressed, Fig. 4.7(a,b) showing a suppression in the density of free carriers at the CuO_2/NaO_2 planar sites in such samples.

In such samples, the holes are free carriers in the superconducting state, and the lower density of free carriers in the superconducting state showed that the CuO_2/NaO_2 planar sites' electron-hole recombination is enhanced, which in turn reduces the concentration of carriers and, consequently, the values of dielectric constant in Na-doped samples. As a result of the holes moving into the valance band and their energy increasing there, as well as the density of available free electrons decreasing in Na-doped samples, dielectric loss is also suppressed in these samples, as shown in Fig. 8d shows that Na-doped materials' ac-conductivity is suppressed in comparison to un-doped samples due to the decreased density of free holes in the CuO_2/NaO_2 planes.

4.3.1.6. SEM Analysis:

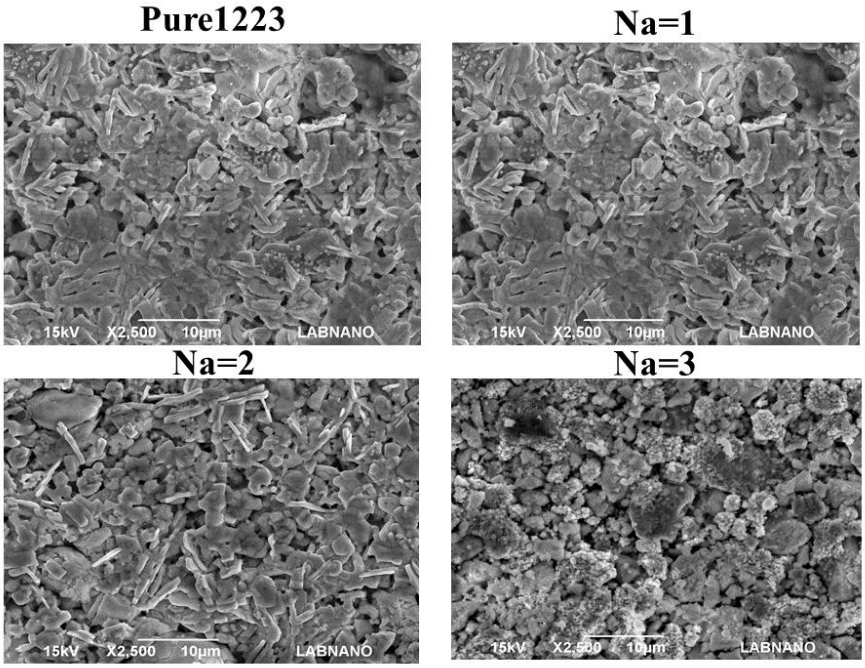

Figure 4.8a: SEM for the samples of $Cu_{0.5}Tl_{0.5}Ba_2Ca_2Cu_{3-x}Na_xO_{10-\delta}$ (x=0, 1, 2, 2.5,3) at ×2500 magnification

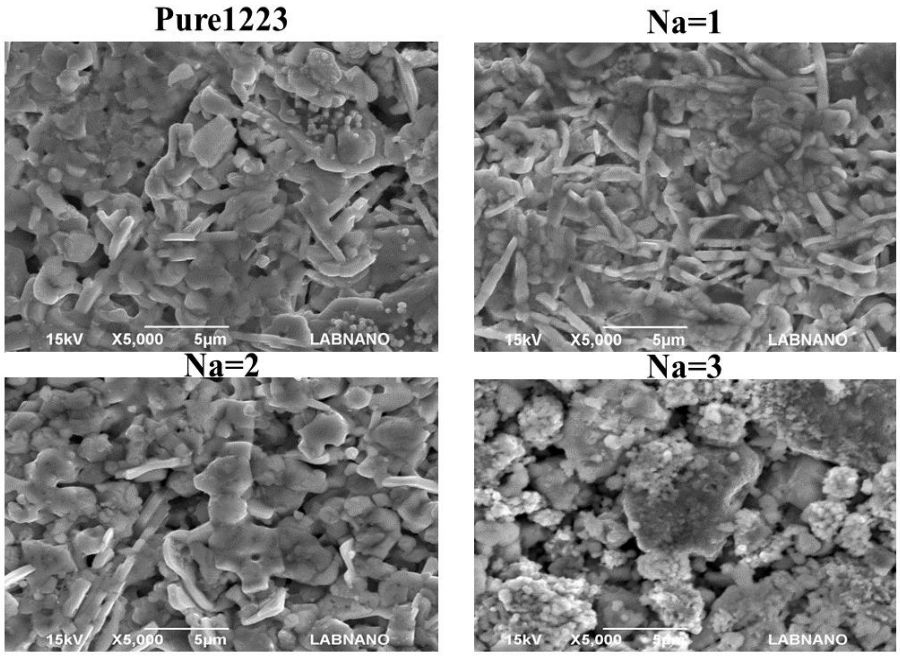

Figure 4.8b: SEM for the samples of $Cu_{0.5}Tl_{0.5}Ba_2Ca_2Cu_{3-x}Na_xO_{10-\delta}$ (x=0, 1, 2, 2.5,3) at ×5000 magnification

Fig 4.8: Shows that there is change of shape of rod-like grains into circular shaped grains on doping. The doped samples show that there is an effect on grain morphology **[11-12]** after doping of Na at CuO2 planes of CuTl1223 samples which supports the XRD data that c-axis length and also Volume of unit cell decreases.

4.3.2 $Cu_{0.5}Tl_{0.5}Ba_2CaMgCu_{3-x}Na_xO_{10-\delta}$ (x=0, 1, 2, 3) Samples:

4.3.2.1 Analysis of X-ray diffraction

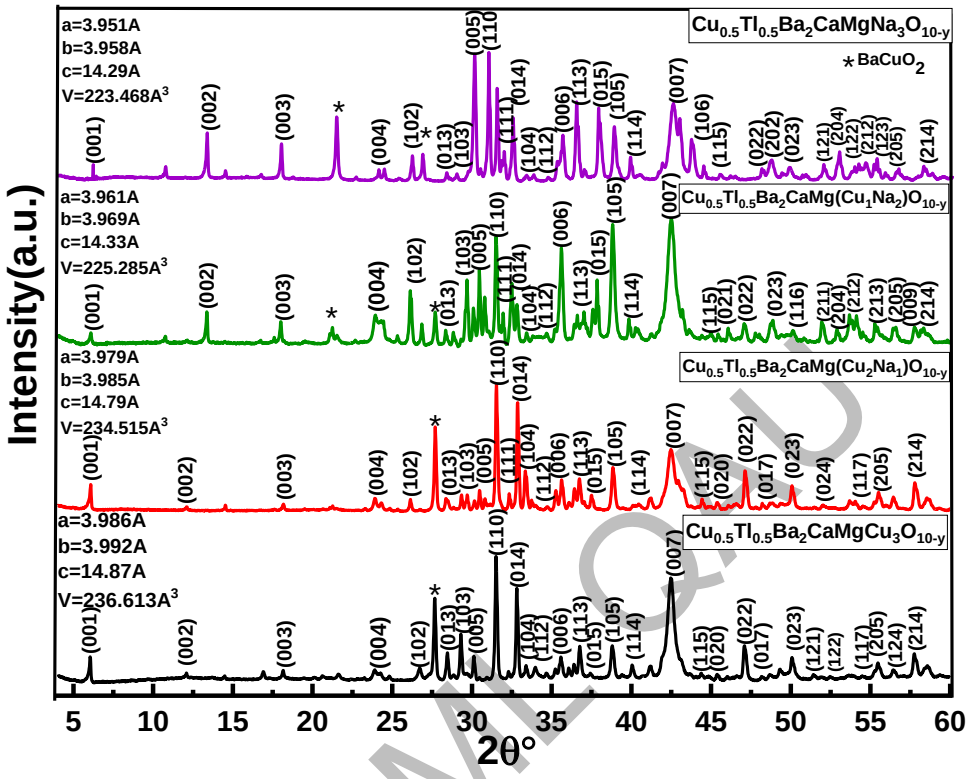

Fig. 4.9: The scanned diffraction of X-rays for the samples of $Cu_{0.5}Tl_{0.5}Ba_2CaMgCu_{3-x}Na_xO_{10-\delta}$ (x=0, 1, 2, 3)

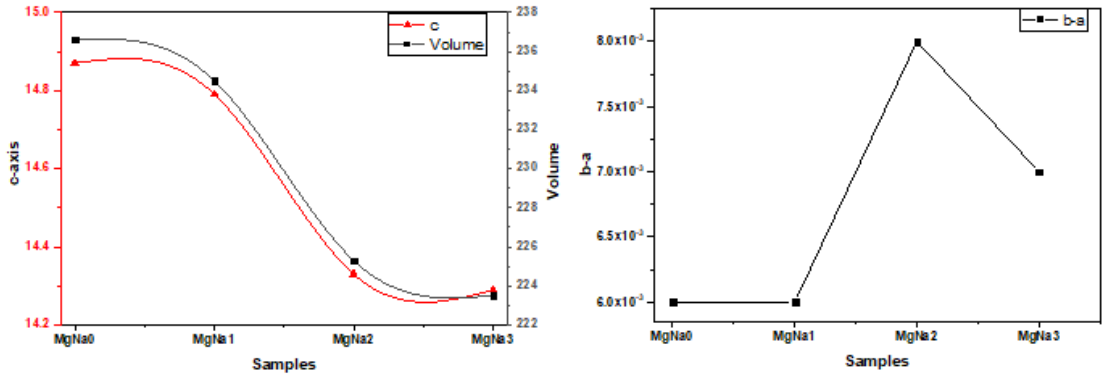

Figure 4.9a: Comparison of b-a axis of $Cu_{0.5}Tl_{0.5}Ba_2CaMgCu_{3-x}Na_xO_{10-\delta}$ (x=0, 1, 2, 3)

Figure 4.9b: Comparison between the c-axis and Volume of the samples of $Cu_{0.5}Tl_{0.5}Ba_2CaMgCu_{3-x}Na_xO_{10-\delta}$ (x=0, 1, 2, 3)

The scanned diffraction of X-rays for the $Cu_{0.5}Tl_{0.5}Ba_2CaMgCu_{3-x}Na_xO_{10-\delta}$ (x=0, 1,2, 3) samples in Fig. 4.8. Additionally, these samples have an orthorhombic crystal structure, with shorter c-axes and smaller unit cell volumes in the final compound. By increasing the doping concentration of Magnesium in the final doped compound, the orthorhombic distortions in these samples are also suppressed. The improvement of interlayer coupling(J) is demonstrated by the reduction of the length of c-axis. The orthorhombic distortion decreases in such samples as a result of higher Mg incorporation in the Final Compound shown in fig. 4.9(a, b). In comparison to un-doped(pure) samples, the larger density of carriers in Mg doping is likely to raise the critical temperature of these compounds.

4.3.2.2 Temperature-dependent measurements of resistivity

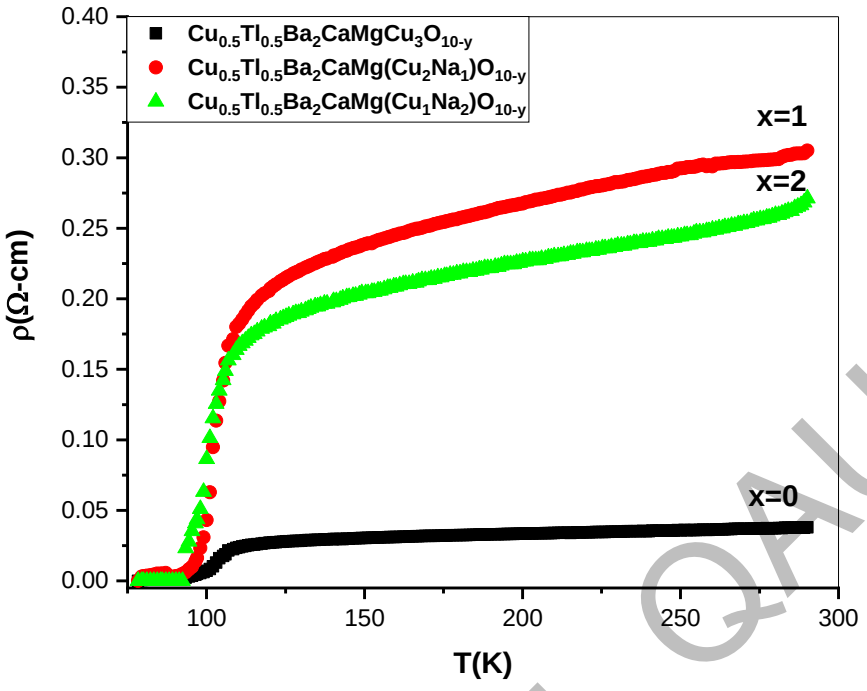

Fig 4.10: temperature-dependent measurements of resistivity for the samples of $Cu_{0.5}Tl_{0.5}Ba_2CaMgCu_{3-x}Na_xO_{10-\delta}$ (x=0, 1, 2) samples respectively

Figure 4.10 displays the temperature-dependent measurements of resistivity for $Cu_{0.5}Tl_{0.5}Ba_2CaMgCu_{3-x}Na_xO_{10-\delta}$(x=0, 1, 2) samples . From Troom till the Onset of superconductivity, all of these samples displayed variation of metallic behavior in resistivity. These superconductors have shown the onset temperature at 113.14K, 112.57K, and 92.76 K and the critical temperature for zero resistivity at 95.2K, 93.57K, and 92.76 K respectively. When comparing the $Cu_{0.5}Tl_{0.5}Ba_2CaMgCu_{3-x}Na_xO_{10-\delta}$ (x=0, 1, 2) samples with the $Cu_{0.5}Tl_{0.5}Ba_2Ca_2Cu_{3-x}Na_xO_{10-\delta}$ (x=0, 1, 2, 3) samples, it can be seen that the former Mg-doped samples perform better than the later Mg-free samples due to their higher carrier density.

4.3.2.4. Fluctuation-induced conductivity analyses:

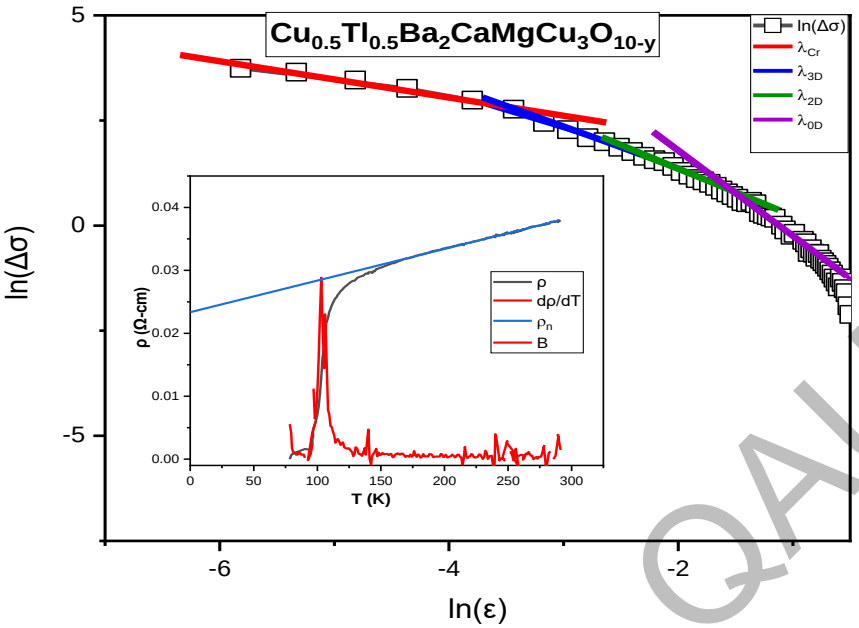

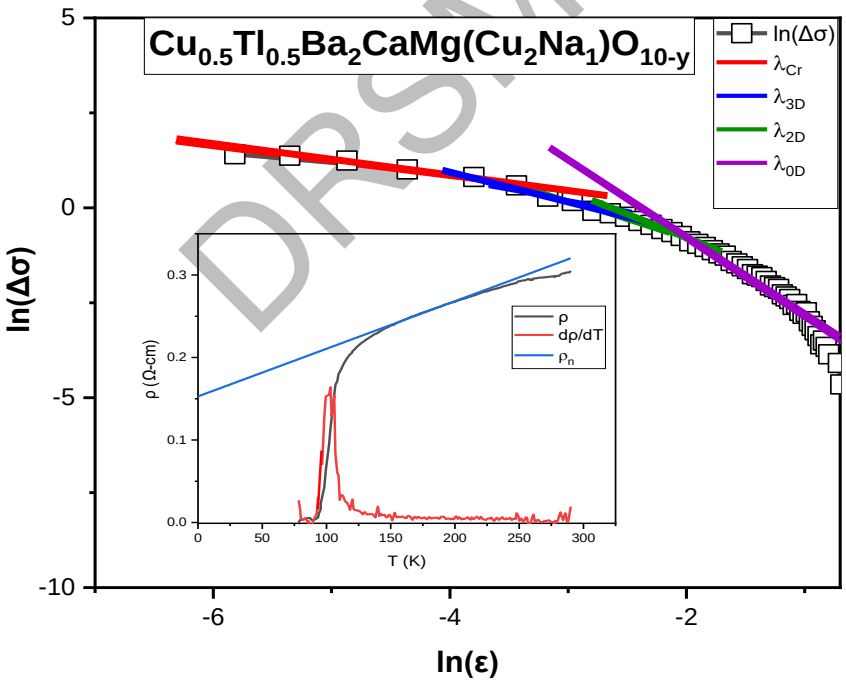

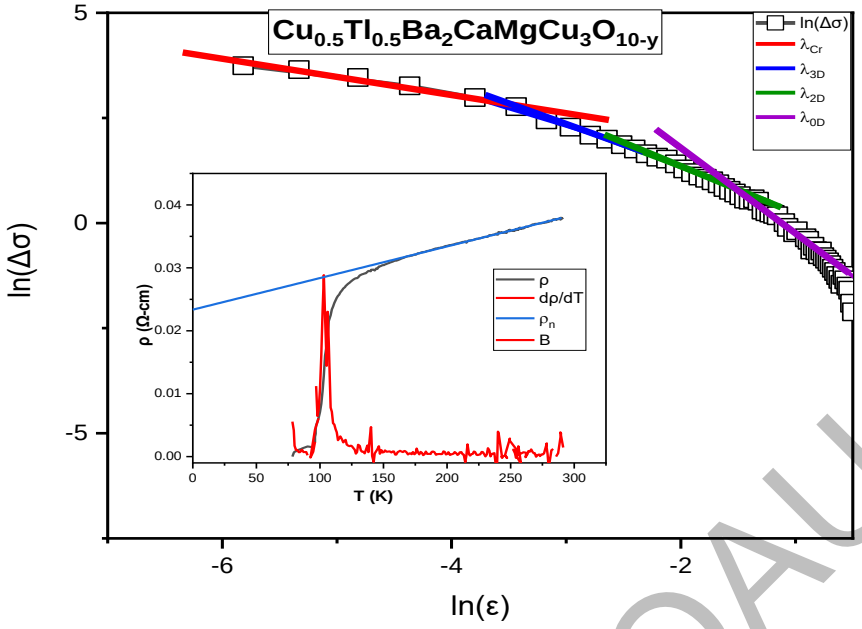

Fig 4.11(a,b,c): Plot between $\ln\Delta\sigma_{(T)}$ and $\ln\varepsilon$ of $Cu_{0.5}Tl_{0.5}Ba_2CaMgCu_{3-x}Na_xO_{10-\delta}$ (x=0, 1, 2)samples respectively

By performing fluctuation conductivity analyses (FIC) on the conductivity data described in the earlier part, it is also possible to identify the parameters relating to the intrinsic superconductivity in such samples. Fig:4.11(a, b, c) represents the results of these analyses. All MgNa-doped samples showed an increase in the number of inadvertent defects in the Final Compound as the α raised in magnitude, as seen in Table.4.3. Mg and Na-doped samples $Cu_{0.5}Tl_{0.5}Ba_2CaMgNa_3O_{10-\delta}$ (x=0, 1, 2) have a slightly increased in inter-layer coupling (J) and the ξc(0), as seen in Table 4.4. The density of Superconducting carriers is not greatly changed by the addition of Mg and Na-doping to the final compound, as evidenced by a little rise in the values of these parameters. Additionally, with Mg and Na-doped materials, the energy required to separate the Cooper pairs is insignificant.

Samples	λ_{CR}	λ_{3D}	λ_{2D}	λ_{0D}	$T_{CR-3D} = T_G$ (K)	T_{3D-2D} (K)	T_{2D-0D} (K)	T_c^{mf} (K)	T^* (K)	$\alpha = \rho_n(0K)$ (Ω-cm)
MgNa0	0.34	.58	1.03	2.01	107.37	108.37	121.42	103.05	159	0.022
MgNa1	0.33	.56	1.01	2.06	107.37	108.37	110.38	103.05	152	0.134
MgNa2	0.33	.59	1.13	2.07	104.36	105.36	116.4	100.05	157	0.137

Samples	$\xi_c(0)$ (Å)	J	N_G	$\lambda_{p.d.}$ x 10^2 (Å)	$B_{c(0)}$ (T)	B_{c1} (T)	B_{c2} (T)	κ	$J_{c(0)}$ x 10^3 (A/cm^2)	V_F x 10^7 (m/s)	E_{Break} (eV)	τ_φ x 10^{-13} (s)
MgNa0	1.136	.052	.042	332.4	4.38	0.45	128.7	20.8	7.16	0.93	.046	0.9
MgNa1	1.136	.052	.042	335.3	4.34	0.44	128.7	21	7.04	0.91	.027	1.52
MgNa2	1.15	.053	.043	347.2	4.21	0.42	128.7	22	6.61	0.91	.04	1

Table 4.3: Superconducting parameters from the plot of $\ln\Delta\sigma_{(T)}$ and $\ln\varepsilon$ of $Cu_{0.5}Tl_{0.5}Ba_2CaMgCu_{3-x}Na_xO_{10-\delta}$ (x=0, 1, 2)samples respectively

Table 4.4: Superconducting parameters calculated from the FIC of $Cu_{0.5}Tl_{0.5}Ba_2CaMgCu_{3-x}Na_xO_{10-\delta}$ (x=0, 1, 2) samples respectively

The marginally lowered values of $B_{c0}(T)$, $B_{c1}(T)$, and $J_c(0)$ in Mg and Na-doped samples demonstrate that the population of unintentional defects serving as the pinning centers is increased by Na inclusion in the final compounds. It is also evident from a little rise in the Ginzburg-Landau (GL) parameter and London penetration depth in Na-doped samples (Table.4.4).

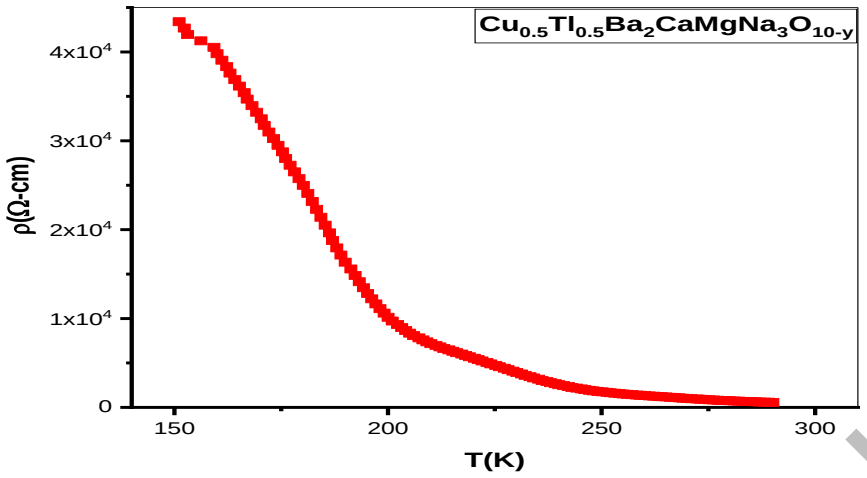

Fig 4.12: temperature-dependent resistivity measurements of $Cu_{0.5}Tl_{0.5}Ba_2CaMgCu_{3-x}Na_xO_{10-\delta}$ (x=3) samples

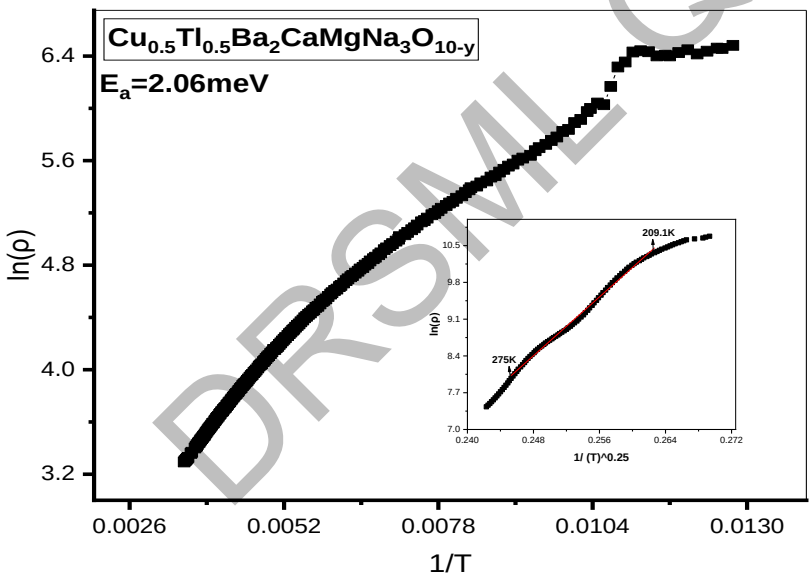

Fig 4.13: Activation energy curve of $Cu_{0.5}Tl_{0.5}Ba_2CaMgCu_{3-x}Na_xO_{10-\delta}$ (x=3) sample

$Cu_{0.5}Tl_{0.5}Ba_2CaMgNa_3O_{10-\delta}$ samples that followed the relationship of equation (12), which has demonstrated temperature-dependent semiconductor-like resistivity fitted in the regime of 77K to 300K, Fig. 4.12, have (VRH) conductivity. The Mott Varying Range Hopping (VRH) is predicted theoretically, which has provided the energy of activation 2.06 MeV in such compounds, is plotted as ln $\boldsymbol{\rho}$ vs. $1/T^{1/4}$.

4.3.2.4 Fourier Transform Infrared spectroscopy(FTIR) measurements

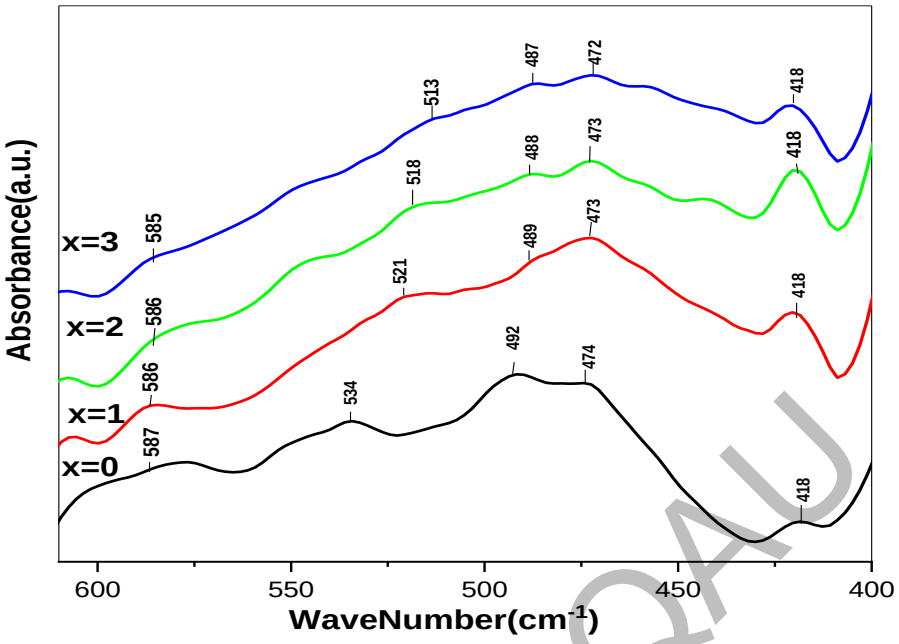

Figure 4.13: results of FTIR measurements of $Cu_{0.5}Tl_{0.5}Ba_2CaMgCu_{3-x}Na_xO_{10-\delta}$ (x=0, 1, 2,3) samples

Fig.12 shows the results of the $Cu_{0.5}Tl_{0.5}Ba_2CaMgCu_{3-x}Na_xO_{10-\delta}$ (x=0, 1, 2, 3) samples' FTIR absorption measurements. Two apical O_2 atoms of type Tl-OA-Cu(2) and Cu(1)-OA-Cu(2) at 420-450 and 480-540 cm^{-1} and a CuO2 planar oxygen mode at 580 cm^{-1} are the three phonon's modes connected to the vibrations of different oxygen atoms in the unit cell. Due to the weaker oscillator strength in Na-doped materials than in Cu-containing compounds, all three of these modes are softened in $Cu_{0.5}Tl_{0.5}Ba_2CaMgCu_{3-x}Na_xO_{10-\delta}$ (x=0, 1, 2, 3).

4.3.2.5 Dielectric measurements

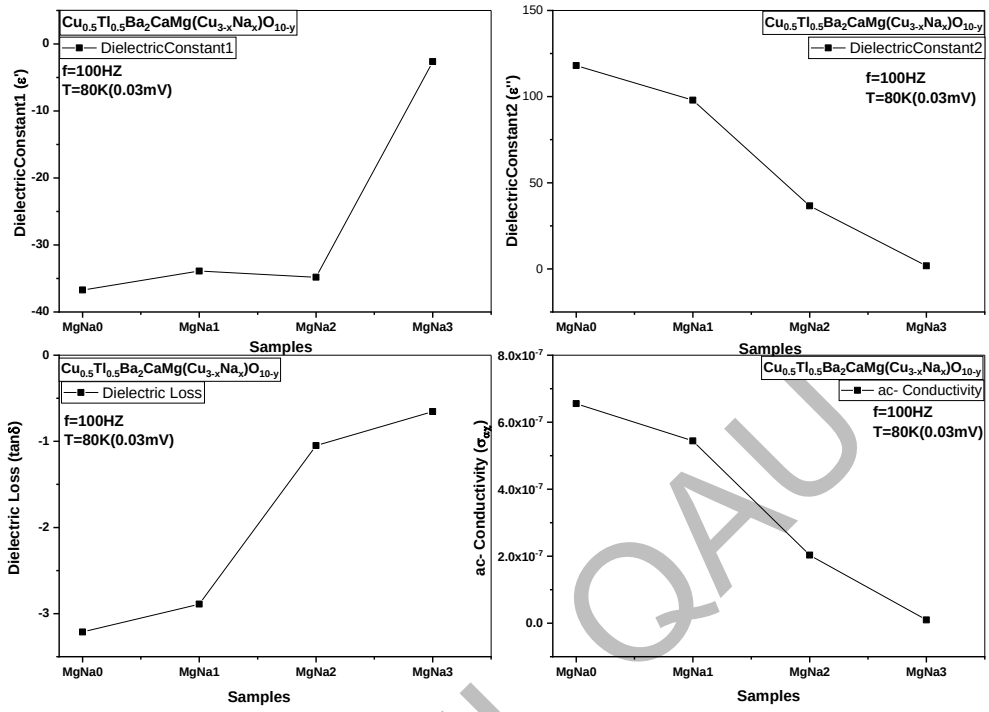

Figure 4.13(a,b,c,d) shows the dielectric measurements of $Cu_{0.5}Tl_{0.5}Ba_2CaMgCu_{3-x}Na_xO_{10-\delta}$ (x=0, 1, 2,3) samples

Figure 13(a,b,c,d) represents the results of the dielectric measurements made on the samples of $Cu_{0.5}Tl_{0.5}Ba_2CaMgCu_{3-x}Na_xO_{10-\delta}$ (x=0, 1, 2, 3) at 78K and 100Hz (a,b,c,d). In $Cu_{0.5}Tl_{0.5}Ba_2CaMgCu_{3-x}Na_xO_{10-\delta}$ (x=0, 1, 2, 3), the dielectric constant is lowered by a factor of more than three times compared to its value in $Cu_{0.5}Tl_{0.5}Ba_2Ca_2Cu_{3-x}Na_xO_{10-\delta}$ (x=0, 1, 2, 2.5, 3) samples. The inter-plane coupling enhancement in previous samples, which is promoted by Mg doping and results in an increase in the thickness of the CRL, is the main cause of this suppression, as seen by the greater volume of unit cells in $Cu_{0.5}Tl_{0.5}Ba_2Ca_2Cu_{3-x}Na_xO_{10-\delta}$ (x=0, 1, 2) samples. The charge transfer mechanism from the charge reservoir layer and, consequently, the density-free carriers in the conducting CuO_2/NaO_2 planes are slowed down by the CRL increased thickness (Fig. 13(a, b)); dielectric loss is also suppressed in such Mg-doped samples (Fig. 13c). Such Mg-doped samples exhibit less ac-conductivity in the superconducting state as compared to un-doped samples show the less conductivity in the superconducting state, as seen in Fig. 13d.

4.4 Conclusions:

In order to better understand how lighter alkali atoms, contribute to high Tc superconductivity in oxides, $Cu_{0.5}Tl_{0.5}Ba_2Ca_2Cu_{3-x}Na_xO_{10-\delta}$ (x=0, 1, 2, 3) and $Cu_{0.5}Tl_{0.5}Ba_2CaMgCu_{3-x}Na_xO_{10-\delta}$ (x=0, 1, 2, 3) samples have been created. When doped at the CuO_2 planar sites, Na is almost three times lighter than Cu and is capable of donating its $3s^1$ electron to the solid-state medium. These investigations focus on two key aspects: (1) the significance of interactions of electrons with phonons in high Tc superconductivity mechanism; and (2) the involvement of excess electrons in the CuO_2 planes in the mechanism. The Synthesization of samples using the two-step solid-state reaction process, and they are assessed for the measurements of x-ray diffraction, resistivity, dielectric properties, and (FTIR) absorption. While $Cu_{0.5}Tl_{0.5}Ba_2Ca_2Cu_{3-x}Na_xO_{10-\delta}$(x=0, 1, 2) and $Cu_{0.5}Tl_{0.5}Ba_2CaMgCu_{3-x}Na_xO_{10-\delta}$(x=0, 1, 2) samples have orthorhombic crystal structure, $Cu_{0.5}Tl_{0.5}Ba_2Ca_2Cu_{3-x}Na_xO_{10-\delta}$ (x=0, 1, 2) and $Cu_{0.5}Tl_{0.5}Ba_2CaMgCu_{3-x}Na_xO_{10-\delta}$ (x=2.5, 3) samples displayed variable range hopping conductivity with band gaps of 10.9 &9meV and 2.06meV, respectively. The resistivity measurements of $Cu_{0.5}Tl_{0.5}Ba_2Ca_2Cu_{3-x}Na_xO_{10-\delta}$ (x=0, 1, 2) samples have revealed metallic variations of resistivity down to 77K with superconductivity onset around 109.85K, 108.65K, 108.01K and the zero resistivity critical temperatures at 94.91K, 94.39K, 91.63K, whereas $Cu_{0.5}Tl_{0.5}Ba_2CaMgCu_{3-x}Na_xO_{10-\delta}$ (x=0, 1, 2) samples have shown onset of superconductivity 113.14K,112.57K, 107.8K and the zero resistivity critical temperature at 95.2K, 93.57K, 92.76K, respectively. The inter-layer coupling J, the Fermi velocity V_F, coherence length along the c-axis $\xi c(0)$, and the phase relaxation time $\tau\phi$ of the carriers are suppressed, suggesting loss in the density of superconducting carriers in Na-doped, according to excess conductivity analyses of $Cu_{0.5}Tl_{0.5}Ba_2Ca_2Cu_{3-x}Na_xO_{10-\delta}$ (x=0, 1, 2) samples by formula $K_F= [3\pi^2N/V]^{½}$. Also compared to un-doped samples, the values of $B_{c0}(T)$, $B_{c1}(T)$, and $J_c(0)$ are increased. While $Cu_{0.5}Tl_{0.5}Ba_2CaMgCu_{3-x}Na_xO_{10-\delta}$ (x=0, 1, 2) samples show an increase in inter-layer coupling J, the Fermi velocity 'V_F', coherence length along the c-axis '$\xi c(0)$', and the phase relaxation time '$\tau\phi$' of the carriers indicated enhancement of their Fermi-vector along the c-axis and hence the density of carriers with Mg-doping in the final compound. The values of $B_{c0}(T)$, $B_{c1}(T)$, and $J_c(0)$, however, is decreased in comparison with un-doped samples showing increase in the population of inadvertent defects . The Critical temperature 'Tc' and some superconducting parameters (as mentioned above) of the MgNa-doped are increased in comparison with that of Na-doped samples demonstrating that Mg doping produces more perfect material.

$Cu_{0.5}Tl_{0.5}Ba_2Ca_2Cu_{3-x}Na_xO_{10-\delta}$ (x=0, 1, 2, 3) and $Cu_{0.5}Tl_{0.5}Ba_2CaMgCu_{3-x}Na_xO_{10-\delta}$ (x=0, 1, 2, 3) samples both showed softening of the phonon modes associated with the vibrations of oxygen atoms with increased Na doping. Since the oscillator strength is suppressed in Na-doped samples compared to those with Cu concentration compounds, this softening of these modes results from this. With the doping of Na in the final compound, the real part of the dielectric constant, the imaginary part of it, and the ac-conductivity are suppressed, as shown by the reduction in the density of free carriers at the CuO_2/NaO_2 planar sites of $Cu_{0.5}Tl_{0.5}Ba_2Ca_2Cu_{3-x}Na_xO_{10-\delta}$ (x=0, 1, 2, 3) and $Cu_{0.5}Tl_{0.5}Ba_2CaMgCu_{3-x}Na_xO_{10-\delta}$ (x=0, 1, 2, 3) samples. The free holes have lowered density in the superconducting state of such samples shows that electron-hole recombination processes in the

CuO_2/NaO_2 planar are enhanced to suppress the concentration of carrier and these parameters as well. This is because holes are free carriers in oxide superconductors in the superconducting state. The disappearance of high Tc superconductivity in $Cu_{0.5}Tl_{0.5}Ba_2Ca_2Cu_{3-x}Na_xO_{10-\delta}$ (x=2.5, 3) and $Cu_{0.5}Tl_{0.5}Ba_2CaMgCu_{3-x}Na_xO_{10-\delta}$ (x=3) samples have shown the significance of interactions of electrons with phonons which is important for the mechanism of high Tc superconductivity.

References

[1] M. Mumtaz *et al.*, "Infield superconductivity of carbon nanotubes $Cu_{0.5}Tl_{0.5}Ba_2Ca_2Cu_3O_{10-\delta}$ superconductor composites," *AIP Advances*, vol. 5, no. 10, p. 107148, Oct. 2015, doi: 10.1063/1.4935191.

[2] N. A. Khan and M. Mumtaz, "A new $Cu_{0.5}Tl_{0.5}Ba_2Ca_2Cu_{3-y}Zn_yO_{10-\delta}$high-temperature superconductor with three ZnO_2planes," *Superconductor Science and Technology*, vol. 19, no. 8, pp. 762–766, Jun. 2006, doi: 10.1088/0953-2048/19/8/012.

[3] M. Rekaby, N. H. Mohammed, M. Ahmed, and A. I. Abou-Aly, "Synthesis, microstructure and indentation Vickers hardness for ($Y_3Fe_5O_{12}$) x/Cu0.5Tl0.5Ba2Ca2Cu3O10-δ composites," *Applied Physics A*, vol. 128, no. 4, Mar. 2022, doi: 10.1007/s00339-022-05394-3.

[4] A. Bedoya, "SUPERCONDUCTIVITY IN COMPOSITE MATERIALS AUTHOR," *www.academia.edu*, Accessed: Sep. 01, 2022. [Online]. Available: https://www.academia.edu/16308860/SUPERCONDUCTIVITY_IN_COMPOSITE_MATERIALS_AUTHOR

[5] A. I. Larkin and A. A. Varlamov, "Fluctuation Phenomena in Superconductors," *arXiv: cond-mat/0109177*, Sep. 2001, Accessed: Aug. 31, 2022. [Online]. Available: https://arxiv.org/abs/cond-mat/0109177

[6] L. G. Aslamasov and A. I. Larkin, "The influence of fluctuation pairing of electrons on the conductivity of normal metal," *Physics Letters A*, vol. 26, no. 6, pp. 238–239, Feb. 1968, doi: 10.1016/0375-9601(68)90623-3.

[7] A. K. Ghosh, S. K. Bandyopadhyay, P. Barat, P. Sen, and A. N. Basu, "Fluctuation-induced conductivity of polycrystalline Y1−xCaxBa2Cu3O7−δ superconductors," *Physica C: Superconductivity*, vol. 264, no. 3–4, pp. 255–260, Jun. 1996, doi: 10.1016/0921-4534(96)00257-2.

[8] A. L. Solovjov, H.-U. Habermeier, and T. Haage, "Fluctuation conductivity in YBa2Cu3O7−y films with different oxygen content. II. YBCO films with Tc≈80 K," *Low Temperature Physics*, vol. 28, no. 2, pp. 99–108, Feb. 2002, doi: 10.1063/1.1461921.

[9] Sarmiento, M.R., et al., "*Conductivity fluctuation and superconducting parameters of the YBa2Cu3− x (PO4) xO7–δ material,"* Physica B: Condensed Matter, vol.398, no.2s, pp. 360-363,2007.

[10] L. Essaleh, S. M. Wasim, G. Marín, C. Rincón, S. Amhil, and J. Galibert, "Mott type variable range hopping conduction and magnetoresistance in p-type CuIn3Te5 semiconductor compound," *Journal of Applied Physics*, vol. 122, no. 1, p. 015702, Jul. 2017, doi: 10.1063/1.4991004.

[11] M. U. Muzaffar, S. H. Safeer, N. A. Khan, A. A. Khurram, T. Subhani, and R. Nazir, "Grain Boundary Shortening in CuTl-1234 Superconductor by the Addition of ZnO Nanoparticles," *Journal of Superconductivity and Novel Magnetism*, vol. 31, no. 6, pp. 1669–1675, Oct. 2017, doi: 10.1007/s10948-017-4385-x.

[12] A. Kanwal and N. A. Khan, "(Cu0.5Tl0.5)(Ba2–yCay)(CaMg)(Cu3–x Znx)O10–δ (y = 0, 1; x = 0, 2, 2.5, 2.8, 3) and (MxTl1–x)(BaCa)(CaMg) Zn3O10–δ (M = Ag, K; x = 0, 0.5) Superconductors for the Studies the role of Spin Density Waves in the Mechanism of High Tc Superconductivity," *Journal of Superconductivity and Novel Magnetism*, vol. 34, no. 12, pp. 3163–3174, Oct. 2021, doi: 10.1007/s10948-021-05960-5.